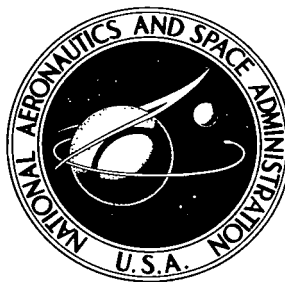


NASA TECHNICAL NOTE



NASA TN D-7981

2. u/u

NASA TN D-7981



LOAN COPY: RETURN
AFWL TECHNICAL LIBRARY
KIRTLAND AFB, N.M.

4.
**EXPERIMENTAL STUDY OF
A FREE TURBULENT SHEAR FLOW
AT MACH 19 WITH ELECTRON-BEAM
AND CONVENTIONAL PROBES**

William D. Harvey and William W. Hunter, Jr.

*Langley Research Center
Hampton, Va. 23665*



3. NATIONAL AERONAUTICS AND SPACE ADMINISTRATION • WASHINGTON, D. C. • OCTOBER 1975



0133538

1. Report No. NASA TN D-7981	2. Government Accession No.	3. Recipient's Catalog No.	
4. Title and Subtitle EXPERIMENTAL STUDY OF A FREE TURBULENT SHEAR FLOW AT MACH 19 WITH ELECTRON-BEAM AND CONVENTIONAL PROBES		5. Report Date October 1975	
		6. Performing Organization Code	
7. Author(s) William D. Harvey and William W. Hunter, Jr.		8. Performing Organization Report No. L-10138	
9. Performing Organization Name and Address NASA Langley Research Center Hampton, Va. 23665		10. Work Unit No. 505-06-41-01	
		11. Contract or Grant No.	
12. Sponsoring Agency Name and Address National Aeronautics and Space Administration Washington, D.C. 20546		13. Type of Report and Period Covered Technical Note	
		14. Sponsoring Agency Code	
15. Supplementary Notes Appendix by William W. Hunter, Jr., and James I. Clemmons, Jr.			
16. Abstract <p>An experimental study of the initial development region of a hypersonic turbulent free mixing layer has been made. Data were obtained at three stations downstream of a $M = 19$ nozzle over a Reynolds range of 1.3×10^6 to 3.3×10^6 per meter (4.0×10^5 to 9.2×10^5 per foot) and at a total temperature of about 1670 K (3000° R). In general, good agreement was obtained between electron-beam and conventional probe measurements of local mean flow parameters. Measurements of fluctuating density indicated that peak root-mean-square (rms) levels are higher in the turbulent free mixing layer than in boundary layers for Mach numbers less than 9. The intensity of rms density fluctuations in the free stream is similar in magnitude to pressure fluctuations in high Mach number flows. Spectrum analyses of the measured fluctuating density through the shear layer indicate significant fluctuation energy at the lower frequencies (0.2 to 5 kHz) which correspond to large-scale disturbances in the high-velocity region of the shear layer.</p>			
17. Key Words (Suggested by Author(s)) Electron beam Conventional probes Free shear flow		18. Distribution Statement Unclassified - Unlimited Subject Category 34	
19. Security Classif. (of this report) Unclassified	20. Security Classif. (of this page) Unclassified	21. No. of Pages 70	22. Price* \$4.25

EXPERIMENTAL STUDY OF A FREE TURBULENT SHEAR FLOW AT MACH 19 WITH ELECTRON-BEAM AND CONVENTIONAL PROBES

William D. Harvey and William W. Hunter, Jr.
Langley Research Center

SUMMARY

An experimental study of the initial development region of a hypersonic turbulent free mixing layer has been made. Data were obtained at three stations downstream of a $M = 19$ nozzle over a Reynolds range of 1.3×10^6 to 3.3×10^6 per meter (4.0×10^5 to 9.2×10^5 per foot) and at a total temperature of about 1670 K (3000° R). In general, good agreement was obtained between electron-beam and conventional probe measurements of local mean flow parameters. Measurements of fluctuating density indicated that peak root-mean-square (rms) levels are higher in the turbulent free mixing layer than in boundary layers for Mach numbers less than 9. The intensity of rms density fluctuations in the free stream is similar in magnitude to pressure fluctuations in high Mach number flows. Spectrum analyses of the measured fluctuating density through the shear layer indicate significant fluctuation energy at the lower frequencies (0.2 to 5 kHz) which correspond to large-scale disturbances in the high-velocity region of the shear layer.

INTRODUCTION

One of the more important results of the recent Conference on Free Turbulent Shear Flows (ref. 1) held at Langley Research Center was the identification of inconsistent free shear layer data that are taken in the initial development region of a shear layer or in transitional flows rather than in fully developed turbulent flows. Reference 1 provides an excellent review of the state of the art in turbulent free shear layer flows. In reference 2 the importance of developing accurate calculation methods for turbulent free mixing layers and the concomitant need for accurate experimental data were pointed out. The effects of Mach number and Reynolds number on spreading rates in fully developed turbulent flow are ill-defined; these effects are uncertain because of insufficient experimental data. In addition, turbulence measurements in supersonic and hypersonic shear layers are required before adequate theories can be developed.

Recent measurements have been obtained of mean and turbulence flow quantities in a Mach 5 nozzle shear layer (ref. 3) where the test Reynolds numbers were in the range required to achieve fully developed turbulent flow. These Mach 5 results show the

spreading rate of fully developed shear layers to be considerably lower than those for previous subsonic data. Furthermore, a corresponding reduction in the velocity fluctuation intensity across the shear layer was obtained from hot-wire surveys. Mean profile data in the initial development region of a hypersonic shear layer are presented in reference 4 for a single station about 13 cm (5.25 in.) downstream of the exit of a Mach 19.5 nozzle where the nozzle-wall turbulent boundary layer was 10 cm (4 in.) thick at the exit. Estimates indicate that distances downstream from the exit of the Mach 19.5 nozzle (ref. 4) on the order of 12 boundary-layer thicknesses would be required to achieve self-similar turbulent flow profiles.

The purpose of the present study is to investigate the initial development region of a hypersonic free shear layer by the analysis of mean profile data at several longitudinal stations obtained with both conventional probes and the electron-beam technique. Conventional probes were used to measure the mean static pressure, pitot pressure, and total temperature profiles. The electron beam was also utilized to measure the mean density and temperature as well as fluctuations in density across the hypersonic turbulent shear layer. The present data are believed to be unique in that no other detailed data on the initial development of a hypersonic turbulent free mixing layer at Mach 19 are available.

SYMBOLS

Measurements are presented in SI and U.S. Customary Units. Calculations and measurements were made in U.S. Customary Units.

A,B,C,D,E,F,G constants

d , diameter

f frequency

Δf frequency bandwidth

I current

K coefficient including geometry, optical, and electronic system parameters

M Mach number

N number density

N_2^+	nitrogen ion
$N_2X^1\Sigma_g^+$	neutral state of nitrogen molecule
$N_2B^2\Sigma_u^+$	excited ionized state of nitrogen molecule
$N_2X^2\Sigma_g^+$	ground ionized state of nitrogen molecule
N_R	ratio of photodetector output to total beam current
p	pressure
$p_{t,2}$	pitot pressure
R_∞	free-stream Reynolds number per unit length at nozzle exit
$R_{\infty,\bar{x}}$	free-stream Reynolds number based on distance from nozzle exit
S_T	measured spectral ratio
T	temperature
T_r	rotational temperature
t	time
u	velocity
V	voltage
x	longitudinal distance
\bar{x}	longitudinal distance from nozzle exit
y	normal distance from nozzle center line
\bar{y}	normal distance from wall boundary or from where $u/u_e = 0.05$ in shear layer

δ	boundary-layer or shear-layer thickness (\bar{y} at $u/u_e = 0.999$ for boundary layer and $0.999 \leq u/u_e \leq 0.05$ for shear layer)
ρ	mass density
σ	spreading rate, $\frac{\bar{x}}{\frac{dy}{d(u/u_e)} 0.5642}$
Φ	normalized power spectral density, $\frac{[\overline{V'(f)}]^2}{(V')_{\text{total}}^2}$
ω	wave number, $2\pi f/u$

Subscripts:

a	ambient
B	test-box conditions
e	edge values
o	settling chamber conditions
t	local stagnation conditions
w	wall conditions
δ	boundary-layer or shear-layer thickness

Bars over symbols denote time mean values and primes denote fluctuating values.

APPARATUS AND TESTS

A schematic sketch of the Langley hypersonic nitrogen tunnel and test equipment used in the present experiment is shown in figure 1 (top view of tunnel shown). The flow in the axially symmetrical nozzle exhausts into the vacuum test box. The boundary layer on the nozzle wall at the exit $x = 224.8$ cm ($x = 88.5$ in.) is about 10 cm (4 in.) thick. The nozzle was water-cooled in order to maintain a constant wall temperature. The facility can be operated continuously for 2 hours or more. Preliminary calibrations of

the flow and techniques of operation are given in reference 5. The present tests (table I) were made at a nominal Mach number of 19 in high purity nitrogen (5 parts per million of oxygen) at a nominal total temperature of about 1670 K (3000° R). The jet free-stream Reynolds number was varied from about 1.3×10^6 to 3.3×10^6 per meter (4×10^5 to 10×10^5 per foot). The jet free stream is defined as being the inviscid flow region along the nozzle or jet center line.

Detailed surveys of mean total temperature, pitot pressure, and static pressure were made with conventional probes across the shear-layer region at the nozzle exit and at about 1.3 and 3.5 boundary-layer thicknesses downstream of the exit. The electron-beam technique was utilized to measure the mean density and static temperature simultaneously at about 1.3 boundary-layer thicknesses downstream of the exit. Measurements of total temperature, pitot pressure, and static pressure across the turbulent boundary layer on the nozzle wall, at about 1.6 boundary-layer thicknesses upstream of the exit, are given in reference 6 for about the same flow conditions as presented herein.

INSTRUMENTATION

General

Several methods have been used to measure local flow parameters in nozzle-wall boundary layers and free mixing layers. Conventional probes provide direct measurements of pitot pressure, total temperature, and static pressure from which other local parameters may be calculated. However, probe data are subject to errors because of the presence of the turbulence and/or viscous effects. The nonintrusive electron-beam technique has been employed extensively in recent years for direct measurements of density and temperature. (See refs. 7 to 14.) Electron-beam static density and static temperature measurements are accomplished by determining the level and spectral distributions of local gas fluorescence resulting from fast electron collisions with molecules and subsequent spontaneous emission. (An extensive bibliography of electron-beam techniques and results may be found in ref. 10.) The electron beam has also been used to measure mean and fluctuating density in a Mach 8.5 nozzle-wall boundary layer (ref. 14) and the initial development region of a hypersonic ($M_e = 19.5$) free mixing layer (ref. 4). Most available investigations were limited to stream Mach numbers less than 9, and few comparisons of the electron-beam measurements with conventional probe data have been made.

Conventional probes are subject to numerous errors caused by viscous effects or interference effects. (See ref. 6.) The first step in comparing conventional probe data with electron-beam data must necessarily be on assessment of these probe errors. However, errors caused by interference effects between the probes and flow are difficult to

assess. Since the electron-beam technique provides data free of probe interference effects, the magnitude of such errors can be estimated if all other sources of error in both the probe and electron-beam data can be identified and evaluated. A detailed discussion of the electron-beam instrumentation and calibration is given in the appendix by William W. Hunter, Jr., and James I. Clemmons, Jr.

Conventional Survey Probes

Surveys across the axisymmetric shear layer were made with probes supported by a water-cooled strut (fig. 1) located on the opposite side of the tunnel from the density or temperature apparatus. The probe measurements were made in a horizontal plane through the center line of the tunnel and the beam measurements were made in a vertical plane through the center line. The probe strut-traversing mechanism (ref. 6) allows the probes to be positioned along or normal to the flow center line to within 0.0254 cm (0.01 in.). Sketches of the probes are given as inserts in figures 2(a) and 3(a). Surveys of mean total temperature, mean pitot pressure, and static pressures were made simultaneously across the mixing region at several x-stations. Pitot tubes were 0.3175 cm (0.125 in.) outside diameter stainless-steel tubes which were internally chamfered at the mouth. The static-pressure probes were also constructed of 0.3175-cm-diameter (0.125-in.) tubing with sharp cone tips. The total angle of the conical tips was 35° . Four 0.0787-cm-diameter (0.031-in.) pressure orifices were located 5.08 cm (2 in.) downstream of the cone tip. (See fig. 2.) The orifice locations were determined from inviscid theoretical calculations of the static-pressure distributions along the surface of the probe for the expected Mach number range through the shear layer. (The numerical method used was that of ref. 15.) The pitot- and static-pressure probes have been analyzed for viscous and rarefaction effects (ref. 6) and corrections have been applied where required. Large corrections (about 50 percent maximum) were applied for pitot-pressure data in the low-velocity region of the shear layer, and lesser corrections were applied up to about 15.24 cm (6 in.) approaching the high-velocity region. Pressure transducers of the type described in reference 6 were used for the pitot- and static-pressure measurements.

The sensing element of the total temperature probe (fig. 3(a)) was an alumel wire of 0.0254-cm (0.01-in.) diameter with small chromel wires of 0.00762-cm (0.003-in.) diameter attached at the center and at the ends. The small chromel wires attached to the ends of the alumel wire provided measurements of end temperatures (allowing calculation of heat conduction losses) and the chromel wire attached to the center measured the temperature at the center point of symmetry of the probe. This measured center temperature was then corrected for both radiation and conduction losses by using the method of reference 6 with values of recovery factor and Nusselt number from Yanta (ref. 16). Values of emissivity over a wide temperature range from references 6 and 17 have been

used for the chromel and alumel wires. The total temperature through the shear layer varied about 1670 K (3000° R) to 333 K (600° R). Both measured and corrected total temperature data are shown in figure 3. The maximum correction to the measured total temperature occurred in the jet free stream and was about 20 percent.

RESULTS AND DISCUSSION

Theory

When the nozzle-wall boundary layer leaves the exit, shear stresses in the low-velocity region of the free shear layer rapidly decrease in magnitude with increasing longitudinal distance. In the high-velocity region of the shear layer where values of velocity gradient and shear stress are small, the flow is assumed to be essentially an inviscid rotational flow field. (See ref. 18.) To evaluate whether the present shear profiles are representative of an inviscid rotational flow field, the experimental Mach number and velocity profiles are compared with theoretical predictions by use of the method of reference 19. The computer program of reference 19 calculates nonuniform supersonic flows by a characteristic method in which the molecular transport properties are assumed to be functions only of gradients normal to the streamlines. Initial input profiles to the program of Mach number, velocity, and static pressure perpendicular to the nozzle center line are required. Only the supersonic part of the shear-layer profiles can be calculated by the method of reference 19.

Experimental Mach number and velocity profiles obtained on the nozzle wall at station $x = 208.3$ cm (82.0 in.) (ref. 6) were scaled to a corresponding boundary-layer thickness at the nozzle exit station $x = 224.8$ (88.5 in.), and used to define conditions on the starting line required in the method of reference 19. The initial flow streamlines of the boundary layer at the nozzle exit were turned 2° corresponding approximately to the measured reduction in pressure from p_w at the exit to p_B in the test chamber. Predictions from reference 19 were obtained for a free-stream Mach number, total temperature, and total pressure of 19.42, 1780 K (3200° R), and 4310 N/cm² (6250 psia), respectively. The initial static-pressure profiles used were either equal to the edge value (p_e) or a ramp distribution. (See eq. (1) of ref. 6.) Comparisons of these calculations with data will be presented subsequently.

Mean Data

Typical distributions of pitot and static pressure through the shear layer are shown in figure 2 and listed in table II for three longitudinal stations $x = 225$ cm, $x = 238$ cm, and $x = 260$ cm ($x = 88.75$ in., $x = 93.75$ in., and $x = 102.25$ in.) for various values of

stagnation pressure. All pressures are normalized with the tunnel settling chamber pressure p_0 . Also shown for comparison is a single nozzle wall profile at $x = 208.3$ cm (82.0 in.). The pitot-pressure profiles at all test stations are nearly the same in the high-velocity side of the shear layer for $2.5 \lesssim y \lesssim 15$ cm ($1 \lesssim y \lesssim 6$ in.). Also included in the figure are average measured values of static pressure at the nozzle wall (p_w/p_0) and test box (p_B/p_0). The nozzle-wall and test-box pressures generally increased about 3 percent during a given test. Static pressures p_e/p_0 (symbols with cross) at the free-stream edge of the shear layer calculated from measured pitot pressure $p_{t,2}/p_0$ are also shown. The static-pressure measurements through the shear layer indicate a difference between free-stream values and test-box values that is not large. A minimum in the static-pressure distributions for $15.6 < x < 20.3$ cm ($6 < x < 8$ in.) occurs and is similar to that measured on tunnel walls in previous investigations. (See refs. 20 and 21.) The fact that $p_w > p_e$ at the nozzle exit might be expected since previous investigators (refs. 6 and 22) have also found a similar effect. A maximum of 10-percent error in the measured static pressure through the shear layer due to turbulence (obtained from ref. 23) would only slightly lower the levels presented in figure 2 and would not change the trends. This normal pressure gradient will be further discussed in a following section. A slight spreading of the flow downstream of the nozzle exit is evident for $y > 19$ cm ($y > 7.5$ in.) by comparing the profile at $x = 225$ cm ($x = 88.75$ in.) with those at $x = 260$ cm ($x = 102.25$ in.). This slight spreading of the flow is partially caused by the flow expansion from p_w/p_0 to p_B/p_0 ($p_w/p_B > 1$). No expansion of the hypersonic flow downstream of the exit would be expected if $p_w/p_B = 1$.

Figure 3 shows the measured and corrected total-temperature data for the same survey stations as presented for the pitot profiles. The corrected data (table II) were obtained by use of a ramp-type distribution of static pressure $p(y)/p_0$ in the data reduction procedure. (See eq. (1) of ref. 6.) However, the use of either a constant or ramp-type distribution of pressure had only a small effect on the computed temperature profile shape. (See fig. 3.) Corrections for radiation and conduction losses from the temperature probe amounted to about 25 percent in the free stream and a maximum of about 40 percent for $y \approx 17.75$ cm (7 in.) in the shear layer. Also, included in figure 3 is the total-temperature profile prediction by the method of reference 19. A slight spreading of the flow is again evident for $y > 21.6$ cm ($y > 8.5$ in.) by comparing the profiles just downstream of the exit at $x = 225$ cm ($x = 88.75$ in.) with the profiles at $x = 260$ cm ($x = 102.25$ in.). Shown for comparison are nominal measured values of T_w/T_0 and T_B/T_0 . Static temperatures at the boundary-layer edge T_e/T_0 were calculated from M_e . For $y < 18$ cm ($y < 7$ in.), the experimental shear-layer temperature profiles are similar to those for the nozzle-wall boundary layer (dashed line in fig. 3). The agreement between data and theory (fig. 3) in the outer region $y < 19$ cm ($y < 7.5$ in.) indicates that this part of the shear layer behaves like an inviscid rotational flow field.

Mach number and velocity profiles (see table III for values) across the shear layer for a range of conditions are shown in figures 4 and 5, respectively. A ramp-type distribution of static pressure $p(y)/p_0$ was used in the calculations of Mach number and velocity profiles. Also shown in the figures are upstream nozzle-wall profiles (input to theory) as well as calculated Mach number (fig. 4) and velocity (fig. 5) profiles obtained from theory of reference 19 by use of a ramp-type pressure input. (See eq. (1) of ref. 6.) Calculations were also made by using a constant value of pressure $p_e(y)$ (not shown herein); these calculations indicated that the maximum difference in velocity or Mach number profiles for either static-pressure distribution was about 0.3 percent or 0.4 percent. Values of the edge of the high-velocity side of the shear layer were determined from the pitot profiles and are shown in figure 2. A comparison of the Mach number profiles with theory (fig. 4) indicates that the theory is slightly higher over most of the high-velocity side of the shear layer for all survey stations. Changes in experimental profile shapes with increasing Reynolds number are also observed.

The small differences between experimental and theoretical velocity profiles out to about $y = 15$ cm (6 in.) (fig. 5(a)) and $y = 18$ cm (7 in.) (fig. 5(b)) show that in the relatively short distance from $x = 225$ cm (88.75 in.) to $x = 260$ cm (102.25 in.), there is little effect of shear on velocity in the outer 80 percent of the high-velocity part of the shear layer. The comparison of velocity profiles with theoretical predictions furthermore indicates that this outer region can be computed by the inviscid rotational method of characteristics of reference 19. However, for the low-velocity side of the shear layer ($y > 15$ or 18 cm (6 or 7 in.)), the effects of turbulent mixing are evidently important and must be included in a successful prediction method. A constant value of $M/M_e = 1$ in the inviscid nozzle-flow region was assumed in the data reduction yielding constant values of $u/u_e = 1$.

A study of the high Reynolds number ($R_\infty = 2.95 \times 10^7$ per m; $R_\infty = 7.5 \times 10^5$ per in.) turbulent free shear layer for a Mach 5 jet (ref. 3) showed the spreading rate of the shear layer to be much lower than that found for subsonic shear layer. At lower Reynolds numbers ($R_\infty = 1.58 \times 10^7$ per m; $R_\infty = 4 \times 10^5$ per in.) for the same Mach 5 flow, a higher spreading rate was obtained and thus indicates that the flow was probably not fully developed (ref. 3) for about one nozzle diameter downstream of the exit ($\bar{x}/\sigma \approx 9$). The spreading rates for the present $M = 19$ results were obtained from experimental data and are shown in figure 6 along with similar data from figure 3 of reference 3. Spreading rate calculations were made as in reference 3 by taking the slope of a fairing of the velocity profiles at the different survey stations and at a constant $u/u_e = 0.5$. These values for the slope at $x = 225$ cm (88.75 in.) were used in the following equation (ref. 24) to compute σ :

$$\sigma = \frac{\bar{x}}{0.5642 \left[\frac{dy}{d(u/u_e)} \right]_{u/u_e=0.5}}$$

The value of \bar{x} assumes that the virtual origin begins at the nozzle lip and therefore causes values of σ to be slightly smaller. The present results support the increase in spreading rate as the flow becomes supersonic with a tendency to level out for Mach numbers greater than about 5. As indicated in reference 3, all the higher spreading rates (low σ) shown in figure 6 for $M > 2$ were based on data taken at less than 20δ downstream of the separation point, and the associated low values of Reynolds number suggest that flows were not fully developed. The present values of σ shown in figure 6 are suspect since the data were obtained only up to $\bar{x} = 3.5\delta$, a value too near the nozzle exit for the mean velocity profiles to have become self-similar and fully turbulent.

Comparison of Mean Data From Conventional Probes and From Electron-Beam Surveys

Comparisons of the absolute mean density and temperature measured with the electron beam (table IV) with values calculated from probe measurements through the shear layer are shown in figures 7 and 8 and table II for two test conditions. Calculated density values from probe measurements (open symbols) are shown for the assumptions of $p(y)/p_0 = p_e/p_0$, $p(y)/p_0 = p_B/p_0$, and variable p/p_0 distribution from the static probe measurements. The comparisons (fig. 7) indicate that the density distribution obtained from the beam technique (solid symbols) agrees better with the probe measurements when the measured static-pressure distribution is used. The main source of error in the probe data is the measurements of static pressure. At the higher test pressure condition (fig. 7(b)) the beam data are in good agreement with the probe data based on measured static pressures. For this higher pressure condition, errors in the density from the beam technique are larger because of the unknown effects of quenching at the higher densities and lower static temperatures. This latter effect has been investigated in reference 25 and the results indicate that apparent quenching increases at low static temperatures and high densities. At the low-density levels found through the present shear layer, calibrations show that density varies almost linearly with the fluorescence output and no corrections were applied to account for quenching.

A typical distribution of mean static temperature through the shear layer from the electron beam (solid symbols) is shown in figure 8 and compared with values obtained from the probe measurements by using either $p(y)/p_0 = p_e/p_0$, p_B/p_0 , or the variation of p/p_0 (from fig. 2). Trends in temperature distributions from the probe data are

similar to trends from the electron-beam results but are generally lower in magnitude for $y < 15.25$ cm ($y < 6$ in.) and greater in magnitude for $y > 15.25$ cm ($y > 6$ in.). All the data indicate a possible peak in temperature that is located very near the minimum in $\bar{\rho}/\rho_0$ (fig. 7) or $y = 20.32$ cm ($y = 8$ in.), as would be expected. The electron-beam temperature measurements are less accurate in the low-density region and may partly explain the observed difference of the two measuring techniques at peak values of T/T_0 ($y \approx 20.32$ cm ($y \approx 8$ in.)). See appendix for discussion of electron-beam measurement uncertainties.

Since the largest uncertainties in the probe data are in the static pressures, comparisons of static pressures obtained from the beam measurements of density and temperature and static-pressure probe data are shown in figure 9 for $x = 238$ cm (93.75 in.). Also included are nozzle wall, test box, and free-stream static pressures calculated from the average of $p_{t,2}/p_0$ over $0 < y < 8.9$ cm ($0 < y < 3.5$ in.). The values from the electron beam were obtained from the equation of state, $p/p_0 = (\rho/\rho_0)(T/T_0)$, and the faired curves of figures 7 and 8. The static-pressure data from the electron beam and from the survey probe (fig. 9) indicate that a difference in pressure level exists between the free stream and test box. Variations in static pressure across the shear layer similar to the present data have been observed for a Mach 2.6 free jet flow (refs. 20 and 21). The difficulty in measuring and correcting hypersonic static pressures has been discussed in reference 6. The probe data shown were corrected using a total temperature which was in turn corrected by assuming constant $p/p_0 = p_e/p_0$. No corrections have been applied to the absolute measurements by the electron beam ($\bar{\rho}/\rho_0$ and \bar{T}/T_0) to obtain p/p_0 . Static-pressure probe corrections were about 50 percent in the free stream. The corrected probe data are in fair agreement with the electron-beam data except in the region of the static-pressure gradient.

The variation in mean static pressure across the mixing region for either measuring technique shown in figure 9 may be partly due to the unmatched free-stream and test-box pressures. The electron-beam pressure distribution (solid symbols in fig. 9) does not agree entirely with the probe data but does show a change across the shear layer. In general, the measured density and velocity profiles tend to support the simultaneous occurrence of the static-pressure minimum at about the same radial location from the nozzle center line where the maximum momentum transfer occurs in the shear layer. According to reference 23, turbulence would not affect the static pressures by more than 10 percent; therefore, no corrections for turbulence effects are applied to present data.

Figure 10 shows a comparison of the present static-pressure distributions through the shear layer with similar data for $0.94 \leq M_\infty \leq 2.60$. (See ref. 21.) The results shown are representative of data for measuring stations across the shear layer at various ratios of distance downstream of the exit (\bar{x}). Both the low and high Mach number data

shown (fig. 10) indicate a static-pressure variation across the mixing region of compressible jets. The location at which the static-pressure minimum occurs is probably due to the outward spreading of the jet stream and induction of surrounding fluid. (See ref. 21.)

Fluctuating Density Measurements

In addition to the mean density measurements, fluctuation density measurements (table IV) across the shear layer at a single station were also made with the electron beam. The purpose of these measurements was to determine the intensity or level and frequency spectra of these fluctuations.

Before final ρ' values could be obtained, it was necessary to account for sources of noise in the signal. These sources are divided into two groups. The first source was the tunnel heater element and ambient background, and second was the beam current fluctuations, inherent signal shot noise, and electronic system noise. These noise contributions were accounted for in the following manner. For each series of tunnel runs, the first noise source (radiated field from heater element and ambient background) was recorded and measured with the beam off and the tunnel operating ($\overline{(V')^2_{TN}}$ where TN denotes tunnel noise). The second noise source was recorded and measured ($\overline{(V')^2_{BN}}$ where BN denotes background noise) with no tunnel flow and the tunnel heater off over a range of densities. Then as an approximation, the representative rms readings were squared and subtracted from the squared total rms reading made during a tunnel run, and the square root taken of the resultant difference. The total voltage and the rms voltage are related to the total or average rms density fluctuations by the calibration results given in the appendix; the relation is

$$\frac{\sqrt{\overline{(V')^2}}}{\bar{V}} = \frac{\sqrt{\overline{(V')^2_{total}} - \overline{(V')^2_{TN}} - \overline{(V')^2_{BN}}}}{\bar{V}} \propto \frac{\sqrt{\overline{(\rho')^2}}}{\bar{\rho}}$$

Data tape signals (noise and total signal) were passed through a scanning spectrum analyzer by using an effective bandwidth of $\Delta f = 50$ Hz, detected by a true rms voltmeter, and recorded on a strip chart recorder. A smooth curve was faired through the recorded data and rms data points were taken from the smoothed curve at 100-Hz intervals up to 1 kHz and 1-kHz intervals up to 50 kHz.

Plotted in figure 11 are values of the ratio of the average rms fluctuating density to the mean density. The rms data shown for two test conditions were obtained from true rms voltmeter readings of the analog tape recordings. The frequency response of the overall system limited the frequency content of the measurements. The lower and upper frequency -6-dB points occur at 0.1 kHz and 50 kHz, respectively. This frequency range

represents the practical response of the system. The upper frequency limit was determined by the expected signal-to-noise ratio.

The measured values of rms density (fig. 11) are relatively flat in the flow core for $0 < y < 7.62$ cm ($0 < y < 3$ in.) and rapidly increase with distance from the tunnel center line ($y = 0$) until peaks occur in the region $15.25 < y < 17.8$ cm ($6 < y < 7$ in.). The magnitude and location of the peaks appear to vary with total pressure. The peaks occur in the vicinity of the inflection point of the $\bar{\rho}/\rho_0$ profiles (fig. 7) in accordance with simple mixing theory. The magnitude of the normalized rms data for the lower pressure test is higher than that for the higher pressure data. This difference in level is probably caused by the changing boundary-layer structure with Reynolds number as pointed out in the discussion of figure 4. Other factors such as acoustical sources, settling chamber geometry, and valve-piping effects were not checked as possible disturbance generators, but are not expected to be important. (See ref. 26.)

The intensity of density fluctuations in the free stream is about 2.5 percent which is comparable to pressure fluctuation intensities in high Mach number flows. (See refs. 27 and 28.) If these fluctuations are assumed to be sound, then $\frac{p'}{p_e} \approx 1.4 \frac{\rho'}{\rho_e} \approx 3.5$ percent which may be compared with values in figure 7 of reference 28. A comparison of the present intensities of density fluctuations with those obtained in a Mach 8.5 turbulent nozzle-wall boundary layer (ref. 14 and fig. 5 of ref. 29) also using the electron-beam technique is shown in figure 12. The present shear-layer thickness δ was determined from the difference between \bar{y} at $u/u_e = 0.999$ and \bar{y} at $u/u_e = 0.05$. The present $M_\infty \approx 19$ results generally agree in trend in that the peak intensity occurs in the low-velocity side of both the boundary layer and shear layer. The magnitude of the fluctuations for the shear-layer data is considerably higher across the mixing region than for boundary layers and the peak ρ' occurs in the peak gradient region as might be expected when compared with wall boundary layers.

Figure 13 shows the energy spectra or power spectral density, divided by the local mean density squared, as a function of frequency for the various measuring stations across the shear flow. Values of the power spectral density function of the stationary random signal measured were approximated from

$$\lim_{\Delta f \rightarrow 0; T \rightarrow \infty} \frac{1}{\Delta f(T)} \int_0^t [\bar{V}'(f, t)]^2 dt \approx \frac{[\bar{V}'(f)]^2}{\Delta f}$$

where noise sources $[\bar{V}'(f)]_{TN}^2$ and $[\bar{V}'(f)]_{BN}^2$ are subtracted out and $\Delta f = 50$ Hz. The power spectral density function or energy spectrum for random data describes the frequency composition of data in terms of the spectral density of its mean square value. Values of the power spectral density shown in figure 13 have been faired with a solid line

to indicate trends of the data points. The change in the curve for the lowest density ratio $y = 17.8$ cm (7 in.) results from large noise levels relative to test signal levels.

Appreciable amounts of the fluctuation energy occur at the lower frequencies. (See fig. 13.) The overall level of energy in the spectrum increases with increasing distance from the tunnel center line and then decreases for values of $y > 16.5$ cm ($y > 6.5$ in.). Significant energy through the shear layer between $0.2 < f < 1$ kHz is evident, and indicates large-scale disturbances existing in the shear layer. Energy levels beyond 50 kHz could not be obtained for the present tests because of instrumentation "cutoff" at this frequency. (See fig. 17.)

A comparison of the power spectra obtained for the present study to that in a Mach 5 free shear layer by use of hot-wire techniques (ref. 30) is shown in figure 14. This comparison is made to show relative orders of magnitude in energy between the two experiments and to aid in evaluating measuring techniques. Values of the nondimensional power spectral density Φ are shown plotted against a nondimensional wave number $\omega = 2\pi f\delta/u$. The shear-layer thickness δ for both experiments shown was determined from the difference between \bar{y} at $u/u_e = 0.999$ and \bar{y} at $u/u_e = 0.05$. Local velocity u was calculated from the values of u/u_e shown in figure 5. For the present $M \approx 19$ data the power spectra are presented for a \bar{y} -location corresponding to u/u_e values at the peak intensity of density fluctuations (from fig. 11) and for $u/u_e = 0.6$ for reference 30. The values of Φ shown in figure 14 were obtained by taking the ratio of the power spectral density to the total mean squared fluctuation as follows:

$$\Phi = \frac{[\overline{v'(f)}]^2}{(\overline{v'})_{\text{total}}^2}$$

The electron-beam results shown in figure 14 were calculated from values of $\overline{[\rho'(f)]^2}/\bar{\rho}^2\Delta f$ over the frequency range at the $y = 16.5$ -cm ($y = 6.5$ -in.) station for the lowest Reynolds number and $y = 17.8$ cm ($y = 7.0$ in.) for the highest Reynolds number test. The electron-beam measured values of the power spectral density were then normalized by the corresponding rms to mean values squared (fig. 11). Measured values of the hot-wire signal and corresponding noise signals over the maximum frequency are shown in figure 15 of reference 30. These data were obtained by using the spectral survey bandwidth of $\Delta f = 1$ kHz. The difference between the squared values of the hot-wire and noise signals over the frequency range divided by the bandwidth Δf gave the power spectra over the maximum frequency range at the $u/u_e = 0.6$ station. Then integration of the power spectra over the total frequency range gave the mean squared value.

The $M \approx 19$ results shown in figure 14 were obtained at a location downstream of the nozzle exit equal to 1.31 initial boundary thicknesses compared with about 35 for the

$M = 5$ results. The shear flow results for $M = 5$ (ref. 30) are for a higher Reynolds number and a turbulent mixing region further downstream of the exit than the $M \approx 19$ data. The accuracy of all data presented is somewhat questionable at the extremes of the nondimensional wave number abscissa. This is because of the large-amplitude fluctuations at low frequencies and low signal-to-noise ratio at high frequencies. The comparison indicates that relative to the $M = 5$ results, there are large-scale fluctuations present in the $M_\infty \approx 19$ shear layer; however, significant small-scale turbulence also is present. It is possible that these large-scale fluctuations indicated by the present data result from a pulsating or wavering axial motion of the entire shear layer. Effects of turbulent scales of the disturbances in the shear flow are to some extent, however, accounted for in the nondimensional wave number through δ where δ/u for reference 30 is about 3.5 times smaller than that for the present $M \approx 19$ results.

CONCLUSIONS

An experimental study of the developing region of a hypersonic shear layer has been made. The investigation was made in the free turbulent mixing layer downstream of the exit of a Mach 19 nozzle over a Reynolds number range from 1.3×10^6 to 3.3×10^6 per meter (4.0×10^5 to 9.2×10^5 per foot) and at a total temperature of about 1670 K (3000° R). The electron beam was utilized to measure fluctuations in density across the mixing layer and these results along with the measured mean values of density and temperature from both the beam and conventional probes have led to the following conclusions:

1. In general, good agreement was obtained between electron-beam and corrected conventional probe measurements for local mean flow parameters.
2. Peak relative density fluctuation levels were higher than those observed in boundary layers for Mach numbers less than 9. However, the intensity of the relative density fluctuations in the free stream was similar in magnitude to intensities in pressure fluctuations found in high Mach number flows.
3. Spectrum analysis of the measured fluctuating signals through the hypersonic turbulent free mixing region indicated that significant fluctuation energy was at lower frequencies (between 0.5 and 1 kHz for the present tests) and suggested that large-scale disturbances exist in the shear layer, particularly near the stream edge of the layer.

Langley Research Center
National Aeronautics and Space Administration
Hampton, Va. 23665
May 27, 1975

APPENDIX

ELECTRON-BEAM INSTRUMENTATION SYSTEM

William W. Hunter, Jr., and James I. Clemmons, Jr.
Langley Research Center

The electron-beam instrumentation system consists of four subsystems: electron-beam system, temperature measurement system, density measurement system, and a digital data recording system. An overall instrumentation system block diagram is shown in figure 15. Details and function of each subsystem are described.

Theoretical Basis for Electron-Beam Measurements

A beam of 28-keV electrons was used to excite neutral $N_2X^1\Sigma_g^+$ nitrogen molecules to the $N_2B^2\Sigma_u^+$ excited ionized state, from which the molecules spontaneously decay to the ground ionized state $N_2X^2\Sigma_g^+$ with the emission of photons. The relative population distributions of vibrational and rotational molecular states of $N_2X^1\Sigma_g^+$ are functions of the vibrational and rotational temperature, respectively. (See ref. 31.) Through analysis of the spectrum produced by the $N_2B^2\Sigma_u^+$ to $N_2X^2\Sigma_g^+$ transition to the ground state, the $N_2X^1\Sigma_g^+$ molecular state temperature is determined.

The temperature measurement technique used in this work is as follows: The rotational spectrum was divided into parts; relative distribution of rotational energy in the vibrational band between the two parts or channels changes with rotational temperature. Therefore, a variable ratio between the channels and temperatures can be established analytically or through a calibration procedure. A calibration procedure was used in this work and the resultant data were fitted to a sixth-order polynomial through a least-squares procedure, that is,

$$T = A + BS_T + CS_T^2 + DS_T^3 + ES_T^4 + FS_T^5 + GS_T^6 \quad (1)$$

where T is the temperature and S_T is the measured spectral ratio.

Density measurements were determined from the fluorescence intensity resulting from the $N_2B^2\Sigma_u^+$ to $N_2X^2\Sigma_g^+$ spontaneous transition. The relation between the emitted fluorescence and the ground state ($N_2X^1\Sigma_g^+$) number density is not a simple relation. The relation used in this work is

$$N_R = \frac{K(AN + BN^2)}{1 + CN} \quad (2)$$

where N_R is a measured ratio of photodetector output normalized to the total beam current. The coefficient K includes geometry, optical, and electronic system parameters

APPENDIX

whereas the coefficient A accounts for the direct population contribution to the excited state $N_2^+B^2\Sigma_u^+$. These coefficients are directly dependent on the number density N of the ground molecular state $N_2X^1\Sigma_g^+$. Coefficient B includes the population factors which are dependent on N^2 and the coefficient C includes the depopulation factors. (See ref. 32 for a detailed accounting of these coefficients.) In this work, coefficients for this equation were determined through a calibration procedure.

Electron-Beam System

The electron-beam system used in this work is typical and details may be found in references 32, 33, and 34. Nominal beam operating current and potential are 700 mA and 28 kV, respectively. Total beam current is assumed to be the current collected by the tunnel at ground potential. Beam current is measured with a picoammeter. An amplified meter voltage output which is proportional to the measured current is provided as input to the digital data system.

Magnetic shielding installed in the Langley hypersonic nitrogen tunnel is required to reduce electromagnetic field effects on the beam system operation which caused a maximum of 75-percent reduction in beam efficiency. Source of the disturbance is the tunnel heater element and power cables feeding the element. (See ref. 5.) Typical heater element direct-current operating parameters are 5400 amperes at 45 volts. A survey was performed and the magnetic flux density in the vicinity of the beam source is approximately 1 gauss (1×10^{-4} tesla or 1 Wb/m^2). Effective shielding, that is, no noticeable field effects, was accomplished with a pair of concentric Mumetal shields. The concentric cylindrical shields are separated 6.4 mm (0.25 in.) apart and the material is 1.3 mm (0.052 in.) thick.

Temperature Measurement System

Temperature measurements were made by use of a dual-channel spectrometer described and illustrated in reference 35. This instrument is basically a 0.5-m (19.69-in.), $f/5.5$ dual-channel modified Czerny-Turner type of spectrometer with a single entrance slit. Fluorescence from the electron beam is focused onto the variable-width entrance slit, behind which a beam splitter diverts a portion of the input signal to each channel of the spectrometer. The grating-mirror system in each channel constructs a spectrum at each exit plane; the part of each spectrum detected by the photomultipliers is determined by adjusting the grating positions and placing fixed-sized exit slits in each exit plane to delimit the width of the spectrum detected.

Before meaningful measurements could be made with the dual-channel system, it was necessary to compensate for unequal optical efficiencies in each channel. The fluorescence from the electron beam was focused onto the entrance slit; with identical grating

APPENDIX

positions and exit slit widths, the gain of the two photomultipliers was adjusted to give a ratio of unity in the output signals. This check was made each day, and the drift was found to be negligible and required no additional compensation. The grating positions in each channel were calibrated by using the 3888.65 Å (1 angstrom = 10^{-10} meter) helium line of a helium discharge lamp radiation as a reference. Exit slit widths were set to cover wavelength intervals 3895.0 Å to 3907.0 Å and 3907.0 Å to 3910.2 Å. Photomultiplier current values were measured with a picoammeter. (See fig. 15.) Each picoammeter has an amplified voltage output which is proportional to the detected current and this output is used as an input to the digital data system.

The experimental setup is illustrated in figure 1. Fluorescence from the electron beam is collected by the lens with a magnification of 0.4 and focused onto the entrance slit. Since the entrance slit and the electron beam were each aligned in the vertical direction, a Dove prism was placed in front of the entrance slit to rotate the beam image by 90° . This arrangement insured a uniform distribution of light across the entrance slit width and guaranteed good spatial resolution in the wind tunnel. The entrance slit used for the dual-channel spectrometer was 1 cm (0.3937 in.) high and 400 micrometers (39.37×10^{-6} in.) wide. Small spatial fluctuations of the beam merely resulted in a small vertical movement of its image on the slit. In regions of flow where the gradient of the stream parameters was especially steep, the increased resolution resulted in a more accurate description of flow parameters. On the other hand, in the lowest density regions where the beam intensity was weakest (and where in this work the gradient was less steep) the decrease in total signal-to-noise ratio increased the measured uncertainty.

During a tunnel run, approximately 100 data points at a given observation position were obtained and required about 1.5 minutes run time. The temperatures were determined with an uncertainty varying from 1 percent at the lowest temperature and greatest density to 12 percent at the highest temperatures and lowest density. These stated uncertainties for temperature and also for the density measurements are based on the standard deviation of the respective ratio measurements.

Measurements through the free mixing region were made by traversing the spectrometer and density apparatus, to be described in the next section, in the vertical direction parallel to the beam. Both the spectrometer and density apparatus were mounted on a common platform. Platform position was continuously monitored with an electro-mechanical readout system. With suitable calibration, the optical system center-line location with respect to the tunnel center line was always known within ± 0.25 mm (9.84×10^{-3} in.). The free mixing region that was surveyed extended in the y-direction from 11.42 to 22.85 cm (4.5 to 9.0 in.) from the center line.

APPENDIX

Density Measurement System

The density measurement system consisted of an electro-optical detection apparatus, electronic filter, amplifiers, and an analog recorder. (See fig. 15.) The electro-optical detection apparatus is diagramed in figure 16 and consists of a 60/40 beam splitter, 0.16-cm by 5.1-cm entrance slit, 19-cm focal length lens, mirrors, interference filter, and photomultiplier detector with an S-20 photocathode. The interference filter was used to isolate the nitrogen ion first negative system, (0-0) vibrational band, and its bandpass was centered at 3924 Å and had a 61 Å half-width. The beam splitter was used to allow simultaneous measurements of density and temperature at the same mean position in the flow. This was accomplished by using a common lens (fig. 1) to image simultaneously a part of the beam-induced fluorescence on the spectrometer and density apparatus entrance slits.

Length and width of the fluorescence observed by the temperature and density devices were determined by the respective entrance slit dimensions and the optical magnification which was 0.4. Spatial resolution of the density apparatus was 0.40 cm by 12.3 cm (0.161 in. by 4.84 in.). To obtain absolute density measurements, it was necessary to size the entrance slit of the density apparatus so that its length (5.1 cm (2 in.)) was sufficient to span a fluorescence region normal to the beam direction. The dimensions of the fluorescence region normal to the beam direction are dependent on the local gas number density and distance from the beam source exit aperture. (See ref. 34.) Expected maximum number density was approximately $3 \times 10^{16}/\text{cm}^3$ ($4.92 \times 10^{17}/\text{in}^3$). To ascertain that the slit size was adequate for this range, tests were conducted in the facility under no flow conditions. These tests simply consisted of traversing the density apparatus along the length of the beam and noting the change of signal as a function of distance from the beam source exit aperture. These tests were performed at several number densities and it was found that for the expected maximum density, a small change of signal occurred between extreme limits of travel. This change was less than 10 percent. It should be noted that these tests were made for maximum unfavorable conditions since the gas number density varied from about 7×10^{14} to $2 \times 10^{16}/\text{cm}^3$ (1.15×10^{16} to $3.28 \times 10^{17}/\text{in}^3$) across the free-mixing-layer survey station. Therefore, under flow conditions the actual beam spreading would be less than under no flow conditions; thus, it was assumed that no additional corrections to the measured density values because of beam spreading would be necessary.

The signal that was obtained from the density apparatus can be described as a biased fluctuating voltage. The fluctuating component is shifted above the ground potential by the average or mean component value. The combined signal was transmitted through the cabling system, amplifier, active filter, and notch filter. (See fig. 15.) A 50-Ω coaxial

APPENDIX

cable system was terminated at the transmitting and receiving ends with $50\text{-}\Omega$ resistors to ground. The amplifier was a high input and low output impedance dc amplifier with a bandwidth of 100 kHz. The amplifier gain was variable from 1 to 1000 in 1, 2, and 5 steps. The amplifier was used in conjunction with the oscilloscope to obtain the proper output for both data recording systems (digital and analog).

Two filters were used. The first was an active 5-pole Butterworth with a gain of 27 and the 3-dB point at 22.8 kHz. The rolloff was 13 dB/octave. The second filter was a passive 60-Hz parallel-T notch filter with an attenuation of 52 dB.

The total signal at this point was received by the buffer amplifier and the oscilloscope. The buffer amplifier had a gain of one-third and was used for the isolation of the density measurement system and the digital data recording system. The dc integrating digital voltmeter of the data recording system was set at 0.1 second. The integration technique produced a relatively smooth mean or dc component of the total signal without unduly affecting the response of the mean variations.

The oscilloscope was used in the ac coupled mode to remove the dc component of the total signal. The oscilloscope also provided gain to prepare the signal properly for the analog data recording system. A direct record channel with a response of 100 Hz to 100 kHz was used for the fluctuating component. The total signal was recorded on an FM channel (response 0 to 10 kHz) of the analog tape recorder. Root-mean-square voltmeters and the oscilloscope were used for monitoring the signal at the appropriate points.

Figure 17 gives the response curve for the entire electronic system. The curve was generated with discrete frequencies each of which was recorded on the analog tape recorder and then played back to obtain the higher frequency data (denoted by triangles). Since the tape-recorder response was limited below approximately 100 Hz, the remaining data (denoted by squares) were obtained from the output of a root-mean-square voltmeter.

Digital Data System

A digital data system (figs. 15 and 18) is used to accept and record data generated by the temperature, density, and electron-beam systems. Simultaneous measurements of these parameters were made by four active data channels. Each channel consists of the primary instrumentation, that is, photomultiplier tube, amplifiers, and ammeters, and the secondary instrumentation, analog-to-digital converters (digital voltmeters).

A measurement control circuit (fig. 18) insures the simultaneous start of data acquisition by the data system. The circuit issues a trigger pulse to each converter to initiate a measurement. The circuit awaits the "measurement complete" signal from each converter before a new trigger pulse is generated. Converters with different sample

APPENDIX

or measurement periods can be used and the number of samples or measurements made by the system can be controlled. Two samples per second were taken by the instruments for this experiment.

An instrument coupler receives each data channel and prepares the information for recording. The coupler arranges all data into the desired format for recording. The digit sequence and retention of digits can be controlled by a coupler patchboard. The acquired data are recorded on a magnetic tape which is processed by an appropriate computer program.

Temperature System Calibration

Calibration of the temperature measurement apparatus was accomplished by scanning the N₂ (0-0) vibrational band of the first negative system of nitrogen with a 0.5-m (19.69-in.) Ebert-Fastie type spectrometer. The spectrometer was placed in the position occupied by the density detection apparatus shown in figure 1 and with a beam splitter, simultaneous measurements were made with the dual-channel spectrometer. From the resolved spectrum, the rotational temperature could be determined from the relative rotational transition intensities. (See refs. 7, 13, and 32.) The ratios of output levels from the dual channel were plotted against the rotational temperature determined from the scanning spectrometer (fig. 19). By using the calibration temperature and dual-channel-ratio information, a sixth-order polynomial least-squares fit was made and this equation was used to reduce all tunnel data. The resultant equation was:

$$T = 7.7377 + (66.467)S_T + (64.864)S_T^2 + (-96.295)S_T^3 \\ + (58.065)S_T^4 + (-15.743)S_T^5 + (1.6168)S_T^6$$

where S_T is the measured channel spectral ratio and T is the temperature.

Density System Calibration

Because of the tunnel leakage, density calibrations were performed with air at ambient temperature (296 K (534° R)) by varying the static pressure in the tunnel box enclosing the nozzle and diffuser. (See fig. 1.) Static-pressure values were measured with an untrapped McLeod gage. An untrapped gage was used to eliminate the effects of condensables in the static tunnel environment on the pressure measurements. Effects of gage mercury backstreaming were neglected. Range of calibration pressures was approximately 0.1 to 10 torr (1 torr = 0.133 kN/m²). Partial pressure of nitrogen was calculated based on a standard atmosphere constituent of 78.1 percent of the total pressure. By using the partial pressure, the nitrogen number density was calculated by use of

APPENDIX

the ideal gas equation. Simultaneous with the pressure measurement, the measured photomultiplier output, which was proportional to the fluorescence intensity, normalized to the total beam current was recorded and shown in figure 20.

By using a method of least squares to fit the calibration data, measured normalized detector output, and nitrogen number density, the coefficients of equation (2) were determined. The resultant equation used to reduce the tunnel data was

$$N_R = \frac{(1.9 \times 10^{-19})N + (9.15 \times 10^{-38})N^2}{1 + (2.3 \times 10^{-17})N} \quad (4)$$

where the numerator coefficients are products KA and KB, respectively, of equation (2).

Electron-Beam Measurement Uncertainties

Measurements of the mean number density and rotational temperature, \bar{N} and \bar{T}_r , fluctuating density, N' , and power density spectra of the fluctuating density were made with the electron beam. Uncertainties associated with these measurements may be grouped under the broad categories of random and systematic.

Random uncertainties are due to the statistical variation of the measured quantity, subsequent noise-inducing detection process, and other extraneous noise sources such as electromagnetic interference from the tunnel resistive heater filament and its supply cables. Estimates of the random uncertainties of the mean number density and temperature were based on the measured standard deviation about the mean and were found to be ± 1 to 4 percent and ± 1 to 12 percent, respectively. The larger values are related to the measurements in the lower density flow regions. Standard deviation of the measured fluctuating density values was calculated to be less than ± 1 percent. This calculation and those subsequently performed were based on the information outlined in reference 36 for estimating the standard deviation of a quantity with assumed normal statistical distribution. The equation used was

$$\text{Error function} = \frac{1}{\sqrt{t\Delta f}}$$

where Δf is the analyzing system bandwidth and t , the integration time. For N' the bandwidth was approximately 50 kHz and integration time was 1 second. Similarly, the power spectra uncertainty based on a 50-Hz bandwidth and an integration time of 1 second was calculated. The power spectra uncertainty was calculated to be ± 18 percent.

Systematic uncertainties were more difficult to estimate. Major systematic uncertainties are associated with the basic beam techniques for measuring temperature and

APPENDIX

density. Temperature measurements have been found to be dependent on the gas density and the number of specific rotational quantum states used in the spectral analyses. (See refs. 9, 37, and 38.) A study of these dependencies and an empirical correction have been reported in reference 39. These data were used to correct the temperature measurements in this work. Corrections ranged from -19 percent for the lower temperatures to 0 percent for temperatures above approximately 250 K. No further corrections or estimates of systematic errors were made for the temperature measurements.

Systematic uncertainty enters the density measurements primarily through the calibration procedure. This uncertainty arises because the calibration is performed at ambient temperatures (≈ 296 K) whereas the test measurements are performed over a range of temperatures, ≈ 50 K to 365 K. The reason for the difference between measurements performed at ambient temperature and those performed at lower or higher temperatures is because the collision deexcitation rate of the excited states is temperature dependent. A preliminary study of this effect has been reported in reference 25. By using the data of reference 25 it is estimated that the maximum systematic error in the mean density measurements reported herein is -6 percent.

No estimate of systematic errors in the fluctuating density and power spectral density measurements was made. It was assumed that bias instrument errors may be neglected and that N' and power spectral density measurements have 0-percent systematic errors.

REFERENCES

1. Birch, Stanley F.; and Eggers, James M.: A Critical Review of the Experimental Data for Developed Free Turbulent Shear Layers. Free Turbulent Shear Flows. Vol. I – Conference Proceedings, NASA SP-321, 1972, pp. 11-40.
2. Bushnell, D. M.: Calculation of Turbulent Free Mixing Status and Problems. Free Turbulent Shear Flows. Vol. I – Conference Proceedings, NASA SP-321, 1972, pp. 1-10.
3. Mean Flow and Turbulence Measurements in a Mach 5 Shear Layer. ASME Applied Mechanics/Fluids Engineering Conference (Atlanta, Georgia), June 1973. Part I – Morrisette, E. Leon; and Birch, Stanley F.: The Development and Spreading of the Mean Flow. Part II – Wagner, Richard D.: Hot-Wire Measurements of the Mean Flow and Turbulence Intensities.
4. Harvey, William D.; and Bolton, Robert L.: Initial Development of a Hypersonic Free Mixing Layer. NASA TM X-2602, 1972.
5. Clark, Frank L.; Ellison, James C.; and Johnson, Charles B.: Recent Work in Flow Evaluation and Techniques of Operations for the Langley Hypersonic Nitrogen Facility. Vol. I of Fifth Hypervelocity Techniques Symposium, Univ. of Denver, Mar. 1967, pp. 347-373. (Available from DDC as AD 819 715.)
6. Beckwith, Ivan E.; Harvey, William D.; and Clark, Frank L. (With appendix A by Ivan E. Beckwith, William D. Harvey, and Christine M. Darden and appendix B by William D. Harvey, Lemuel E. Forrest, and Frank L. Clark): Comparisons of Turbulent-Boundary-Layer Measurements at Mach Number 19.5 With Theory and an Assessment of Probe Errors. NASA TN D-6192, 1971.
7. Harbour, P. J.: Absolute Determination of Flow Parameters in a Low Density Hypersonic Tunnel. Rarefied Gas Dynamics, Volume II, Leon Trilling and Harold Y. Wachman, eds., Academic Press, Inc., 1969, pp. 1713-1722.
8. Hoppe, John C.: Rotational and Vibrational Temperature Measurements in the 12-Inch Hypersonic Ceramic-Heated Tunnel. NASA TN D-4892, 1968.
9. Ashkenas, Harry: Rotational Temperature Measurements in Electron-Beam Excited Nitrogen. Physics Fluids, vol. 10, no. 12, Dec. 1967, pp. 2509-2520.
10. Muntz, E. P.: The Electron Beam Fluorescence Technique. AGARDograph 132, Dec. 1968.
11. Demetriades, Anthony; and Doughman, Ernest L.: Mean and Intermittent Flow of a Self-Preserving Plasma Jet. AIAA J., vol. 7, no. 4, Apr. 1969, pp. 713-722.

12. Petrie, Stuart L.: Flow Field Analyses in a Low Density Arc-Heated Wind Tunnel. Proceedings of the 1965 Heat Transfer and Fluid Mechanics Institute, Andrew F. Charwat, ed., Stanford Univ. Press, 1965, pp. 282-300.
13. Cunningham, James W.; Fisher, C. H.; and Price, L. L.: Density and Temperature in Wind Tunnels Using Electron Beams. IEEE Trans. Aerosp. & Electron. Systems, vol. AES-3, no. 2, Mar. 1967, pp. 269-284.
14. Wallace, J. E.: Hypersonic Turbulent Boundary Layer Measurements Using an Electron Beam. CAL Rep. No. AN-2112-Y-1 (Contract No. NSR 33-009-029), Cornell Aeronaut. Lab., Inc., Aug. 1968.
15. Lomax, Howard; and Inouye, Mamoru: Numerical Analysis of Flow Properties About Blunt Bodies Moving at Supersonic Speeds in an Equilibrium Gas. NASA TR R-204, 1964.
16. Yanta, William J.: A Hot-Wire Stagnation Temperature Probe. NOLTR 68-60, U.S. Navy, June 18, 1968.
17. Harvey, William D.; Forrest, Lemuel E.; and Clark, Frank L.: Measurements of Total Hemispherical Emittance for Chromel and for Alumel Wires. NASA TM X-2359, 1971.
18. Brinich, Paul F.; and Neumann, Harvey E.: Some Effects of Acceleration on the Turbulent Boundary Layer. AIAA J., vol. 8, no. 5, May 1970, pp. 987-989.
19. Dash, S.: An Analysis of Internal Supersonic Flows With Diffusion, Dissipation and Hydrogen-Air Combustion. ATL TR-152 (Contract NAS 1-9560), Advanced Technology Lab., Inc., May 1970. (Available as NASA CR-111783.)
20. Pitkin, Edward T.; and Glassman, Irvin: Experimental Mixing Profiles of a Mach 2.6 Free Jet. J. Aerosp. Sci., vol. 25, no. 12, Dec. 1958, pp. 791-793.
21. Warren, Walter R., Jr.: The Static Pressure Variation in Compressible Free Jets. J. Aeronaut. Sci., vol. 22, no. 3, Mar. 1955, pp. 205-207.
22. Fischer, M. C.; Maddalon, D. V.; Weinstein, L. M.; and Wagner, R. D., Jr.: Boundary-Layer Pitot and Hot-Wire Surveys at $M_\infty \approx 20$. AIAA J., vol. 9, no. 5, May 1971, pp. 826-834.
23. Fage, A.: On the Static Pressure in Fully-Developed Turbulent Flow. Proc. Roy. Soc. (London), ser. A: vol. 155, no. 886, July 1, 1936, pp. 576-596.
24. Sirieix, M.; and Solignac, J. L.: Contribution a l'Etude Experimentale de la Couche de Melange Turbulent Isobare d'un Eculement Supersonique. Separated Flows, Pt. I, AGARD CP No. 4, May 1966, pp. 241-270.

25. Lillicrap, D. C.: Collision Quenching Effects in Nitrogen and Helium Excited by a 30-keV Electron Beam. NASA TM X-2842, 1973.
26. Harvey, William D.; Cary, Aubrey M., Jr.; and Harris, Julius E.: Experimental and Numerical Investigation of Boundary-Layer Development and Transition on the Walls of a Mach 5 Nozzle. NASA TN D-7976, 1975.
27. Wagner, R. D.; Maddalon, D. V.; Weinstein, L. M.; and Henderson, A., Jr.: Influence of Measured Free-Stream Disturbances on Hypersonic Boundary-Layer Transition. Paper presented at the AIAA Second Fluid Plasma Dynamics Conference (San Francisco, Calif.), June 1969.
28. Stainback, P. C.; Fischer, M. C.; and Wagner, R. D.: Effects of Wind-Tunnel Disturbances on Hypersonic Boundary-Layer Transition. Pts. I and II. AIAA Paper No. 72-181, Jan. 1972.
29. Harvey, William D.; Bushnell, Dennis M.; and Beckwith, Ivan E.: Fluctuating Properties of Turbulent Boundary Layers for Mach Numbers up to 9. NASA TN D-5496, 1969.
30. Wagner, Richard D.: Mean Flow and Turbulence Measurements in a Mach 5 Free Shear Layer. NASA TN D-7366, 1973.
31. Muntz, E. P.: Measurement of Rotational Temperature, Vibrational Temperature, and Molecular Concentration in Non-Radiating Flows of Low Density Nitrogen. Report No. 71 (AFOSR TN 60-499), Inst. Aerophys., Univ. Toronto, Apr. 1961.
32. Hunter, William W., Jr.; and Leinhardt, T. E.: Temperature Dependence of the 3^1P Excitation Transfer Cross Section of Helium. J. Chem. Phys., vol. 58, no. 3, Feb. 1, 1973, pp. 941-947.
33. Hillard, Mervin E., Jr.; Ocheltree, Stewart L.; and Storey, Richard W.: Spectroscopic Analysis of Electron-Beam-Induced Fluorescence in Hypersonic Helium Flow. NASA TN D-6005, 1970.
34. Ocheltree, S. L.; and Storey, R. W.: Apparatus and Techniques for Electron Beam Fluorescence Probe Measurements. Rev. Sci. Instrum., vol. 4, no. 4, Apr. 1973, pp. 367-374.
35. Hookstra, Carl R., Jr.; Hoppe, John C.; and Hunter, William W., Jr.: Dual-Channel Spectrometer for Rotational-Temperature Measurements. NASA TM X-2135, 1970.
36. Piersol, Allan G.: The Measurement and Interpretation of Ordinary Power Spectra for Vibration Problems. NASA CR-90, 1964.

37. Hunter, William W., Jr.: Rotational Temperature Measurements 300° K to 1000° K With Electron Beam Probe. 21st Annual ISA Conference Proceedings, Vol. 21, Part II – Physical and Mechanical Measurement Instrumentation, Oct. 1966, pp. 1-16.
38. Hunter, William W., Jr.: Investigation of Temperature Measurements in 300° to 1100° K Low-Density Air Using an Electron Beam Probe. NASA TN D-4500, 1968.
39. Lillicrap, D. C.; and Lee, Louise P.: Rotational-Temperature Determination in Flowing Nitrogen Using an Electron Beam. NASA TN D-6576, 1971.

TABLE I. - NOMINAL TEST CONDITIONS

[Nozzle exit is at $x = 225$ cm (88.75 in.); $T_w \approx 300$ K (540° R)]

T _O		p _O		(p _{t,2}) _e /p _O	M _e	Reynolds number		p _B /p _O	p _w /p _O
K	°R	N/cm ²	lb/in ²			per meter	per foot		
x = 225 cm (88.75 in.)									
1640	2950	2710	3922	0.1434 × 10 ⁻³	18.85	1.82 × 10 ⁶	5.54 × 10 ⁵	2.03 × 10 ⁻⁷	4.0 × 10 ⁻⁷
1665	3000	3970	5750	.1271	19.34	2.41	7.34	1.50	3.7
1675	3010	4410	6400	.1317	19.20	2.58	8.16	1.40	3.8
1655	2980	5810	8410	.1221	19.50	3.12	9.51	1.00	3.8
x = 238 cm (93.75 in.)									
1640	2950	2480	3595	0.1484 × 10 ⁻³	18.74	1.67 × 10 ⁶	5.06 × 10 ⁵	1.80 × 10 ⁻⁷	2.95 × 10 ⁻⁷
1665	3000	3820	5540	.1300	19.25	2.32	7.07	1.71	1.72
1665	3000	4320	6266	.1324	19.18	2.63	8.00	1.45	1.48
1655	2980	5520	8000	.1167	19.68	3.00	9.14	1.40	1.65
x = 260 cm (102.25 in.)									
1665	3000	2590	3750	0.1468 × 10 ⁻³	18.78	1.74 × 10 ⁶	5.29 × 10 ⁵	1.30 × 10 ⁻⁷	3.9 × 10 ⁻⁷
1675	3010	5460	7910	.1144	19.76	2.93	8.94	1.50	3.7

TABLE II. - CORRECTED PITOT PRESSURE, STATIC PRESSURE, AND TOTAL TEMPERATURE

(a) $p_0 \approx 2710 \text{ N/cm}^2$ (3922 psia); $x = 225 \text{ cm}$ (88.75 in.)

y		$P_{t,2}/p_0$	p/p_0	T_t/T_0
cm	in.			
1.552	0.611	1.517×10^{-4}	-----	----
2.06	.811	1.491	-----	----
2.575	1.011	1.443	-----	1.00
3.040	1.211	1.458	-----	↓
3.59	1.411	1.450	-----	↓
4.09	1.611	1.461	-----	↓
4.60	1.811	1.414	-----	↓
5.11	2.011	1.439	2.85×10^{-7}	↓
5.62	2.211	1.414	2.78	↓
6.13	2.411	1.442	2.70	↓
6.64	2.611	1.388	2.68	↓
7.14	2.811	1.315	2.65	↓
7.65	3.011	1.265	2.60	↓
8.15	3.211	1.255	2.59	↓
8.66	3.411	1.1191	2.50	↓
9.16	3.611	1.1131	2.45	↓
9.67	3.811	1.066	2.35	↓
10.20	4.011	.9936	2.25	.998
10.70	4.211	.9792	2.20	.995
11.21	4.411	.9037	2.15	.988
11.72	4.611	.7286	2.10	.968
12.22	4.811	.6009	2.08	.950
12.73	5.011	.5749	2.07	.930
13.25	5.211	.4672	2.05	.915
13.76	5.411	.3936	2.00	.902
14.78	5.611	.3556	1.98	.860
14.80	5.811	.2999	1.98	.825
15.30	6.011	.2545	1.92	.805
15.80	6.211	.1900	1.99	.788
16.30	6.411	.1484	2.00	.775
16.80	6.611	.1010	1.99	.755
17.30	6.811	.05852	1.95	.715
17.82	7.011	.03003	1.90	.685
18.35	7.211	.02375	1.80	.660
18.85	7.411	.01853	1.72	.620
19.35	7.611	.01469	1.75	.600
19.87	7.811	.01207	1.78	.550
20.20	8.011	.01069	1.86	.490
20.85	8.211	.00946	1.95	.450
21.40	8.411	.00739	1.99	.380
21.90	8.611	.00593	1.99	.325
22.95	9.011	.00438	1.99	.280
23.97	9.411	.00390	1.89	.240
24.97	9.811	.00376	1.80	.225
25.45	10.011	-----	1.81	.220
26.45	10.411	-----	1.79	.210
27.50	10.811	-----	1.80	----
28.80	11.35	-----	2.00	----

(b) $p_0 \approx 3970 \text{ N/cm}^2$ (5750 psia); $x = 225 \text{ cm}$ (88.75 in.)

y		$P_{t,2}/p_0$	p/p_0	T_t/T_0
cm	in.			
1.552	0.611	1.467×10^{-4}	-----	----
2.32	.911	1.358	-----	----
2.95	1.161	1.357	-----	1.00
3.59	1.411	1.276	-----	↓
4.22	1.661	1.244	-----	↓
4.86	1.911	1.280	-----	↓
5.50	2.161	1.326	2.12×10^{-7}	↓
6.13	2.411	1.232	2.12	↓
6.76	2.661	1.192	2.12	↓
7.39	2.911	1.165	2.11	↓
8.04	3.161	1.120	2.11	↓
8.66	3.411	1.069	2.13	↓
9.30	3.661	1.067	2.18	↓
9.93	3.911	1.019	2.12	.999
10.58	4.161	.9625	2.08	.995
11.21	4.411	.8807	2.00	.985
11.83	4.661	.7814	1.85	.968
12.49	4.911	.6778	1.80	.942
13.10	5.161	.5657	1.72	.925
13.76	5.411	.4655	1.72	.908
14.40	5.661	.3785	1.65	.885
15.00	5.911	.2831	1.60	.845
15.65	6.161	.2357	1.55	.822
16.30	6.411	.1516	1.56	.785
16.91	6.661	.06809	1.45	.750
17.55	6.911	.03819	1.30	.715
18.20	7.161	.0199	1.15	.680
18.85	7.411	.0152	1.00	.648
19.49	7.661	.01143	1.05	.610
20.10	7.911	.008714	1.10	.522
20.75	8.161	.006094	1.22	.480
21.40	8.411	.003923	1.31	.395
21.90	8.611	.002826	1.37	.349
22.60	8.911	.002379	1.42	.300
23.30	9.161	.002157	1.45	.268
23.97	9.411	.002016	1.42	.235
24.58	9.661	.002006	1.40	.225
25.20	9.911	.001967	1.40	.220
25.80	10.161	.001906	1.39	.219
26.45	10.411	-----	-----	.220
27.00	11.611	-----	-----	.222
27.80	10.911	-----	1.41	----
28.50	11.211	-----	1.47	----

TABLE II. - CORRECTED PITOT PRESSURE, STATIC PRESSURE, AND TOTAL TEMPERATURE - Continued

(c) $p_o \approx 4410 \text{ N/cm}^2$ (6400 psia); $x = 225 \text{ cm}$ (88.75 in.)

y		$P_{t,2}/P_o$	p/p_o	T_t/T_o
cm	in.			
1.552	0.611	1.12×10^{-4}	-----	---
2.95	1.161	1.11	-----	1.00
4.22	1.661	1.31	-----	↓
5.50	2.161	1.32	1.92×10^{-7}	
6.64	2.611	1.35	2.08	
8.05	3.161	1.25	2.10	
8.15	3.211	1.15	2.03	
9.16	3.611	1.05	2.00	↓
9.94	3.911	.995	1.99	.999
10.70	4.211	.875	1.85	.995
11.21	4.411	.850	1.80	.980
11.72	4.611	.730	1.79	.968
12.73	5.011	.675	1.70	.942
13.60	5.351	.535	1.60	.910
14.78	5.611	.440	1.55	.865
14.80	5.811	.400	1.50	.840
15.80	6.211	.300	1.20	.805
16.30	6.411	.245	1.06	.780
16.80	6.611	.201	1.02	.750
17.30	6.811	.255	.99	.715
17.82	7.011	.105	.92	.690
18.35	7.211	.0755	.87	.660
18.85	7.411	.0495	.83	.625
19.35	7.611	.0375	.83	.620
19.87	7.811	.0310	.80	.570
20.20	8.011	.0215	.801	.495
20.85	8.211	.0165	.79	.460
21.40	8.411	.0225	1.01	.430
21.90	8.611	.0095	1.07	.355
22.40	8.811	.00755	1.13	.315
22.95	9.011	.00545	1.25	.260
23.40	9.211	.00405	1.24	.240
23.97	9.411	.00280	1.25	.215
24.97	9.811	.00218	1.22	.210
25.70	10.111	.00178	1.22	.200
26.00	10.211	.00165	1.22	.195
26.45	10.411	.00153	1.26	.194
27.50	10.75	-----	1.28	.190
27.70	10.90	-----	1.29	.189
29.35	11.55	-----	-----	.188

(d) $p_o \approx 5810 \text{ N/cm}^2$ (8410 psia); $x = 225 \text{ cm}$ (88.75 in.)

y		$P_{t,2}/P_o$	p/p_o	T_t/T_o
cm	in.			
1.552	0.611	0.9293×10^{-4}	-----	---
2.19	.861	-----	-----	---
2.82	1.111	.9163	-----	1.00
3.46	1.361	-----	-----	↓
4.09	1.611	.9834	-----	
4.72	1.861	-----	-----	
5.35	2.111	.9571	1.60×10^{-7}	
6.00	2.361	-----	-----	
6.64	2.611	1.120	1.60	
7.26	2.861	-----	-----	
7.90	3.111	1.237	1.73	
8.53	3.361	-----	-----	↓
9.16	3.611	1.183	1.85	
9.80	3.861	-----	-----	
10.44	4.111	1.110	1.82	.998
11.09	4.361	-----	-----	.985
11.42	4.611	.9177	1.72	.970
12.35	4.861	.8515	-----	.950
13.00	5.111	.7410	1.61	.925
13.61	5.361	.5980	-----	.910
14.25	5.611	.4888	1.40	.900
14.90	5.861	.3984	-----	.855
15.52	6.111	.3713	1.16	.830
16.16	6.361	.2800	1.04	.800
16.80	6.611	.3023	1.00	.770
17.42	6.861	.1998	.99	.722
18.08	7.111	.1258	.92	.700
18.70	7.361	.07101	.84	.672
19.34	7.611	.03150	.79	.650
20.00	7.861	.01490	.66	.575
20.60	8.111	.009967	.61	.495
21.22	8.361	.007040	.54	.435
21.85	8.611	.004290	.55	.360
22.50	8.861	-----	.56	.315
23.17	9.111	.001979	.58	.285
23.80	9.361	-----	.59	.255
24.40	9.611	.001338	.60	---
25.02	9.861	-----	.62	---
25.70	10.111	.001202	-----	.240
26.30	10.361	-----	-----	---
26.80	10.55	-----	.655	.235
28.70	11.30	-----	.700	---
29.35	11.55	-----	.725	---

TABLE II.- CORRECTED PITOT PRESSURE, STATIC PRESSURE, AND TOTAL TEMPERATURE - Continued

(e) $p_o \approx 2480 \text{ N/cm}^2$ (3595 psia); $x = 238 \text{ cm}$ (93.75 in.)

y		Pt,2/p _o	p/p _o	T _t /T _o
cm	in.			
1.552	0.611	1.612×10^{-4}	-----	-----
2.19	.861	1.557	-----	-----
2.82	1.111	1.534	-----	1.00
3.46	1.361	1.532	-----	↓
4.09	1.611	1.558	-----	
4.72	1.861	1.501	-----	
5.35	2.111	1.485	2.91×10^{-7}	
6.00	2.361	1.476	2.85	
6.64	2.611	1.395	2.80	
7.26	2.861	1.342	2.70	↓
7.90	3.111	1.301	2.65	1.05
8.53	3.361	1.280	2.50	1.01
9.16	3.611	1.237	2.30	1.00
9.80	3.861	1.200	2.10	1.00
10.44	4.111	1.110	2.00	.991
11.09	4.361	1.087	1.99	.975
11.42	4.611	.8528	1.90	.960
12.35	4.861	.7085	1.85	.935
13.00	5.111	.5926	1.72	.905
13.61	5.361	.4628	1.65	.875
14.25	5.611	.3483	1.60	.847
14.90	5.861	.2496	1.55	.826
15.52	6.111	.1556	1.50	.806
16.16	6.361	.09667	1.51	.772
16.80	6.611	.07289	1.55	.728
17.42	6.861	.05653	1.83	.675
18.08	7.111	.05634	1.75	.633
18.70	7.361	.02551	1.76	.600
19.34	7.611	.01671	1.75	.578
20.00	7.861	.01229	1.74	.505
20.60	8.111	.01178	1.72	.470
21.22	8.361	.007538	1.70	.409
21.85	8.611	.005606	1.70	.343
22.50	8.861	.004745	1.81	.290
23.17	9.111	.003721	1.72	.260
23.80	9.361	.003436	1.85	.241
24.40	9.611	.004384	1.75	.222
25.02	9.861	.002670	1.82	.215
25.70	10.111	.002736	1.83	.211
26.30	10.361	.002660	1.55	.210
27.00	10.611	-----	1.75	.208
27.60	10.861	-----	1.65	.205
28.22	11.111	-----	1.72	---
28.80	11.361	-----	1.69	---
29.50	11.611	-----	1.72	---
30.10	11.861	-----	1.73	---

(f) $p_o \approx 3820 \text{ N/cm}^2$ (5540 psia); $x = 238 \text{ cm}$ (93.75 in.)

y		Pt,2/p _o	p/p _o	T _t /T _o
cm	in.			
1.552	0.611	1.341×10^{-7}	-----	-----
2.19	.861	1.351	-----	-----
2.82	1.111	1.352	-----	1.00
3.46	1.361	1.364	-----	↓
4.09	1.611	1.314	-----	
4.72	1.861	1.255	-----	
5.35	2.111	1.281	2.55×10^{-7}	
6.00	2.361	1.315	2.55	
6.64	2.611	1.301	2.53	
7.26	2.861	1.223	2.50	
7.90	3.111	1.203	2.40	
8.53	3.361	1.163	2.36	
9.16	3.611	1.117	2.28	
9.80	3.861	1.043	2.10	↓
10.44	4.111	.9793	2.00	.996
11.09	4.361	.8937	1.99	.987
11.42	4.611	.8527	1.85	.965
12.35	4.861	.7457	1.76	.949
13.00	5.111	.5599	1.66	.925
13.61	5.361	.4672	1.58	.911
14.25	5.611	.4388	1.52	.883
14.90	5.861	.3667	1.32	.857
15.52	6.111	.2634	1.11	.825
16.16	6.361	.1498	.958	.801
16.80	6.611	.1078	.860	.772
17.42	6.861	.0703	.760	.712
18.08	7.111	.04968	.845	.683
18.70	7.361	.03703	.940	.665
19.34	7.611	.03299	1.12	.586
20.00	7.861	.01866	1.18	.525
20.60	8.111	.01484	1.22	.475
21.22	8.361	.01043	1.36	.425
21.85	8.611	.006868	1.40	.377
22.50	8.861	.004581	1.47	.330
23.17	9.111	.003099	1.49	.272
23.80	9.361	-----	1.50	.255
24.40	9.611	-----	1.51	.243
25.02	9.861	-----	1.52	---
25.70	10.111	-----	1.51	---
26.30	10.361	-----	1.52	---
27.00	10.611	-----	1.52	---

TABLE II. - CORRECTED PITOT PRESSURE, STATIC PRESSURE, AND TOTAL TEMPERATURE - Continued

(g) $p_0 \approx 4320 \text{ N/cm}^2$ (6266 psia); $x = 238 \text{ cm}$ (93.75 in.)					(h) $p_0 \approx 5520 \text{ N/cm}^2$ (8000 psia); $x = 238 \text{ cm}$ (93.75 in.)				
y		$P_{t,2}/p_0$	p/p_0	T_t/T_0	y		$P_{t,2}/p_0$	p/p_0	T_t/T_0
cm	in.				cm	in.			
1.552	0.611	1.16×10^{-4}	-----	----	1.552	0.611	0.9433×10^{-4}	-----	----
2.06	.811	1.17	-----	----	2.19	.861	.90366	-----	----
2.575	1.011	1.18	-----	1.00	2.82	1.111	.90189	-----	1.00
3.43	1.35	1.175	-----	↓	3.46	1.361	.88678	-----	↓
4.19	1.65	1.25	-----	↓	4.09	1.611	.8855	-----	↓
4.95	1.95	1.25	-----	↓	4.72	1.861	.92173	-----	↓
5.48	2.15	1.175	2.53×10^{-7}	↓	5.35	2.111	.9204	2.41×10^{-7}	↓
5.96	2.35	1.170	2.57	↓	6.00	2.361	.9497	2.40	↓
6.35	2.50	1.210	2.54	↓	6.64	2.611	.9930	2.41	↓
6.86	2.70	1.210	2.49	↓	7.26	2.861	1.06049	2.39	↓
7.36	2.90	1.260	2.40	↓	7.90	3.111	1.1279	2.35	↓
8.00	3.15	1.350	2.22	↓	8.53	3.361	1.1672	2.30	↓
8.50	3.35	1.375	2.20	↓	9.16	3.611	1.1723	2.25	↓
8.76	3.45	1.370	2.19	↓	9.80	3.861	1.1783	2.15	↓
9.40	3.70	1.336	2.15	↓	10.44	4.111	1.1445	2.00	.993
9.90	3.90	1.310	2.10	↓	11.09	4.361	1.0961	1.99	.982
10.41	4.10	1.150	2.00	.993	11.42	4.611	1.0008	1.85	.964
10.91	4.30	1.110	1.99	.982	12.35	4.861	.92367	1.76	.950
12.08	4.75	.965	1.78	.962	13.00	5.111	.75866	1.67	.931
12.45	4.90	.865	1.75	.942	13.61	5.361	.65054	1.60	.900
12.97	5.10	.780	1.67	.925	14.25	5.611	.50047	1.58	.865
13.48	5.30	.695	1.58	.912	14.90	5.861	.40533	1.47	.850
13.99	5.50	.600	1.52	.895	15.52	6.111	.31291	1.18	.835
14.61	5.75	.530	1.49	.870	16.16	6.361	.23372	.91	.802
15.11	5.95	.450	1.37	.855	16.80	6.611	.16642	.81	.762
15.89	6.25	.355	1.04	.790	17.42	6.861	.10957	.70	.716
17.15	6.75	.219	.820	.730	18.08	7.111	.07233	.63	.655
17.51	6.90	.165	.755	.715	18.70	7.361	.04809	.65	.632
18.06	7.10	.116	.760	.685	19.34	7.611	.03675	.73	.609
18.55	7.30	.0570	.862	.649	20.00	7.861	.02876	.98	.555
19.20	7.55	.0519	.925	.605	20.60	8.111	.01599	1.08	.491
19.58	7.70	.0319	1.01	.578	21.72	8.361	.011888	1.11	.425
20.05	7.90	.0240	1.12	.525	21.85	8.611	.008344	1.15	.386
20.60	8.10	.0191	1.22	.475	22.50	8.861	.005366	1.19	.341
21.06	8.30	.0145	1.28	.426	23.17	9.111	.003621	1.28	.285
21.75	8.55	.01120	1.32	.377	23.80	9.361	-----	1.36	.255
22.10	8.70	.00810	1.35	.309	24.40	9.611	-----	1.47	.246
22.60	8.90	.00570	1.37	.290	25.02	9.899	.001630	1.45	----
23.10	9.10	.00418	1.39	.268	25.70	10.111	-----	1.45	----
24.62	9.70	.00252	1.48	.215	26.30	10.361	-----	1.46	.217
25.50	10.05	.00193	1.52	.203	26.80	10.55	-----	1.47	----
26.65	10.50	.00159	1.52	.200	28.80	11.36	-----	1.42	----
27.20	10.70	-----	-----	.199					

TABLE II.- CORRECTED PITOT PRESSURE, STATIC PRESSURE, AND TOTAL TEMPERATURE - Concluded

(i) $p_o \approx 2590 \text{ N/cm}^2$ (3750 psia); $x = 260 \text{ cm}$ (102.25 in.)

y		$P_{t,2}/p_o$	p/p_o	T_t/T_o
cm	in.			
1.552	0.611	1.4493×10^{-4}	-----	----
2.19	.861	1.4386	-----	----
2.82	1.111	1.4307	-----	1.00
3.46	1.361	1.4528	-----	↓
4.09	1.611	1.4819	-----	
4.72	1.861	1.5052	-----	
5.35	2.111	1.4778	2.95×10^{-7}	
6.00	2.361	1.4926	2.94	↓
6.64	2.611	1.5107	2.92	
7.26	2.861	1.4661	2.95	
7.90	3.111	1.41161	2.93	
8.53	3.361	1.3537	2.88	
9.16	3.611	1.2787	2.83	
9.80	3.861	1.1924	2.75	
10.44	4.111	1.14988	2.72	
11.09	4.361	.99364	2.68	
11.42	4.611	.89153	2.58	
12.35	4.861	.77212	2.51	.955
13.00	5.111	.66885	2.42	.921
13.61	5.361	.56421	2.36	.895
14.25	5.611	.44963	2.22	.866
14.90	5.861	.37109	2.20	.829
15.52	6.111	.24518	2.15	.799
16.16	6.361	.17986	2.02	.768
16.80	6.611	.099059	1.75	.745
17.42	6.861	.04999	1.35	.696
18.08	7.111	.023307	.955	.638
18.70	7.361	.012677	.875	.601
19.34	7.611	.010491	1.05	.569
20.00	7.861	.009413	1.10	.540
20.60	8.111	.008829	1.34	.479
21.72	8.361	.008448	1.32	.421
21.85	8.611	.008081	1.41	.376
22.50	8.861	.007916	1.63	.330
23.17	9.111	.007754	1.60	.280
23.80	9.361	.007787	1.55	.245
24.40	9.611	.007746	1.52	.211
25.02	9.861	.007624	1.51	.205
25.70	10.111	.007559	1.48	.202
26.30	10.361	.007488	1.42	.201
27.00	10.611	-----	1.39	.200
27.60	10.861	-----	1.41	.199
28.22	11.111	-----	1.40	----
28.80	11.361	-----	1.35	----
29.50	11.611	-----	1.35	----

(j) $p_o \approx 5460 \text{ N/cm}^2$ (7910 psia); $x = 260 \text{ cm}$ (102.25 in.)

y		$P_{t,2}/p_o$	p/p_o	T_t/T_o
cm	in.			
1.552	0.611	0.9433×10^{-4}	-----	----
2.19	.861	.90366	-----	----
2.82	1.111	.90189	-----	1.00
3.46	1.361	.88677	-----	↓
4.09	1.611	.8855	-----	
4.72	1.861	.9217	-----	
5.35	2.111	.9204	2.42×10^{-7}	
6.00	2.361	.9497	2.45	↓
6.64	2.611	.9930	2.44	
7.26	2.861	1.0605	2.45	
7.90	3.111	1.12788	2.52	
8.53	3.361	1.1672	2.66	
9.16	3.611	1.1723	2.82	
9.80	3.861	1.1782	2.95	
10.44	4.111	1.1445	2.90	
11.09	4.361	1.0961	2.86	
11.42	4.611	1.0008	2.73	
12.35	4.861	.9237	2.68	1.00
13.00	5.111	.7587	2.55	.981
13.61	5.361	.6505	2.37	.940
14.25	5.611	.5005	2.22	.920
14.90	5.861	.4053	2.05	.885
15.52	6.111	.3129	1.88	.840
16.16	6.361	.2337	1.81	.800
16.80	6.611	.1664	1.42	.765
17.42	6.861	.1096	1.18	.732
18.08	7.111	.0723	.92	.691
18.70	7.361	.0481	.72	.651
19.34	7.611	.03675	.61	.622
20.00	7.861	.02876	.70	.579
20.60	8.111	.01599	1.09	.530
21.72	8.361	.01888	1.12	.452
21.85	8.611	.00834	1.15	.400
22.50	8.861	.00537	1.21	.348
23.17	9.111	.00362	1.28	.303
23.80	9.361	-----	1.35	.262
24.40	9.611	-----	1.41	.245
25.10	9.899	.00163	1.45	----
25.70	10.111	-----	1.48	----
26.30	10.361	-----	1.47	.215
27.00	10.611	-----	1.49	----
28.80	11.361	-----	1.44	----

TABLE III. - CALCULATED SHEAR-LAYER PROFILES FROM MEAN PROBE MEASUREMENTS

(a) $p_o \approx 2710 \text{ N/cm}^2$ (3922 psia);
 $x = 225 \text{ cm}$ (88.75 in.)

y		M/M _e	u/u _e
cm	in.		
1.552	0.611	0.991	1.00
2.06	.811	.992	
2.575	1.011	1.000	
3.040	1.211	.997	
4.09	1.611	1.000	
4.60	1.811	.995	
5.11	2.011	1.000	
5.62	2.211	1.000	
6.13	2.411	.999	
6.64	2.611	.982	
7.14	2.811	.953	
7.65	3.011	.937	
8.15	3.211	.930	
8.66	3.411	.910	
9.16	3.611	.886	
9.67	3.811	.858	
10.20	4.011	.830	.998
10.70	4.211	.822	.990
11.21	4.411	.793	.988
11.72	4.611	.712	.972
12.22	4.811	.642	.943
12.73	5.011	.629	.933
13.25	5.211	.567	.920
13.76	5.411	.522	.905
14.78	5.611	.495	.887
14.80	5.811	.454	.873
15.30	6.011	.422	.842
15.80	6.211	.372	.835
16.30	6.411	.316	.826
16.80	6.611	.235	.809
17.30	6.811	.197	.765
17.82	7.011	.139	.669
18.35	7.211	.121	.640
18.85	7.411	.105	.615
19.35	7.611	.095	.555
19.87	7.811	.085	.493
20.20	8.011	.078	.435
20.85	8.211	.071	.405
21.40	8.411	.061	.310
21.90	8.611	.055	.238
22.95	9.011	.036	.185
23.97	9.411	.029	.115
24.97	9.811	.024	.072
25.70	10.11	----	.055

(b) $p_o \approx 3970 \text{ N/cm}^2$ (5750 psia);
 $x = 225 \text{ cm}$ (88.75 in.)

y		M/M _e	u/u _e
cm	in.		
1.552	0.611	0.981	1.00
2.06	.811	.987	
2.95	1.161	.989	
3.59	1.411	.999	
4.22	1.661	1.000	
4.86	1.911	.999	
5.50	2.161	.996	
6.13	2.411	.956	
6.76	2.661	.941	
7.39	2.911	.931	
8.04	3.161	.914	
8.66	3.411	.893	
9.30	3.661	.889	
9.93	3.911	.871	
10.58	4.161	.845	.991
11.21	4.411	.809	.986
11.83	4.661	.762	.975
12.49	4.911	.710	.960
13.10	5.161	.650	.950
13.76	5.411	.589	.930
14.40	5.661	.531	.910
15.00	5.911	.457	.899
15.65	6.161	.416	.872
16.30	6.411	.335	.851
16.91	6.661	.221	.833
17.55	6.911	.165	.790
18.20	7.161	.119	.722
18.85	7.411	.101	.660
19.49	7.661	.086	.598
20.10	7.911	.073	.535
20.75	8.161	.059	.447
21.40	8.411	.035	.362
22.60	8.911	.021	.235
23.30	9.161	.019	.170
23.97	9.411	.016	.120
24.58	9.661	.012	----
25.20	9.911	.010	.070
25.80	10.161	.010	.055

TABLE III. - CALCULATED SHEAR-LAYER PROFILES FROM MEAN PROBE MEASUREMENTS - Continued

(c) $p_0 \approx 4410 \text{ N/cm}^2$ (6400 psia);
 $x = 225 \text{ cm}$ (88.75 in.)

y		M/M _e	u/u _e
cm	in.		
1.552	0.611	1.30	1.00
2.95	1.161	1.30	↓
4.22	1.661	1.00	
5.50	2.161	1.00	
6.76	2.611	1.00	
7.51	2.961	1.00	
8.15	3.211	1.00	
8.53	3.361	.988	
9.16	3.611	.958	
9.55	3.761	.936	
10.05	3.961	.905	
10.70	4.211	.879	.993
11.21	4.411	.840	.987
11.83	4.611	.819	.975
12.10	4.761	.775	.965
12.60	4.961	.738	.960
13.10	5.161	.709	.949
13.61	5.361	.661	.923
14.25	5.611	.630	.910
14.90	5.861	.570	.900
15.65	6.161	.522	.886
16.16	6.361	.459	.862
16.91	6.661	.418	.845
17.18	6.761	.372	.820
17.70	6.961	.318	.805
18.35	7.211	.262	.740
18.70	7.361	.208	.700
19.35	7.611	.182	.659
19.70	7.761	.155	.610
20.20	8.011	.125	.540
20.85	8.211	.118	.470
21.40	8.411	.101	.400
21.90	8.611	.085	.342
22.25	8.76	.069	.280
22.95	9.011	.059	.229
23.40	9.211	.048	.181
23.97	9.411	.030	.130
24.58	9.661	.120	----

(d) $p_0 \approx 5810 \text{ N/cm}^2$ (8410 psia);
 $x = 225 \text{ cm}$ (88.75 in.)

y		M/M _e	u/u _e
cm	in.		
1.552	0.611	1.052	1.00
2.19	.861	----	↓
2.82	1.111	1.059	
3.46	1.361	----	
4.09	1.611	1.045	
4.72	1.861	----	
5.35	2.111	1.049	
6.00	2.361	----	
6.64	2.611	1.018	
7.26	2.861	----	
7.90	3.111	.999	
8.53	3.361	----	↓
9.16	3.611	.976	
9.80	3.861	----	
10.44	4.111	.945	
11.09	4.361	----	
11.42	4.611	.859	
12.35	4.861	.826	
13.00	5.111	.770	
13.61	5.361	.692	
14.25	5.611	.625	
14.90	5.861	.565	.899
15.52	6.111	.545	.885
16.16	6.361	.473	.866
16.80	6.611	.440	.834
17.42	6.861	.399	.800
18.08	7.111	.319	.759
18.70	7.361	.238	.722
19.34	7.611	.155	.659
20.00	7.861	.105	.604
20.60	8.111	.085	.511
21.22	8.361	.066	.430
21.85	8.611	.047	.341
22.50	8.861	----	.285
23.17	9.111	.031	.195
23.80	9.361	----	.142
24.40	9.611	.009	.101
25.02	9.861	----	.072
25.70	10.111	.008	.055

TABLE III. - CALCULATED SHEAR-LAYER PROFILES FROM MEAN PROBE MEASUREMENTS - Continued

(e) $p_0 \approx 2480 \text{ N/cm}^2$ (3595 psia);
 $x = 238 \text{ cm}$ (93.75 in.)

y		M/M _e	u/u _e
cm	in.		
1.552	0.611	0.985	1.00
2.19	.861	.989	
2.82	1.111	.995	
3.46	1.361	.996	
4.09	1.611	.991	
4.72	1.861	.989	
5.35	2.111	.992	
6.00	2.361	.988	
6.64	2.611	.972	
7.26	2.861	.952	
7.90	3.111	.938	
8.53	3.361	.927	↓
9.16	3.611	.910	.999
9.80	3.861	.890	.992
10.44	4.111	.861	.990
11.09	4.361	.822	.987
11.42	4.611	.787	.975
12.35	4.861	.737	.967
13.00	5.111	.690	.949
13.61	5.361	.631	.925
14.25	5.611	.666	.905
14.90	5.861	.485	.880
15.52	6.111	.407	.851
16.16	6.361	.321	.816
16.80	6.611	.257	.775
17.42	6.861	.242	.737
18.08	7.111	.192	.686
18.70	7.361	.181	.652
19.34	7.611	.125	.594
20.00	7.861	.103	.530
20.60	8.111	.084	.460
21.22	8.361	.083	.372
21.85	8.611	.061	.289
22.50	8.861	.050	.160
23.17	9.111	.048	.128
23.80	9.361	.025	.102
24.40	9.611	.019	.054
25.02	9.861	.011	.038
25.70	10.111	.010	.025
26.30	10.361	.009	.019

(f) $p_0 \approx 3820 \text{ N/cm}^2$ (5540 psia);
 $x = 238 \text{ cm}$ (93.75 in.)

y		M/M _e	u/u _e
cm	in.		
1.552	0.611	0.996	1.00
2.19	.861	.999	
2.82	1.111	.995	
3.46	1.361	.990	
4.09	1.611	.999	
4.72	1.861	1.000	
5.35	2.111	1.010	
6.00	2.361	.998	
6.64	2.611	.990	
7.26	2.861	.962	
7.90	3.111	.957	
8.53	3.361	.939	↓
9.16	3.611	.917	.999
9.80	3.861	.890	.995
10.44	4.111	.860	.990
11.09	4.361	.825	.986
11.42	4.611	.805	.975
12.35	4.861	.751	.966
13.00	5.111	.650	.949
13.61	5.361	.595	.920
14.25	5.611	.563	.905
14.90	5.861	.527	.890
15.52	6.111	.445	.870
16.16	6.361	.335	.851
16.80	6.611	.286	.826
17.42	6.861	.228	.790
18.08	7.111	.191	.756
18.70	7.361	.168	.695
19.34	7.611	.151	.644
20.00	7.861	.116	.569
20.60	8.111	.100	.490
21.22	8.361	.090	.400
21.85	8.611	.063	.331
22.50	8.861	.049	.202
23.17	9.111	.021	.127

TABLE III. - CALCULATED SHEAR-LAYER PROFILES FROM MEAN PROBE MEASUREMENTS - Continued

(g) $p_0 \approx 4320 \text{ N/cm}^2$ (6266 psia);
 $x = 238 \text{ cm}$ (93.75 in.)

(h) $p_0 \approx 5520 \text{ N/cm}^2$ (8000 psia);
 $x = 238 \text{ cm}$ (93.75 in.)

y		M/M_e	u/u_e	y		M/M_e	u/u_e
cm	in.			cm	in.		
1.552	0.611	1.022	1.00	1.552	0.611	1.040	1.00
2.06	.811	1.025		2.19	.861	1.050	
2.575	1.011	1.026		2.82	1.111	1.051	
3.43	1.35	1.024		3.46	1.361	1.060	
4.19	1.65	1.020		4.09	1.611	1.060	
4.95	1.95	1.021		4.72	1.861	1.050	
5.46	2.15	1.028		5.35	2.111	1.050	
5.96	2.35	1.025		6.00	2.361	1.040	
6.35	2.50	1.025		6.64	2.611	1.030	
6.86	2.70	1.019		7.26	2.861	1.019	
7.36	2.90	1.015		7.90	3.111	1.003	
8.00	3.15	1.001		8.53	3.361	1.001	
8.50	3.35	1.005		9.16	3.611	1.000	
8.76	3.45	1.007		9.80	3.861	1.001	
9.40	3.70	1.010	↓	10.44	4.111	.993	.999
9.90	3.90	.990	.998	11.09	4.361	.970	.998
10.41	4.10	.958	.995	11.42	4.611	.927	.991
10.91	4.30	.930	.990	12.35	4.861	.890	.980
12.08	4.75	.875	.975	13.00	5.111	.806	.965
12.45	4.90	.842	.966	13.61	5.361	.744	.950
12.97	5.10	.795	.952	14.25	5.611	.655	.931
13.48	5.30	.741	.949	14.90	5.861	.589	.991
13.99	5.50	.687	.936	15.52	6.111	.517	.884
14.61	5.75	.636	.920	16.16	6.361	.445	.868
15.11	5.95	.589	.907	16.80	6.611	.372	.841
15.89	6.25	.511	.886	17.42	6.861	.304	.800
17.15	6.75	.400	.822	18.08	7.111	.247	.775
17.51	6.90	.355	.798	18.70	7.361	.205	.745
18.06	7.10	.290	.755	19.34	7.611	.175	.668
18.55	7.30	.217	.722	20.00	7.861	.156	.601
19.20	7.55	.175	.660	20.60	8.111	.115	.520
19.58	7.70	.155	.605	21.22	8.361	.099	.425
20.05	7.90	.135	.538	21.85	8.611	.075	.315
20.60	8.10	.115	.487	22.50	8.861	.060	.225
21.06	8.30	.099	.409	23.17	9.111	.047	.163
21.75	8.55	.085	.339	23.80	9.361	.031	.121
22.10	8.70	.070	.273	24.40	9.611	.025	.089
22.60	8.90	.061	.222	25.02	10.111	.015	.050
23.10	9.10	.046	.127	26.30	10.361	.015	.035

TABLE III - CALCULATED SHEAR-LAYER PROFILES FROM MEAN PROBE MEASUREMENTS - Concluded

(i) $p_o \approx 2590 \text{ N/cm}^2$ (3750 psia);
 $x = 260 \text{ cm}$ (102.25 in.)

y		M/M _e	u/u _e
cm	in.		
1.552	0.611	1.001	1.00
2.19	.861	1.002	
2.18	1.111	1.002	
3.46	1.361	1.000	
4.09	1.611	.999	
4.72	1.861	.997	
5.35	2.111	1.001	
6.00	2.361	1.000	
6.64	2.611	.998	
7.26	2.861	.980	
7.90	3.111	.960	
8.53	3.361	.942	
9.16	3.611	.915	
9.80	3.861	.881	↓
10.44	4.111	.862	.999
11.09	4.361	.809	.995
11.42	4.611	.763	.980
12.35	4.861	.711	.967
13.00	5.111	.662	.946
13.61	5.361	.607	.925
14.25	5.611	.542	.905
14.90	5.861	.491	.887
15.52	6.111	.400	.852
16.16	6.361	.343	.828
16.80	6.611	.256	.777
17.42	6.861	.179	.749
18.08	7.111	.118	.701
18.70	7.361	.085	.655
19.34	7.611	.069	.610
20.00	7.861	.060	.530
20.60	8.111	.049	.465
21.22	8.361	.039	.385
21.85	8.611	.031	.309
22.50	8.861	.026	.261
23.17	9.111	.020	.175
23.80	9.361	.016	.122
24.40	9.611	.012	.079
25.02	9.861	.011	.063
25.70	10.111	.007	.042
26.30	10.361	.006	.022

(j) $p_o \approx 5460 \text{ N/cm}^2$ (7910 psia);
 $x = 260 \text{ cm}$ (102.25 in.)

y		M/M _e	u/u _e
cm	in.		
1.552	0.611	1.035	1.00
2.19	.861	1.040	
2.18	1.111	1.050	
3.46	1.361	1.050	
4.09	1.611	1.049	
4.72	1.861	1.037	
5.35	2.111	1.045	
6.00	2.361	1.038	
6.64	2.611	1.030	
7.26	2.861	1.012	
7.90	3.111	1.000	
8.53	3.361	.996	
9.16	3.611	.999	
9.80	3.861	1.001	
10.44	4.111	.986	
11.09	4.361	.965	
11.42	4.611	.925	↓
12.35	4.861	.885	.999
13.00	5.111	.806	.998
13.61	5.361	.744	.997
14.25	5.611	.652	.982
14.90	5.861	.584	.957
15.52	6.111	.515	.929
16.16	6.361	.445	.911
16.80	6.611	.373	.873
17.42	6.861	.305	.837
18.08	7.111	.247	.792
18.70	7.361	.200	.748
19.34	7.611	.175	.701
20.00	7.861	.149	.654
20.60	8.111	.115	.566
21.22	8.361	.095	.471
21.85	8.611	.077	.373
22.50	8.861	.059	.282
23.17	9.111	.055	.197
23.80	9.361	----	----
24.40	9.611	----	----
25.02	9.861	.038	.094
26.30	10.361	----	.046
27.60	10.861	----	.021

TABLE IV. - ELECTRON-BEAM MEASUREMENTS OF MEAN AND FLUCTUATING DENSITY AND MEAN TEMPERATURE AT $x = 238$ cm (93.75 in.)

(a) $p_0 = 2435$ N/cm ² (3522 psia)					
y		ρ/ρ_0	T/T_0	p/p_0 (calc.)	$\sqrt{\rho'^2/\bar{\rho}}$
cm	in.				
0	0	18.05×10^{-6}	-----	-----	2.75×10^{-2}
2.54	1.0	18.05	-----	-----	2.68
5.08	2.0	18.02	-----	-----	2.91
6.35	2.5	17.25	-----	-----	3.20
7.62	3.0	16.90	-----	-----	4.00
8.90	3.5	15.85	1.6×10^{-2}	-----	5.01
10.16	4.0	13.88	-----	-----	6.50
11.42	4.5	10.95	2.89	3.18×10^{-7}	8.30
12.70	5.0	8.65	3.66	3.16	10.01
13.98	5.5	5.72	5.88	3.34	12.45
15.25	6.0	4.38	7.33	3.25	-----
15.90	6.25	3.95	8.82	3.55	-----
16.51	6.50	2.86	10.1	3.03	16.12
17.15	6.75	1.19	12.2	1.47	-----
17.80	7.0	.912	14.7	1.37	13.75
18.41	7.25	.748	16.9	1.32	-----
19.05	7.5	.715	18.1	1.32	13.50
19.70	7.75	.674	18.9	1.30	-----
20.35	8.0	.631	20.6	1.33	-----
20.99	8.25	.612	20.2	1.27	-----
21.60	8.5	.601	19.9	1.17	-----

(b) $p_0 = 5460$ N/cm ² (7910 psia)					
y		ρ/ρ_0	T/T_0	p/p_0 (calc.)	$\sqrt{\rho'^2/\bar{\rho}}$
cm	in.				
0	0	14.45×10^{-6}	-----	-----	2.65×10^{-2}
2.54	1.0	14.95	-----	-----	2.61
5.08	2.0	15.20	-----	-----	2.75
6.35	2.5	15.25	-----	-----	2.89
7.62	3.0	14.85	-----	-----	3.50
8.90	3.5	13.75	1.45×10^{-2}	-----	4.25
10.16	4.0	11.78	-----	-----	4.73
11.42	4.5	9.29	2.50	2.32×10^{-7}	5.20
12.70	5.0	7.89	3.08	2.45	6.05
13.98	5.5	6.05	4.05	2.45	7.00
15.25	6.0	4.51	5.71	2.57	8.39
16.51	6.5	2.91	6.75	1.96	10.26
17.80	7.0	1.58	8.42	1.33	10.88
18.41	7.25	1.10	11.32	1.24	-----
19.05	7.50	.786	14.81	1.15	6.22
19.70	7.75	.642	18.01	1.13	-----
20.35	8.0	.571	20.75	1.16	3.09
20.99	8.25	.514	22.35	1.12	-----
21.60	8.50	.515	21.42	1.07	2.85
22.20	8.75	.511	19.25	.986	-----
22.85	9.0	.499	18.55	.899	-----

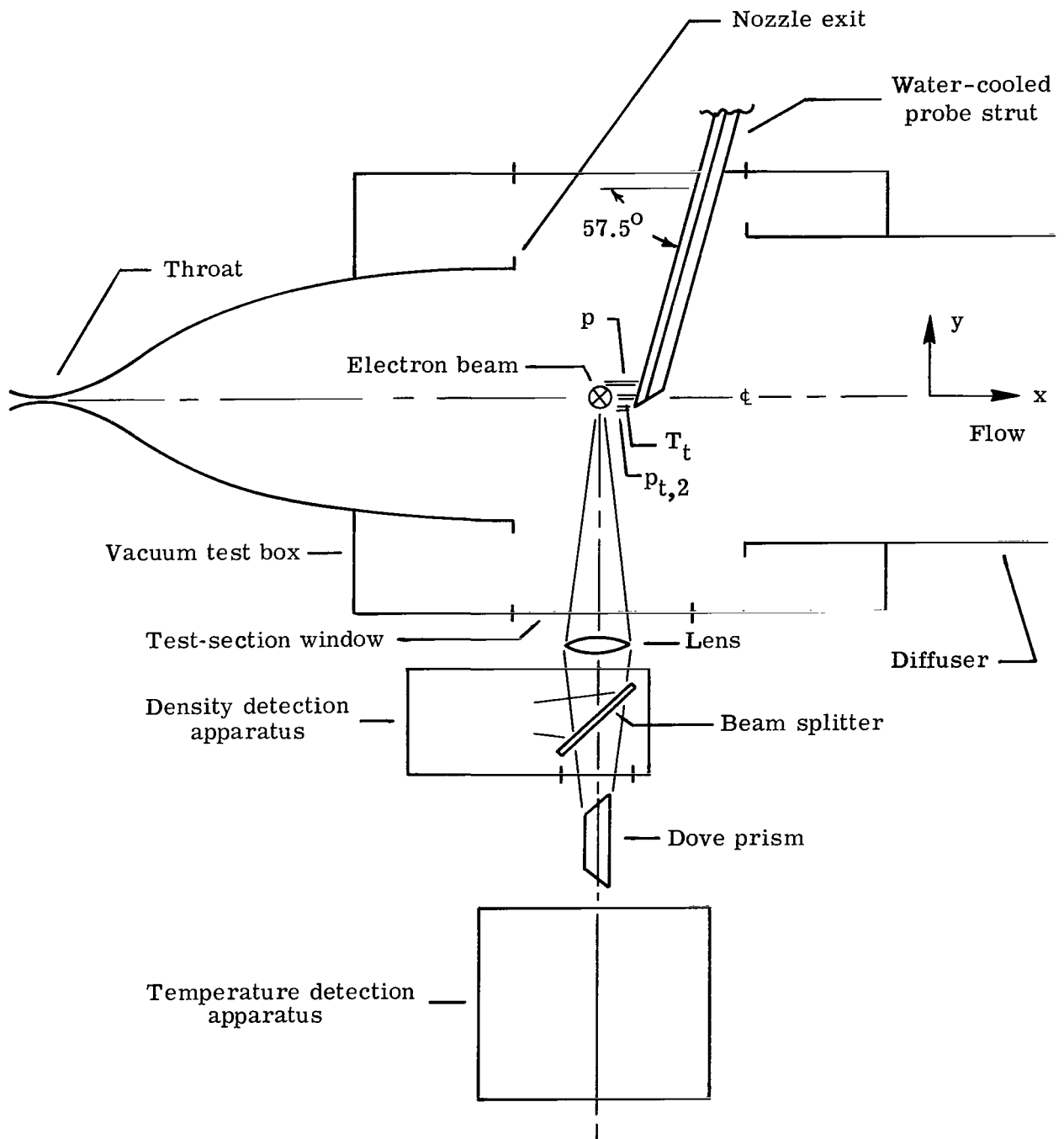
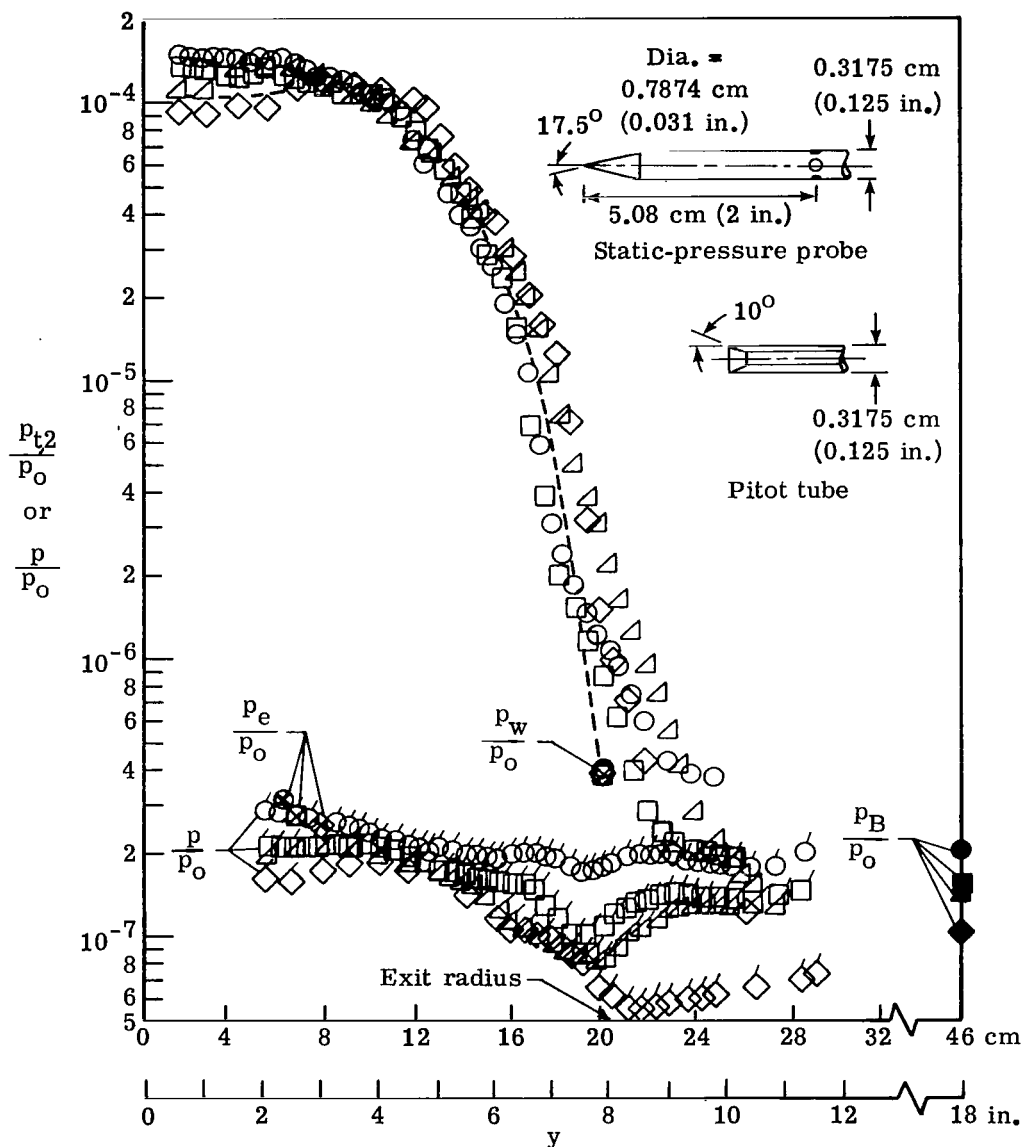


Figure 1.- Schematic of facility and test apparatus.

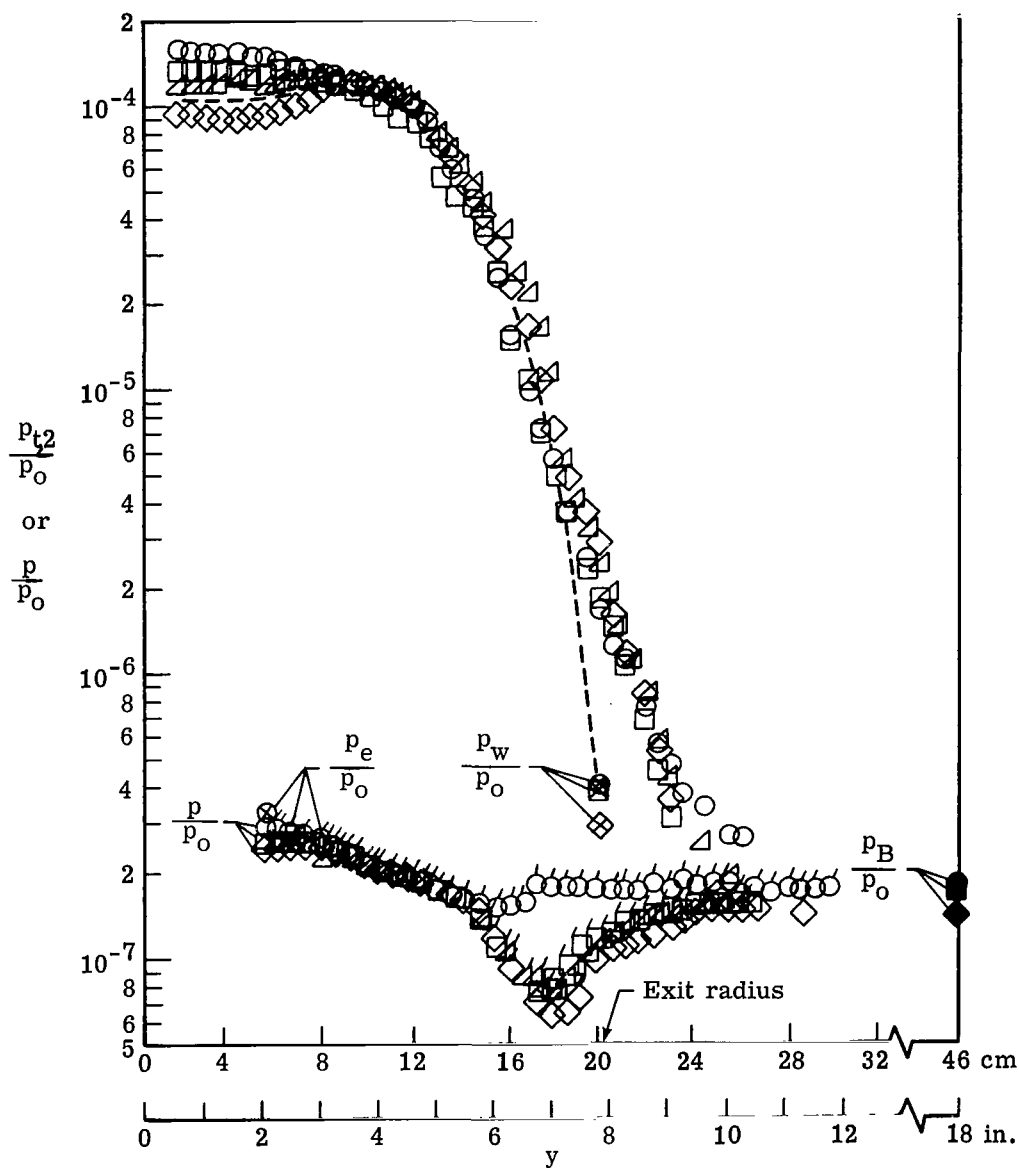
		p_o		T_o		
	M_e	N/cm^2	psia	K	$^{\circ}R$	Ref.
○	18.85	2710	3922	1640	2950	Present
□	19.34	3970	5750	1667	3000	
△	19.20	4410	6400	1672	3010	
◇	19.50	5810	8410	1655	2980	
---	19.4	4309	6250	1778	3200	6
--- { $x = 208.3$ cm (82.0 in.)						



(a) $x = 225$ cm (88.75 in.).

Figure 2.- Measured pitot and static tube pressure distributions through the free shear layer.

		P_o		T_o		
	M_e	N/cm^2	psia	K	$^{\circ}R$	Ref.
○	18.74	2480	3595	1998	2950	Present
□	19.25	3820	5540	1667	3000	
△	19.18	4320	6266	1667	3000	
◇	19.68	5520	8000	1655	2980	
---	19.4	4309	6250	1778	3200	6
{ $x = 208.3$ cm (82.0 in.)						

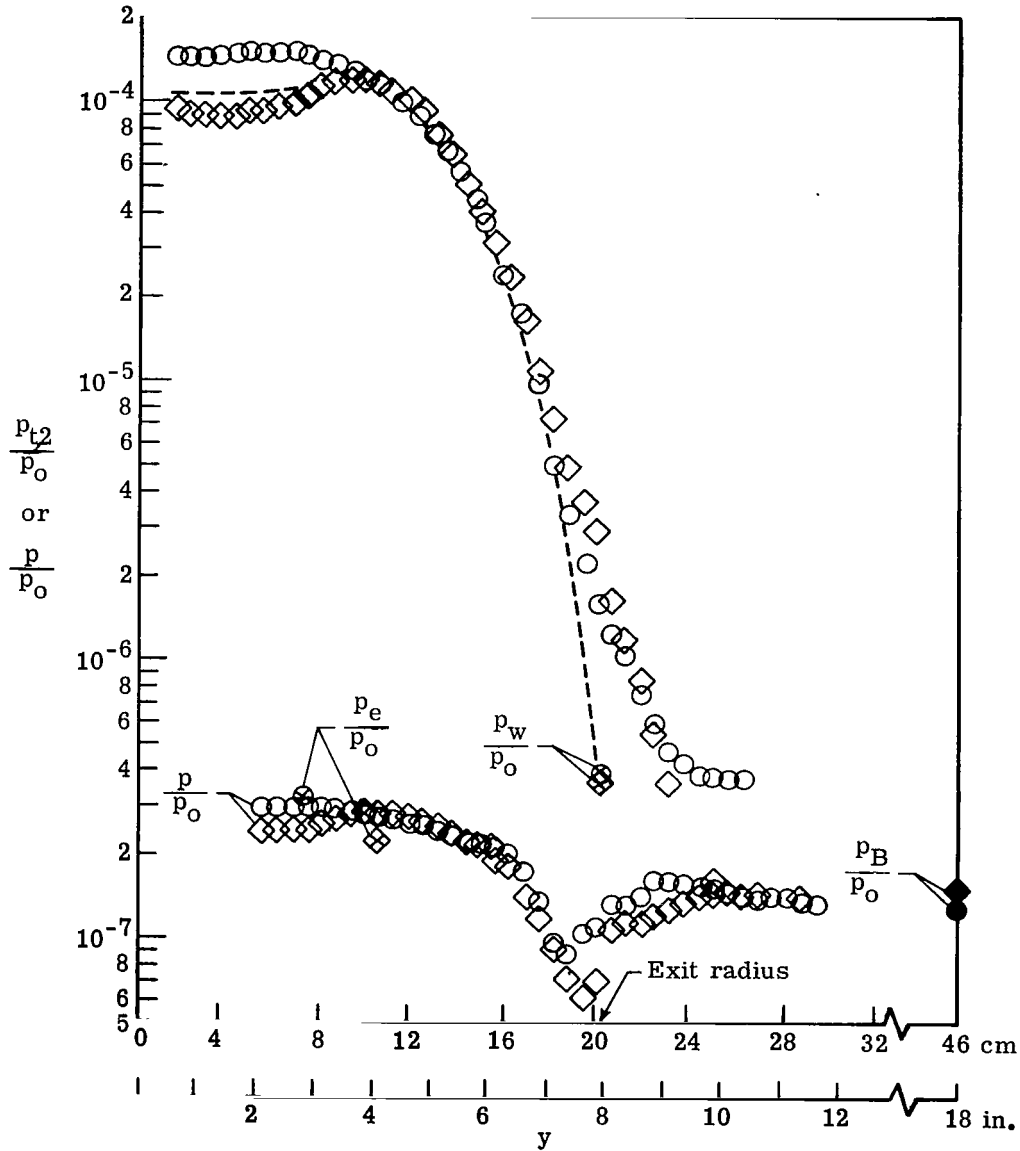


(b) $x = 238$ cm (93.75 in.).

Figure 2.- Continued.

	M_e	p_o		T_o		Ref.
		N/cm^2	psia	K	$^{\circ}R$	
○	18.78	2590	3750	1667	3000	Present
◇	19.76	5460	7910	1672	3010	
---	19.4	4309	6250	1780	3200	6

{ $x = 208.3$ cm (82.0 in.)

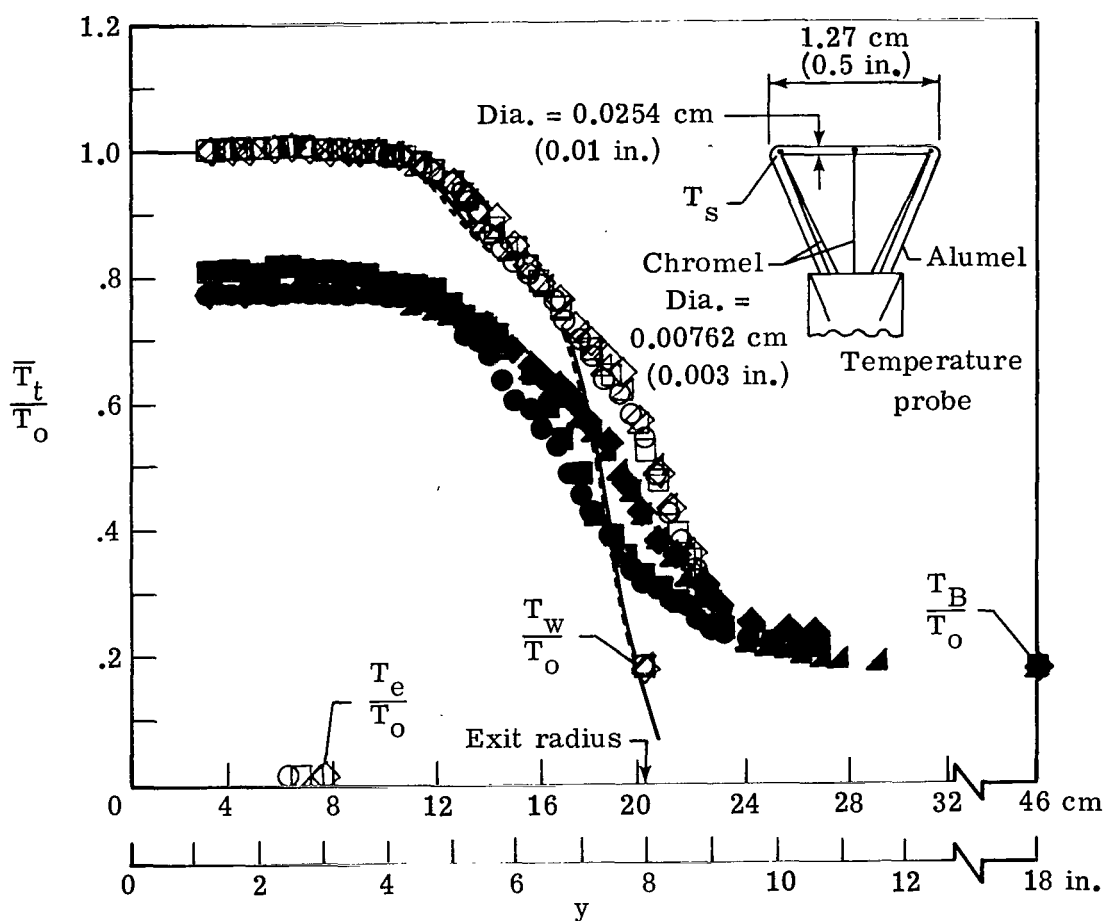


(c) $x = 260$ cm (102.25 in.).

Figure 2. - Concluded.

		p_o		T_o		Reference
	M_e	N/cm^2	psia	K	$^{\circ}R$	
○	18.85	2710	3922	1640	2950	Present
□	19.34	3970	5750	1667	3000	
△	19.20	4410	6400	1672	3010	
◇	19.50	5810	8410	1655	2980	
---	19.4	4309	6256	1778	3200	6 (input to theory)
---	{ $x = 208.3$ cm (82.0 in.)					
—	19.40	4300	6250	1667	3000	19 (theory)

Filled symbols for uncorrected data

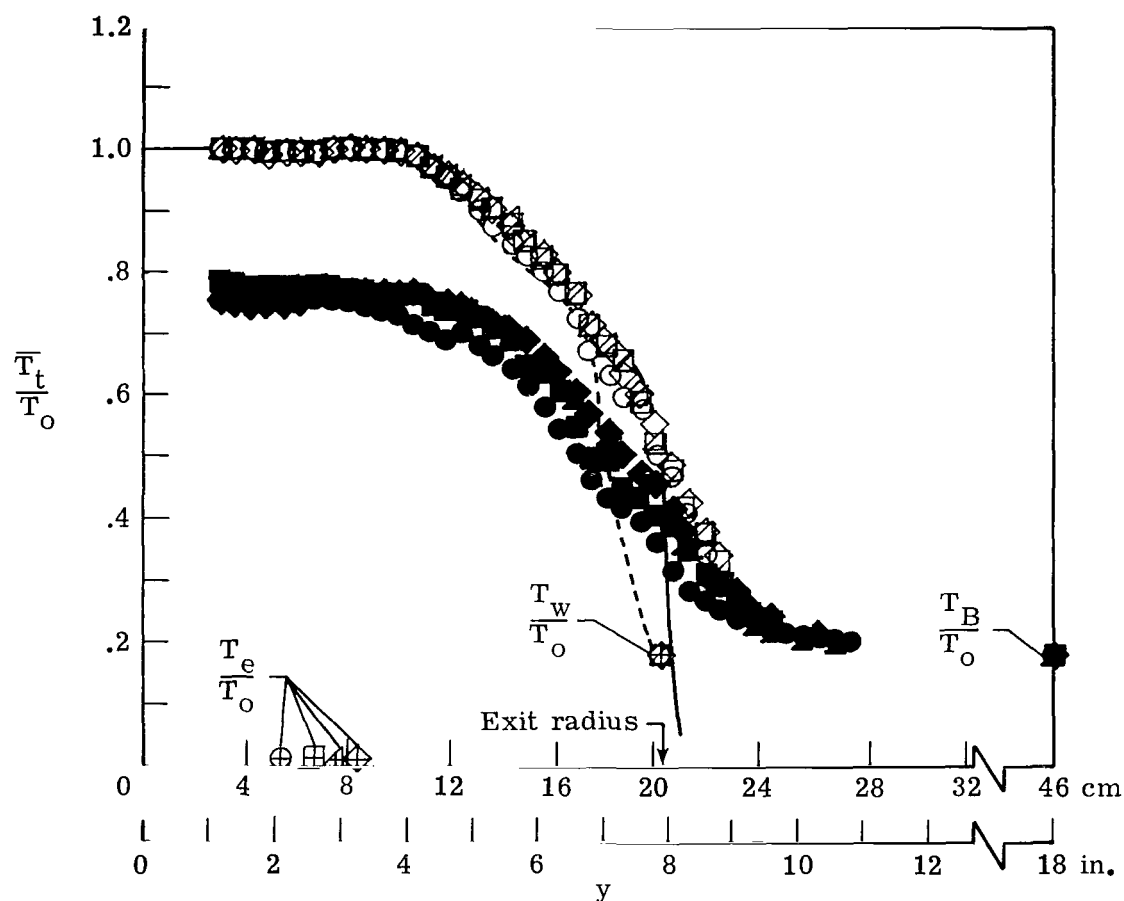


(a) $x = 225$ cm (88.75 in.).

Figure 3.- Measured and corrected total temperature through the shear layer. Constant p_e/p_o used in data reduction for corrected values (open symbols).

	M_e	p_o		T_o		Reference
		N/cm^2	psia	K	$^{\circ}R$	
○	18.74	2480	3595	1640	2950	Present
□	19.25	3820	5540	1667	3000	↓
△	19.18	4320	6266	1667	3000	
◇	19.68	5520	8000	1655	2980	6 (input to theory)
---	19.40	4309	6256	1778	3200	
{ $x = 208.3$ cm (82.0 in.)						19 (theory)
—	19.40	4300	6250	1767	3000	

Filled symbols for uncorrected data

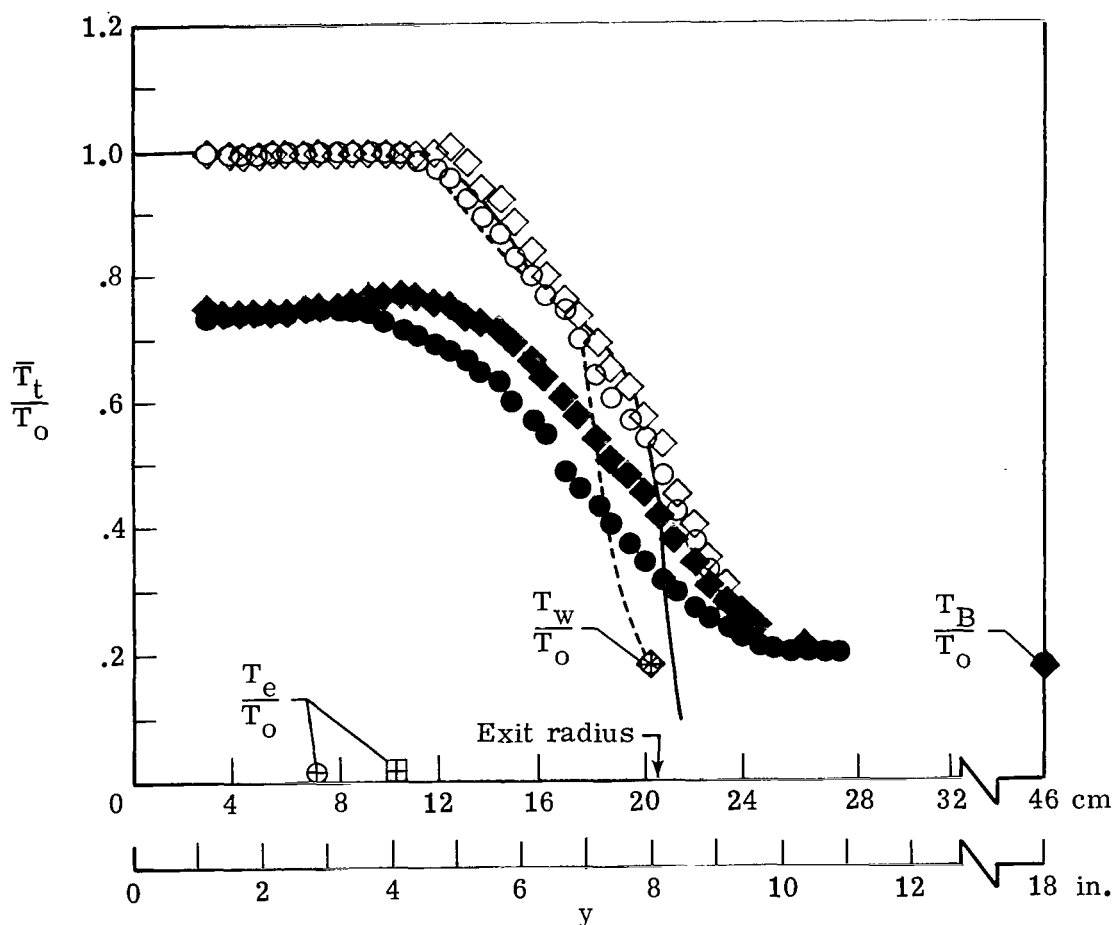


(b) $x = 238$ cm (93.75 in.).

Figure 3.- Continued.

		p_o		T_o		
	M_e	N/cm^2	psia	K	$^{\circ}R$	Reference
○	18.78	2590	3750	1667	3000	Present
□	19.76	5460	7910	1672	3010	
---	19.40	4309	6256	1778	3200	6 (input to theory)
	{ $x = 208.3$ cm (82.0 in.)					
—	19.40	4300	6250	1767	3000	19 (theory)

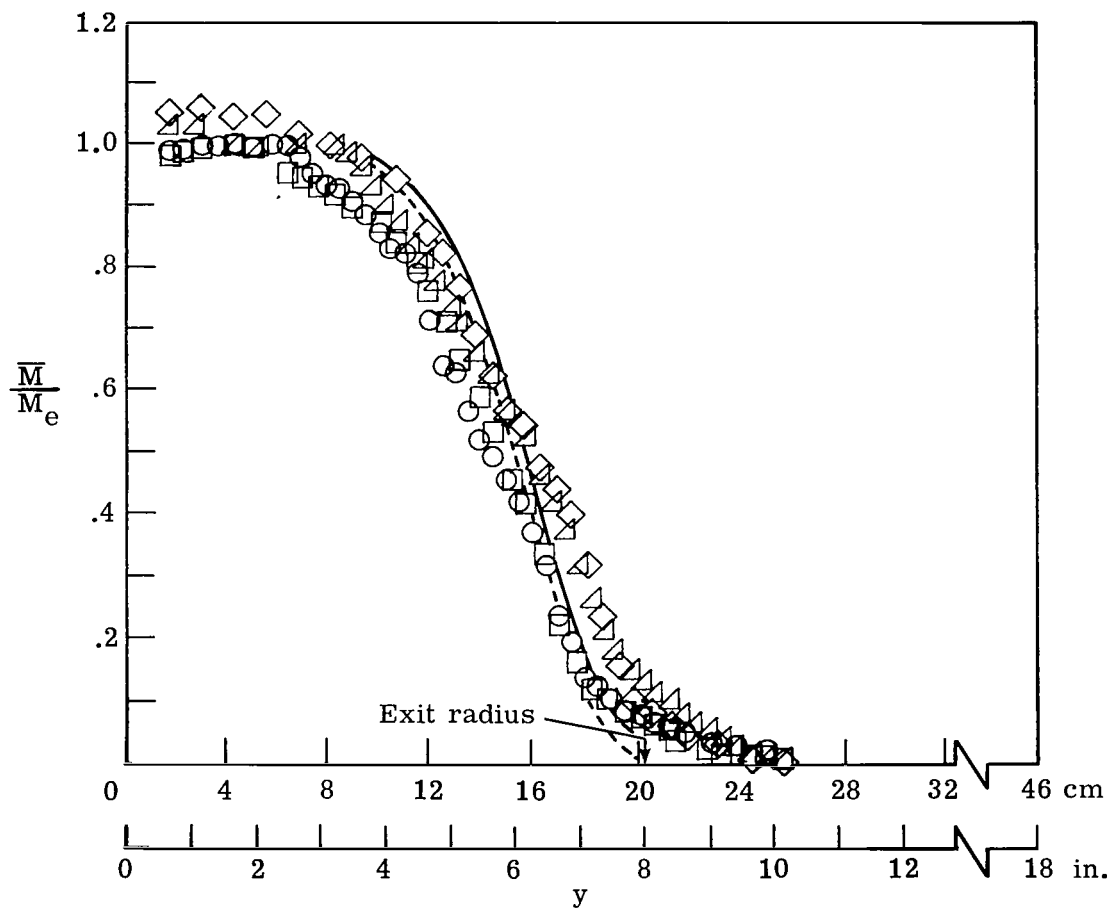
Filled symbols for uncorrected data



(c) $x = 260$ cm (102.25 in.).

Figure 3.- Concluded.

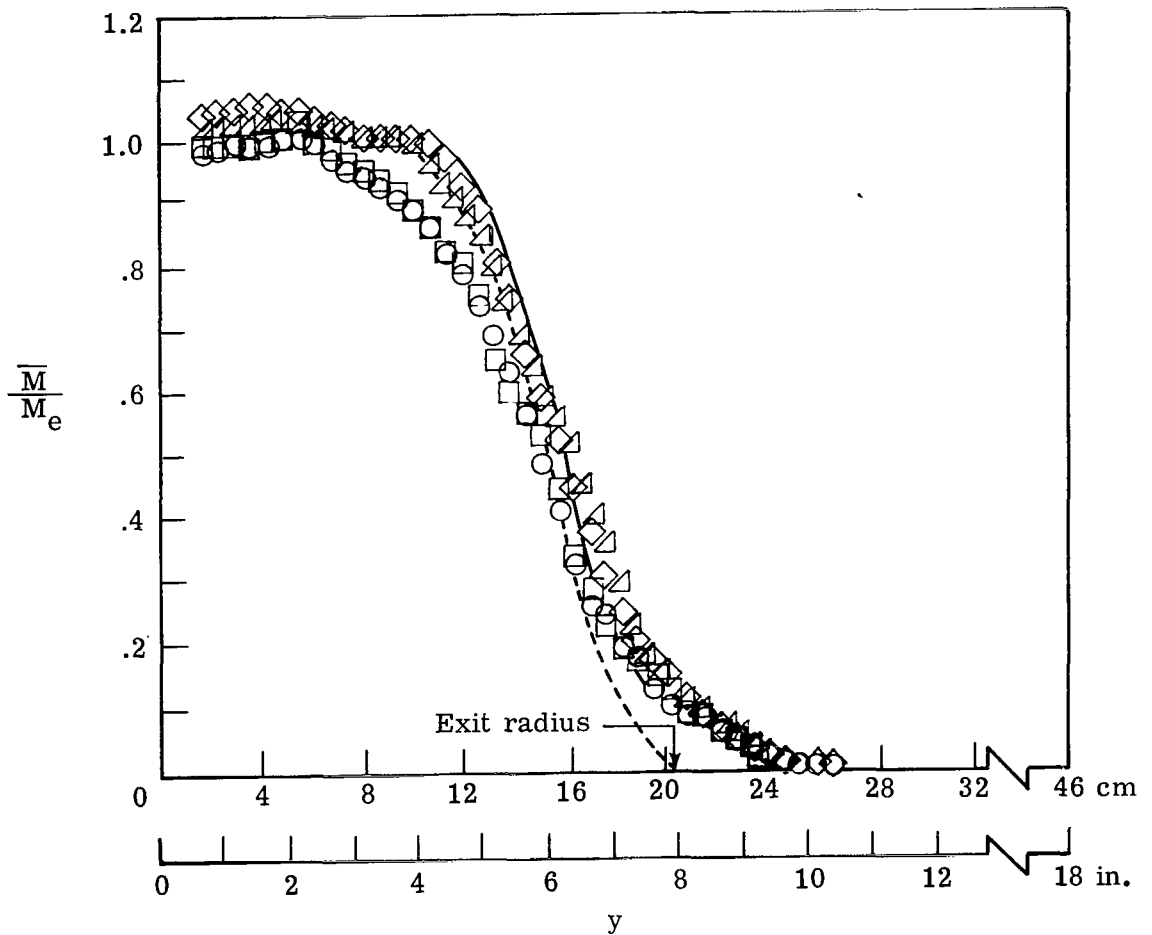
	M_e	p_o		T_o		Reference
		N/cm^2	psia	K	$^{\circ}R$	
○	18.85	2710	3922	1640	2950	Present
□	19.34	3970	5750	1667	3000	
△	19.20	4410	6400	1672	3010	
◇	19.50	5810	8410	1655	2980	
---	19.40	4309	6256	1778	3200	6 (input to theory)
—	19.40	4300	6250	1667	3000	19 (theory)



(a) $x = 225 \text{ cm}$ (88.75 in.).

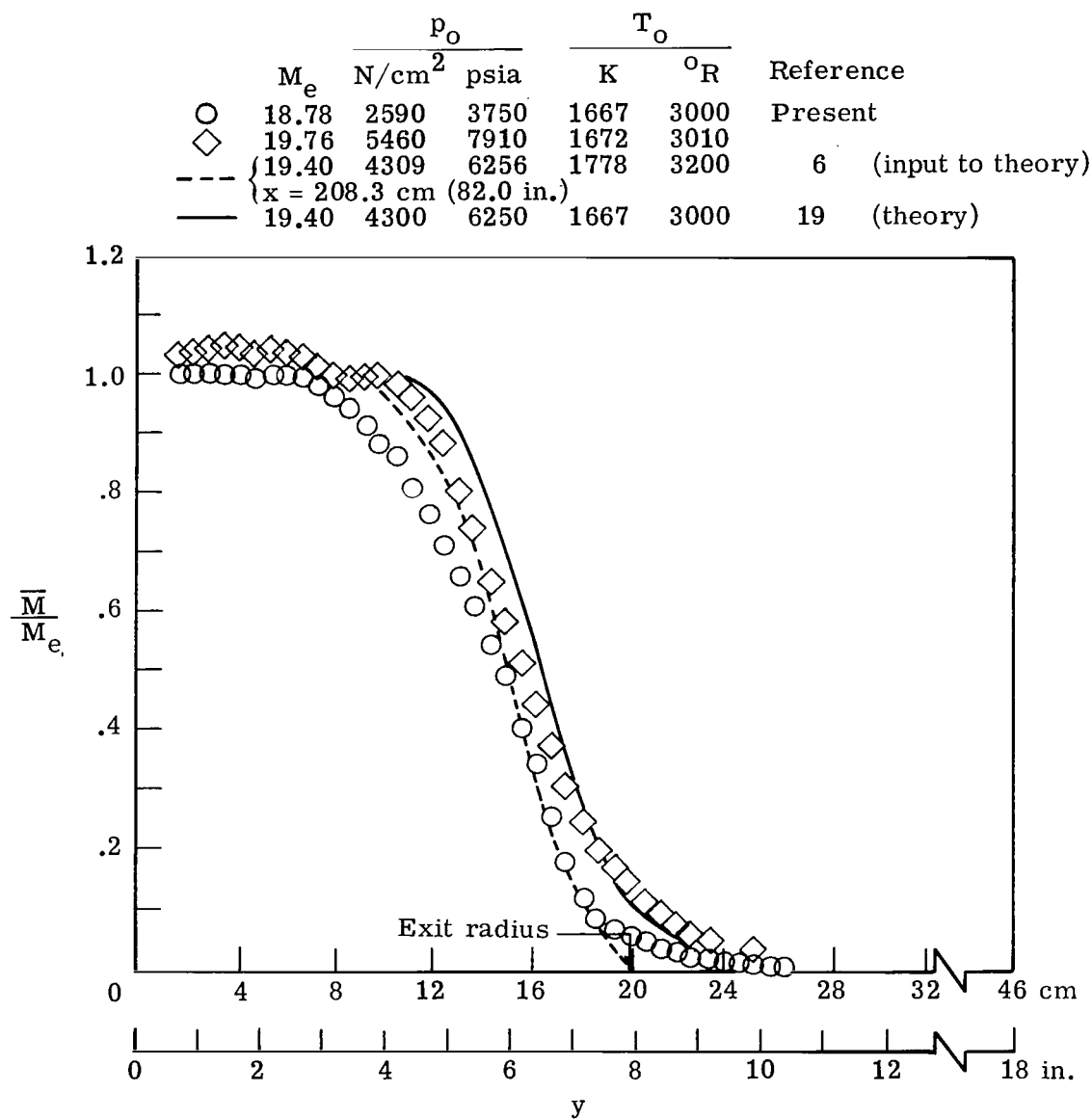
Figure 4.- Comparison of shear flow Mach number profiles with theory and nozzle-wall profile.

	M_e	p_o		T_o		Reference
		N/cm^2	psia	K	$^{\circ}R$	
○	18.74	2480	3595	1640	2950	Present
□	19.25	3820	5540	1667	3000	6 (input to theory)
△	19.18	4320	6266	1667	3000	
◇	19.68	5520	8000	1655	2980	
---	19.40	4309	6256	1778	3200	
---	$x = 208.3 \text{ cm (82.0 in.)}$					19 (theory)
---	19.40	4300	6250	1667	3000	



(b) $x = 238 \text{ cm (93.75 in.)}$.

Figure 4.- Continued.



(c) $x = 260$ cm (102.25 in.).

Figure 4.- Concluded.

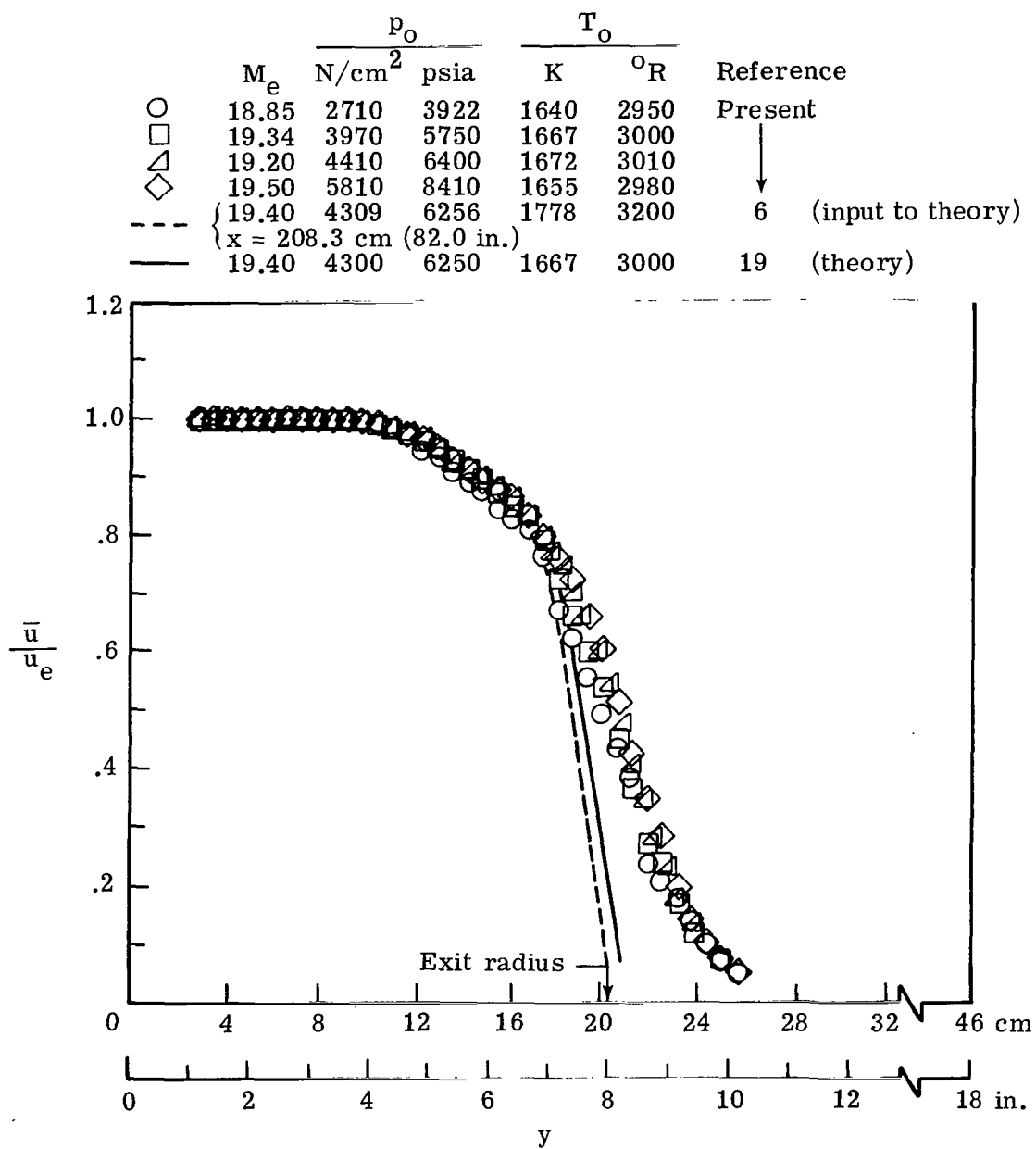
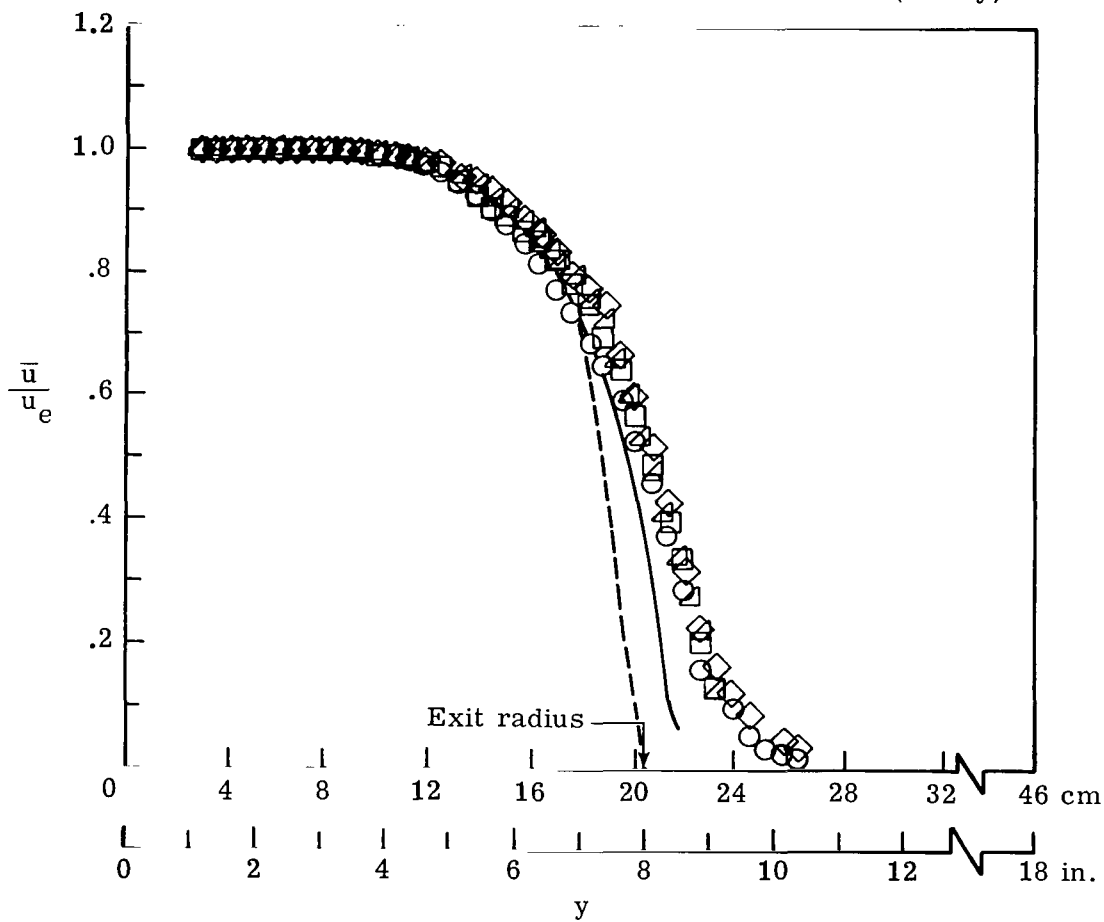


Figure 5.- Comparison of shear flow velocity profiles with theory and nozzle-wall profile.

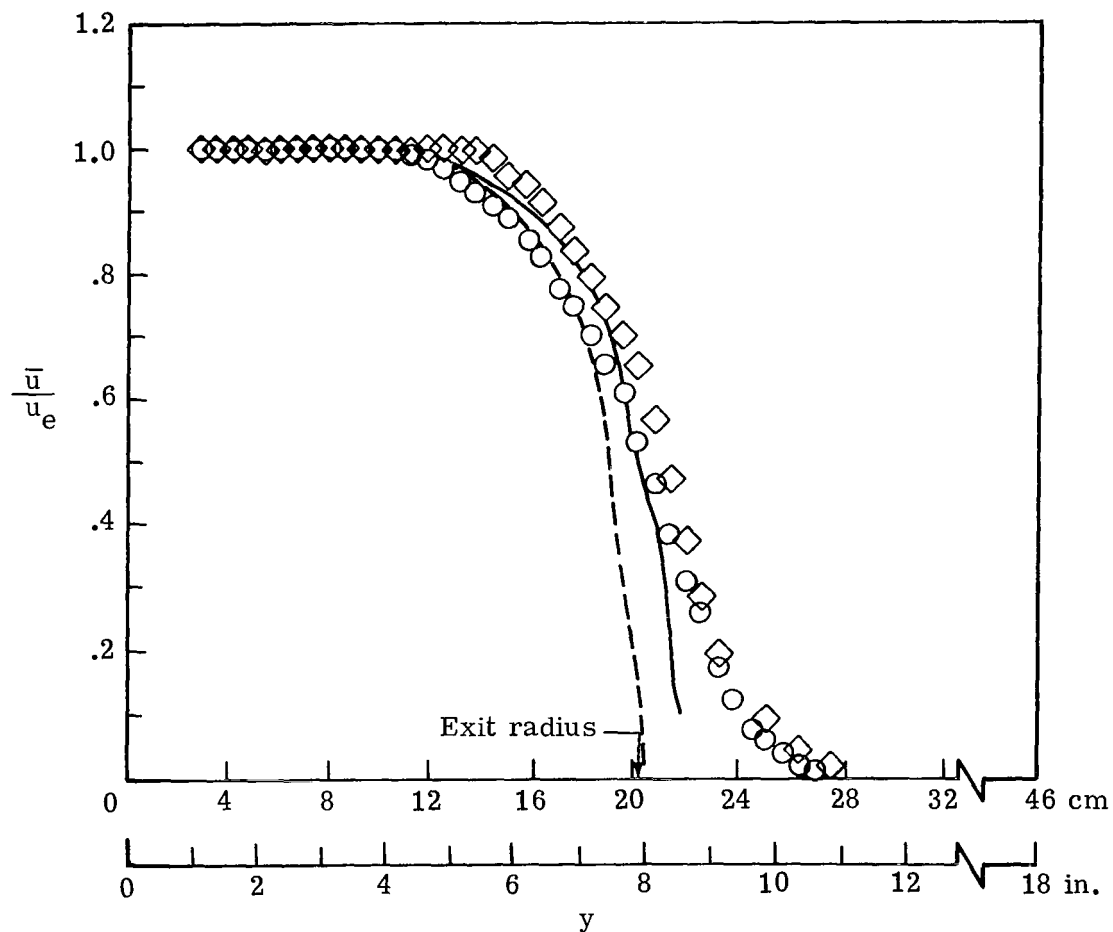
	M_e	p_o		T_o		Reference
		N/cm^2	psia	K	$^{\circ}R$	
○	18.74	2480	3595	1646	2950	Present
□	19.25	3820	5540	1667	3000	↓
△	19.18	4320	6266	1667	3000	
◇	19.68	5520	8000	1655	2980	
---	19.40	4309	6256	1778	3200	6 (input to theory)
—	19.40	4300	6250	1667	3000	19 (theory)



(b) $x = 238$ cm (93.75 in.).

Figure 5.- Continued.

		p_o		T_o		
	M_e	N/cm^2	psia	K	$^{\circ}R$	Reference
○	18.78	2590	3750	1667	3000	Present
◇	19.76	5460	7910	1672	3010	↓
---	19.40	4309	6256	1778	3200	6 (input to theory)
—	19.40	4300	6250	1667	3000	19 (theory)



(c) $x = 260$ cm (102.25 in.).

Figure 5.- Concluded.

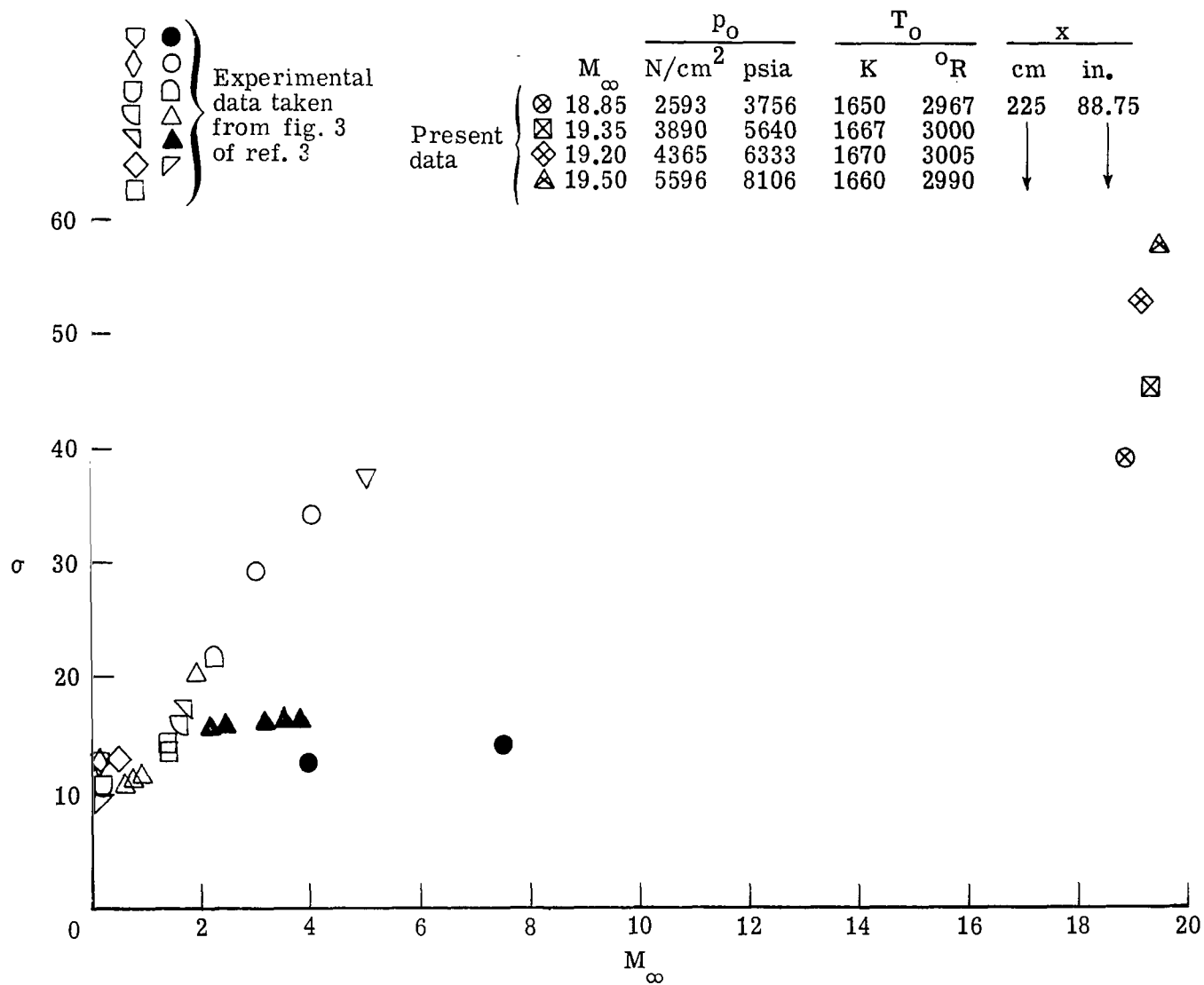
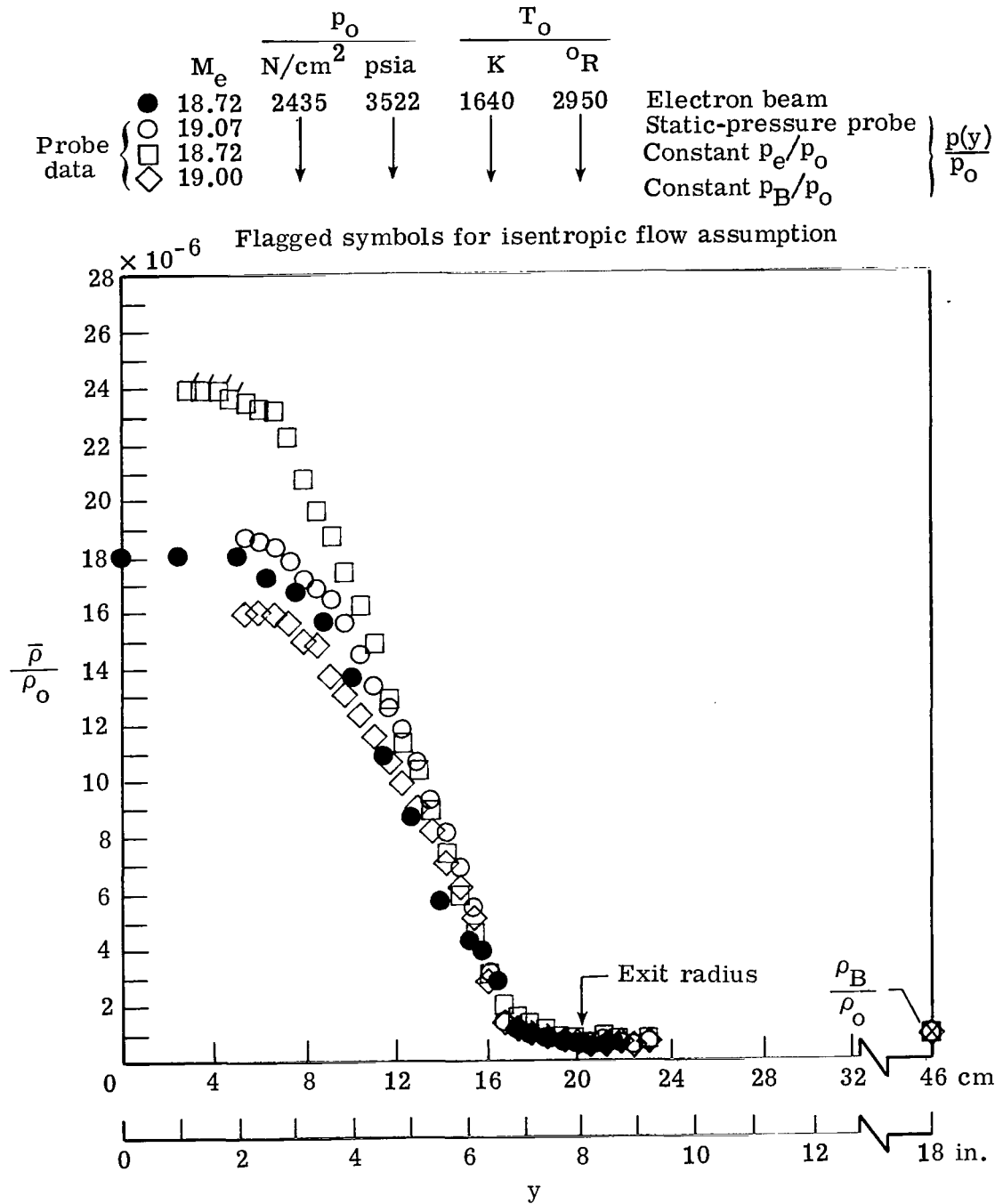


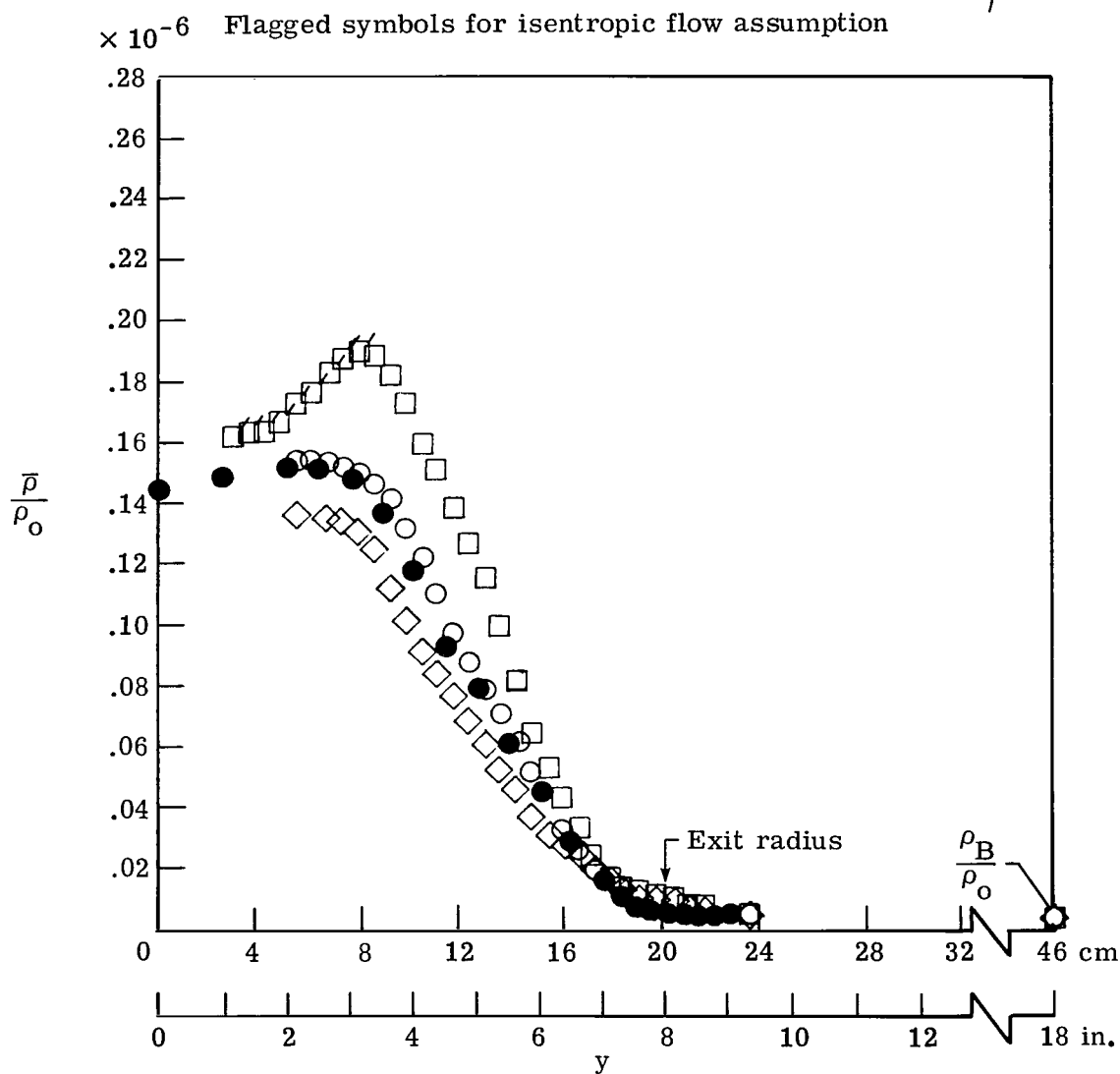
Figure 6.- Variation of spreading parameter with Mach number.



(a) $x = 238 \text{ cm}$ (93.75 in.).

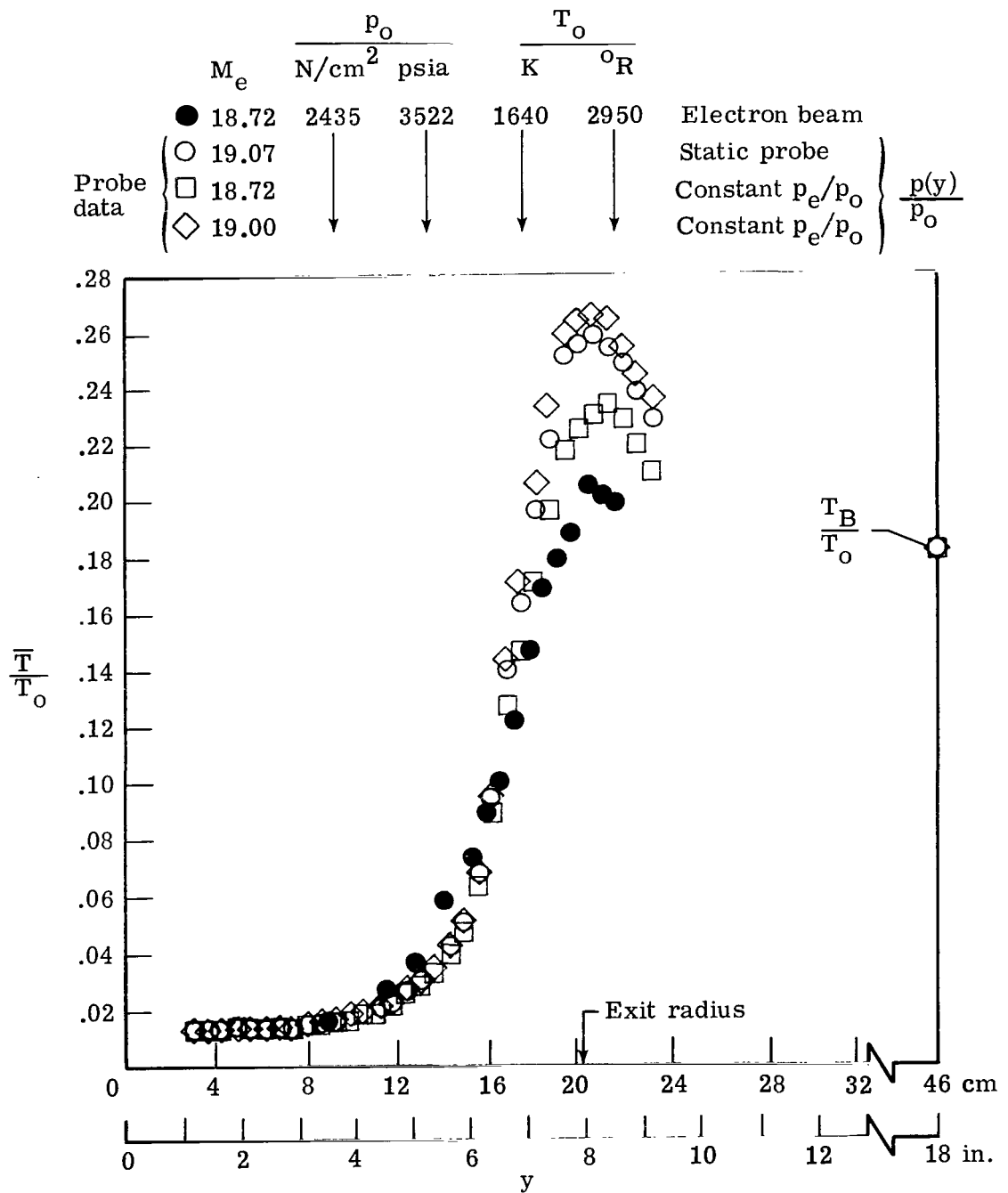
Figure 7.- Comparison of measured density through shear layer by electron beam with calculated density from conventional probe data.

Probe data	M_e	p_o		T_o			$\frac{p(y)}{p_o}$
		N/cm^2	psia	K	$^{\circ}R$		
●	19.76	5460	7910	1722	3010	Electron beam	}
○	20.30					Static-pressure probe	
□	19.58					Constant p_e/p_o	
◇	20.90					Constant p_B/p_o	



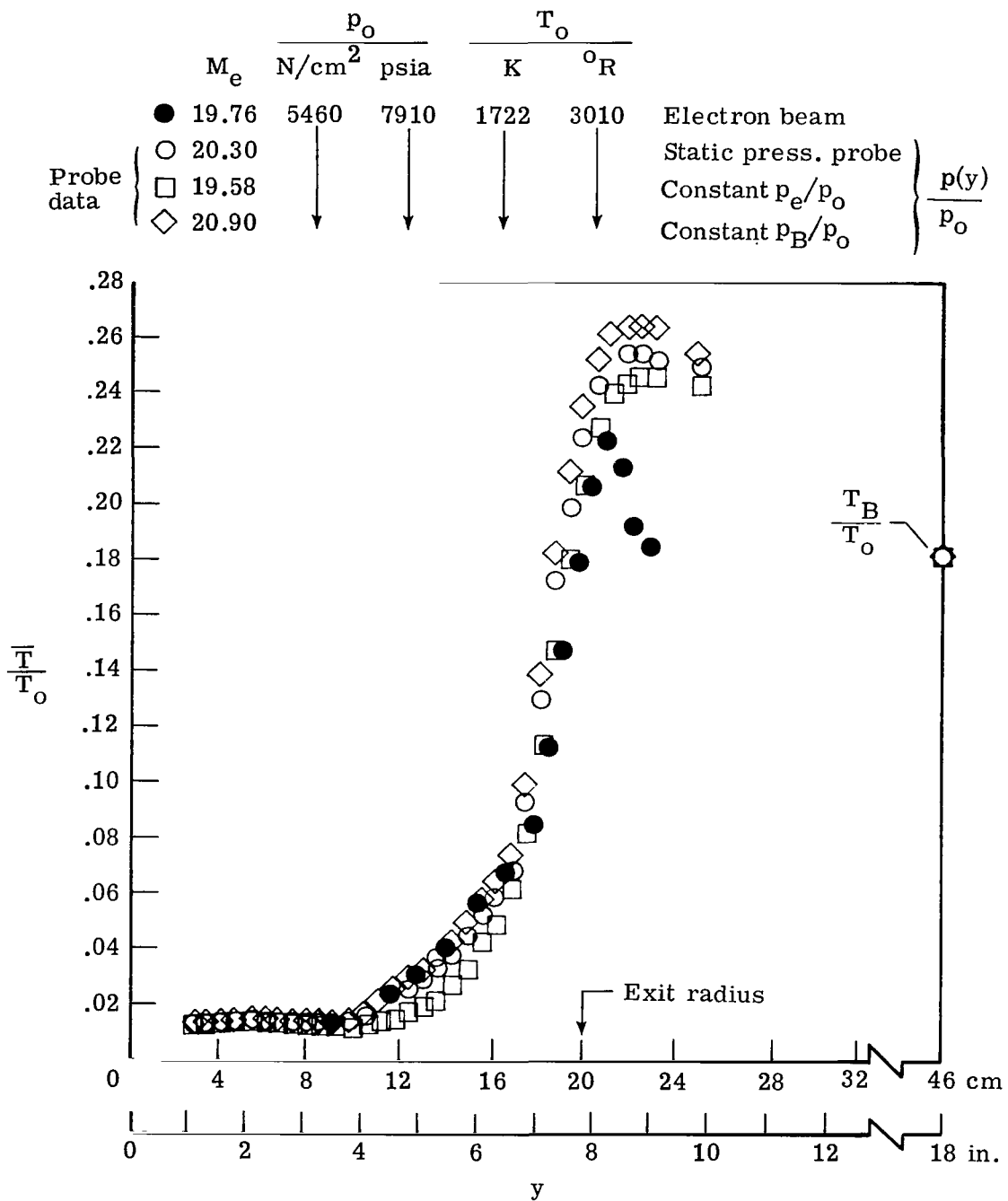
(b) $x = 238 \text{ cm}$ (93.75 in.); $p_o = 5460 \text{ N/cm}^2$.

Figure 7.- Concluded.



(a) $x = 238 \text{ cm}$ (93.75 in.); $p_o = 2435 \text{ N/cm}^2$.

Figure 8.- Comparison of measured temperature through shear layer for electron beam with calculated temperature from conventional probe data.



(b) $x = 238$ cm (93.75 in.); $p_o = 5460$ N/cm².

Figure 8.- Concluded.

	M_e	p_o		T_o		
		N/cm^2	psia	K	$^{\circ}R$	
●	18.72	2435	3522	1640	2950	Electron beam probe
○	19.07	↓	↓	↓	↓	
●	19.76	5460	7910	1670	3010	Electron beam probe
◇	20.30	↓	↓	↓	↓	

Flagged symbols for viscous corrected data.

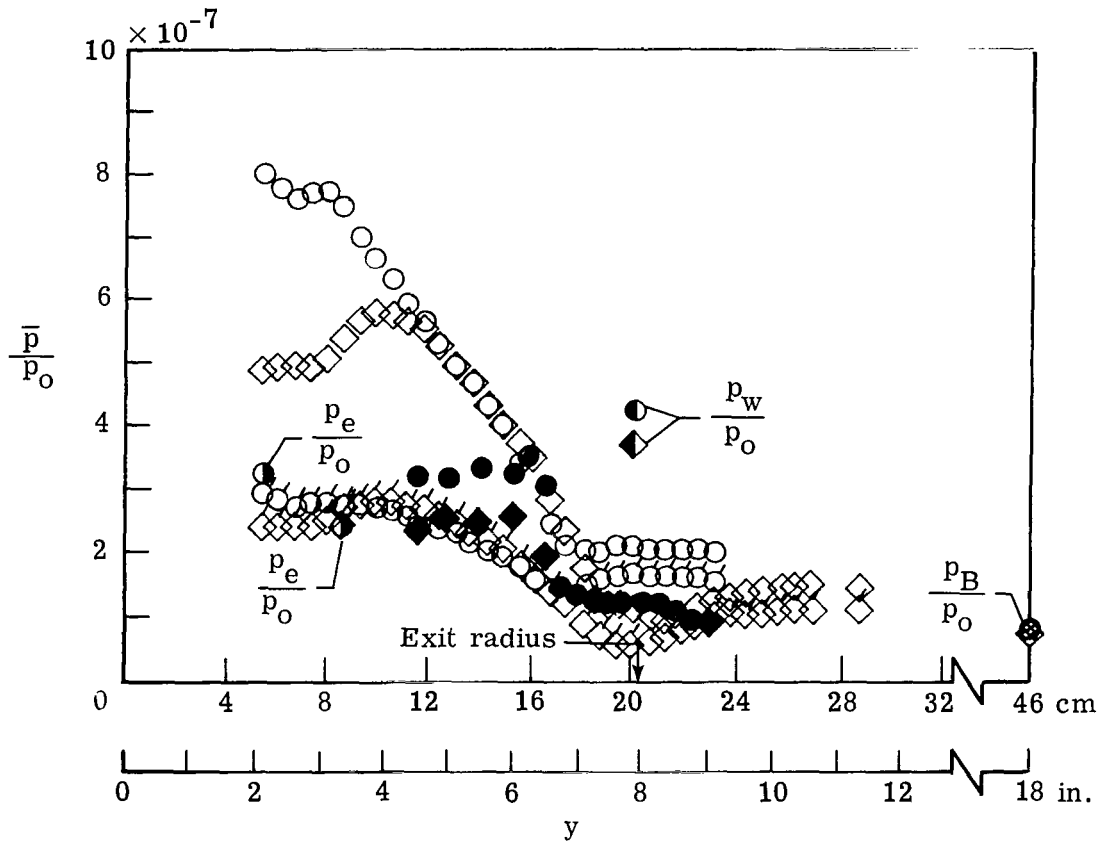


Figure 9.- Comparison of static pressure through shear layer from electron-beam profiles with static-pressure probe.
 $x = 238$ cm (93.75 in.).

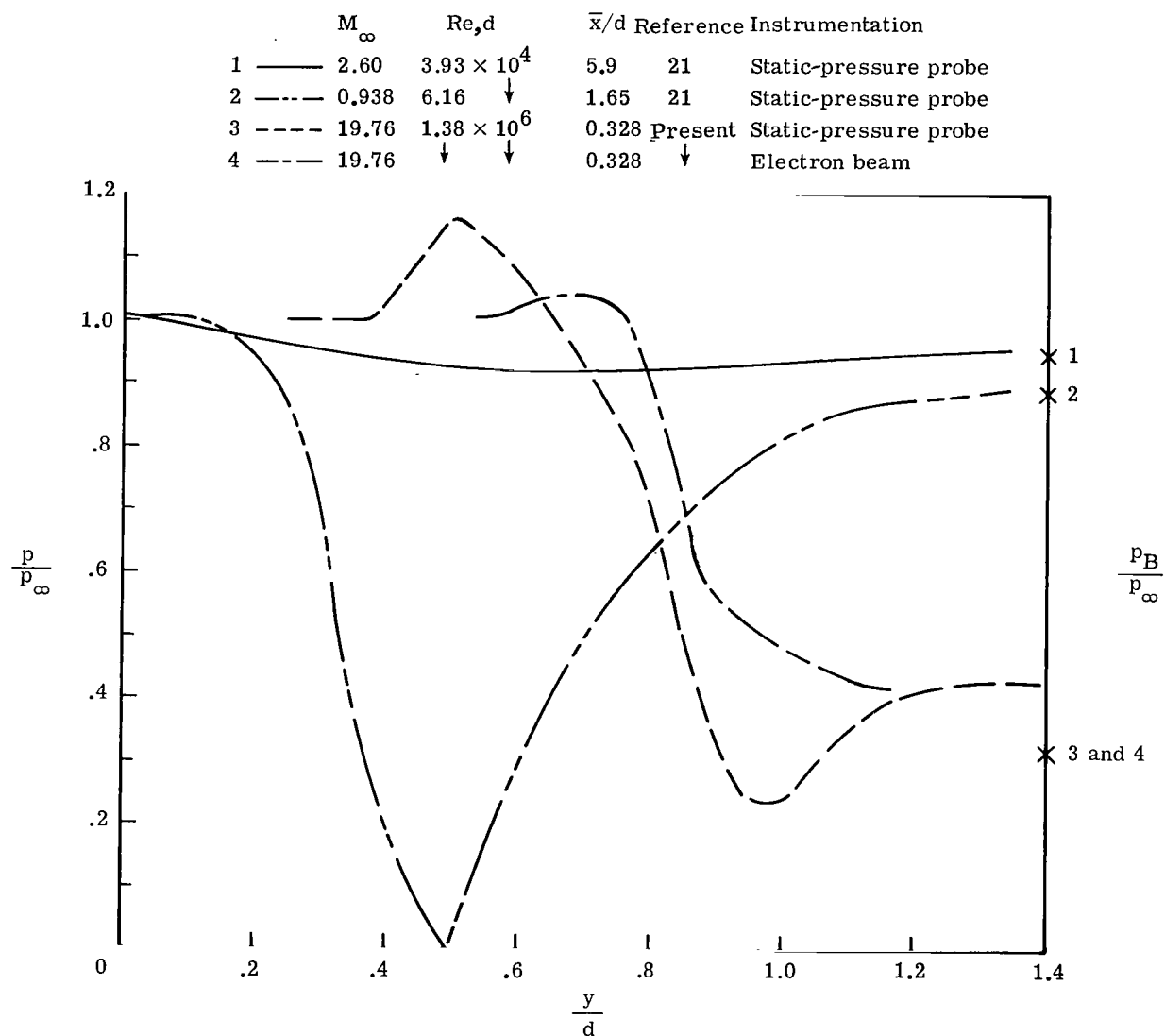


Figure 10.- Comparison of measured static pressure across free shear layers at high and low speeds. \times with arabic number denotes p_B/p_∞ value corresponding to the curves for p/p_∞ .

Data	M_e	p_o		T_o	
		N/cm^2	psia	$^{\circ}R$	K
—○	18.72	2435	3522	1640	2950
---□	19.76	5460	7910	1722	3010

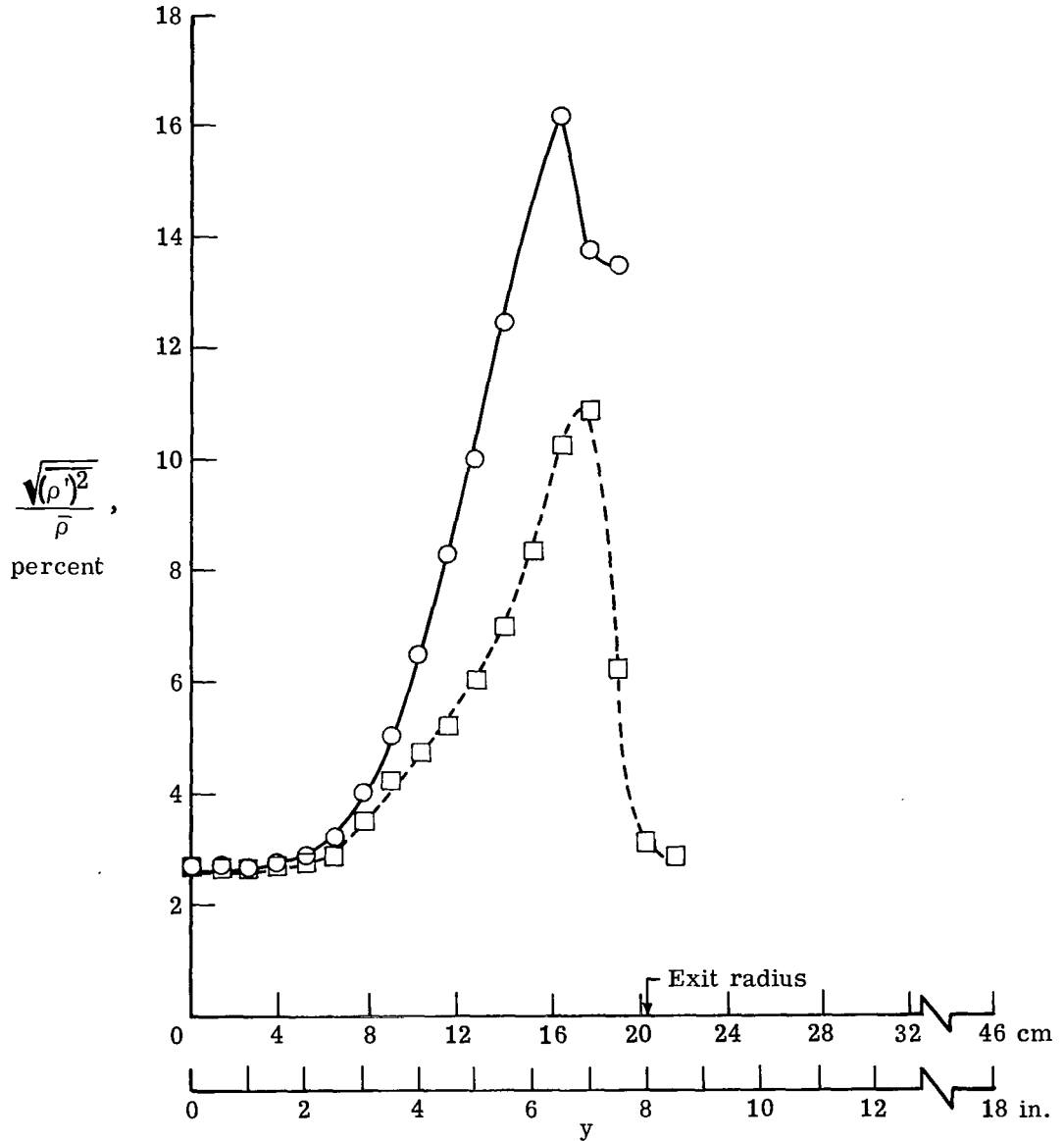



Figure 11.- Root-mean-square density fluctuations through shear layer obtained from electron-beam measurements. $x = 238$ cm (93.75 in.).

	M_e	$R_{\infty, \delta}$	T_W/T_o	$\frac{\delta}{\text{cm} \quad \text{in.}}$		Ref.	$\frac{x}{\text{cm} \quad \text{in.}}$	
	8.25-8.89	$5.37 \text{ to } 10.75 \times 10^4$	0.07 to 0.16	13.2-15.0	5.2-5.9	29	Nozzle wall	
---	18.72	2.33×10^5	0.183	17.8	(7.0)	Present	238	93.75
---	19.76	4.60 ↓	0.180	15.3	(6.0)	↓	↓	↓

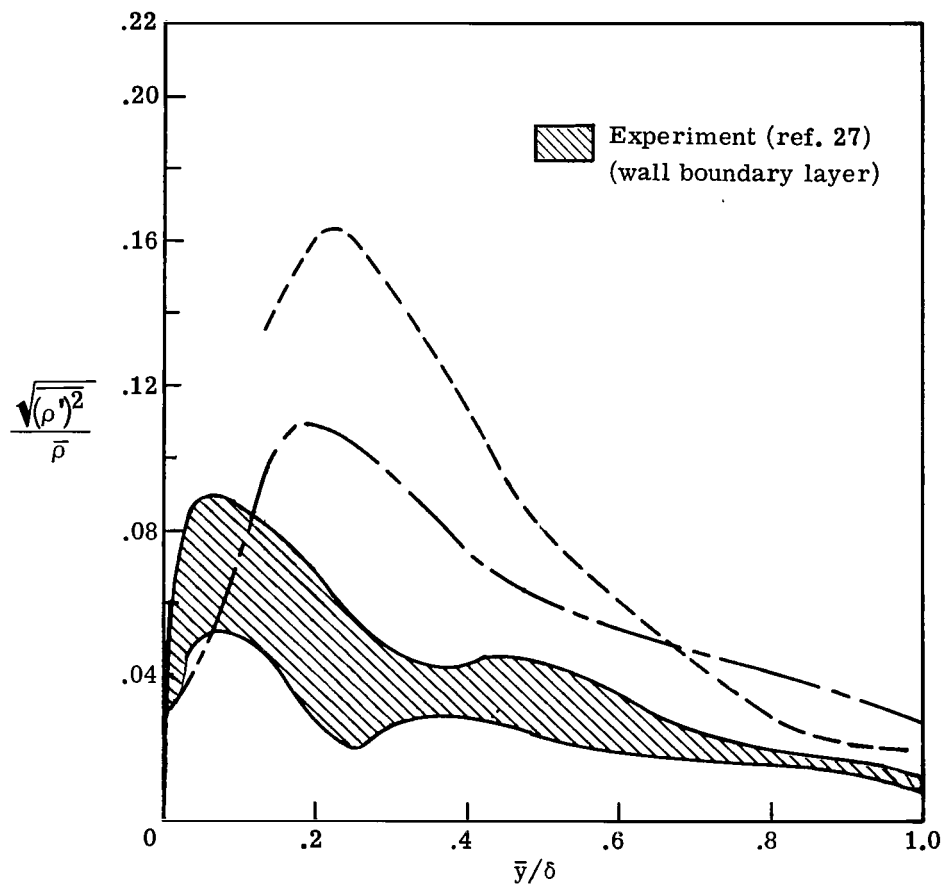
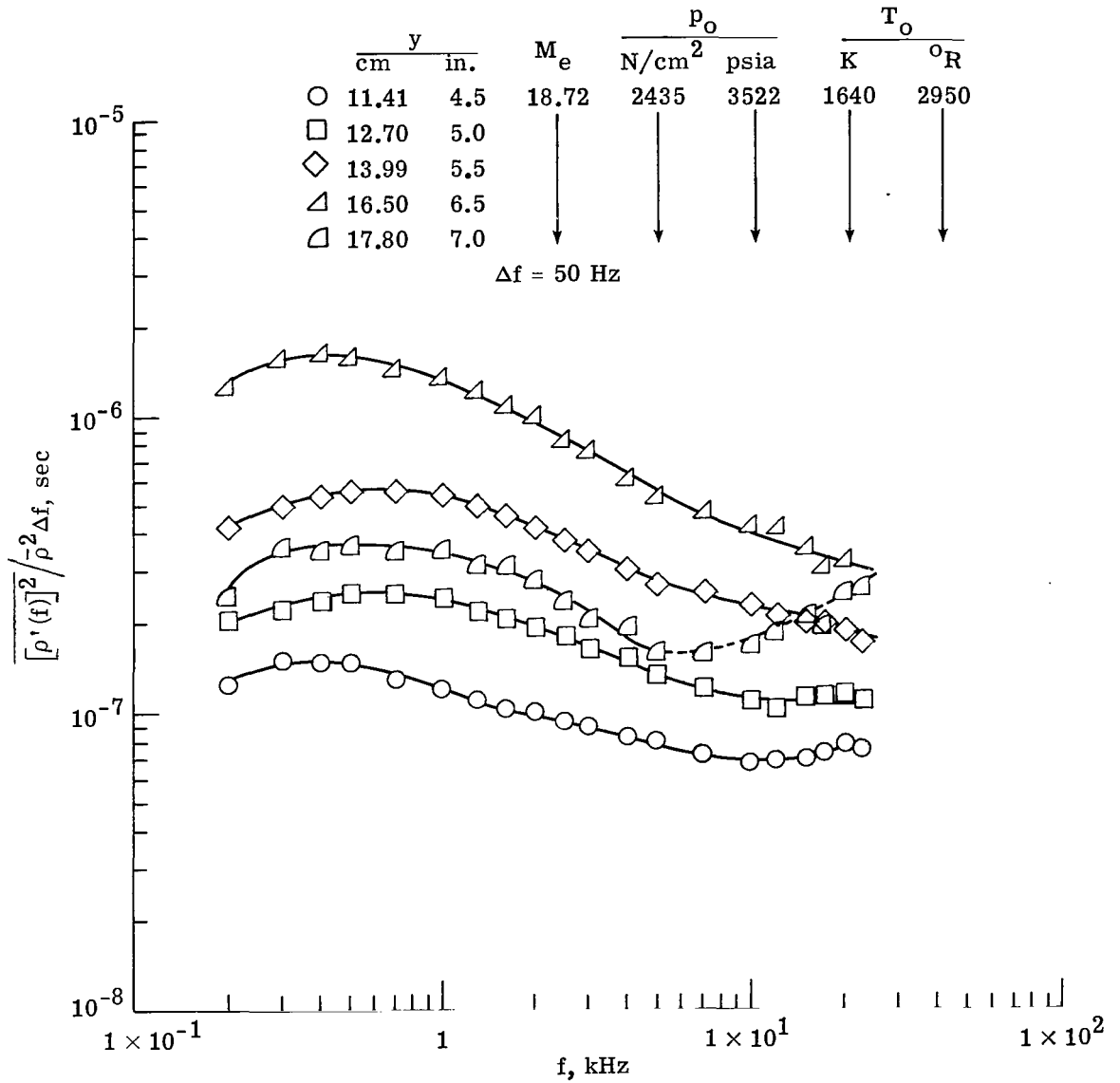
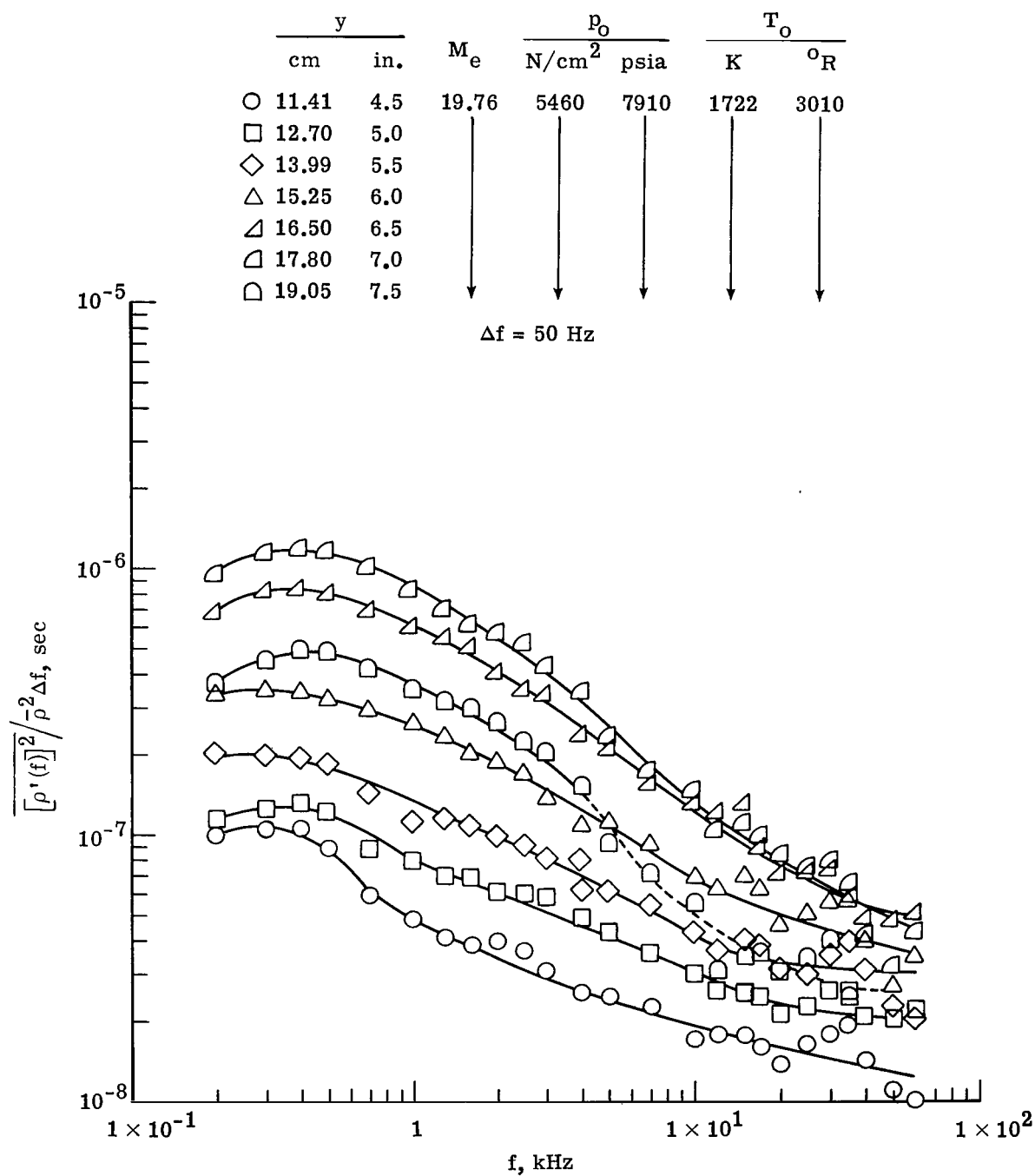


Figure 12.- Comparison of intensity of density fluctuations.



(a) $R_{\infty} = 1.3 \times 10^6$ per m ($R_{\infty} = 4.0 \times 10^5$ per ft).

Figure 13.- Energy spectra of density fluctuations for stations across shear layer. $x = 238$ cm (93.75 in.).



(b) $R_{\infty} = 3.3 \times 10^6$ per m ($R_{\infty} = 9.2 \times 10^5$ per ft).

Figure 13.- Concluded.

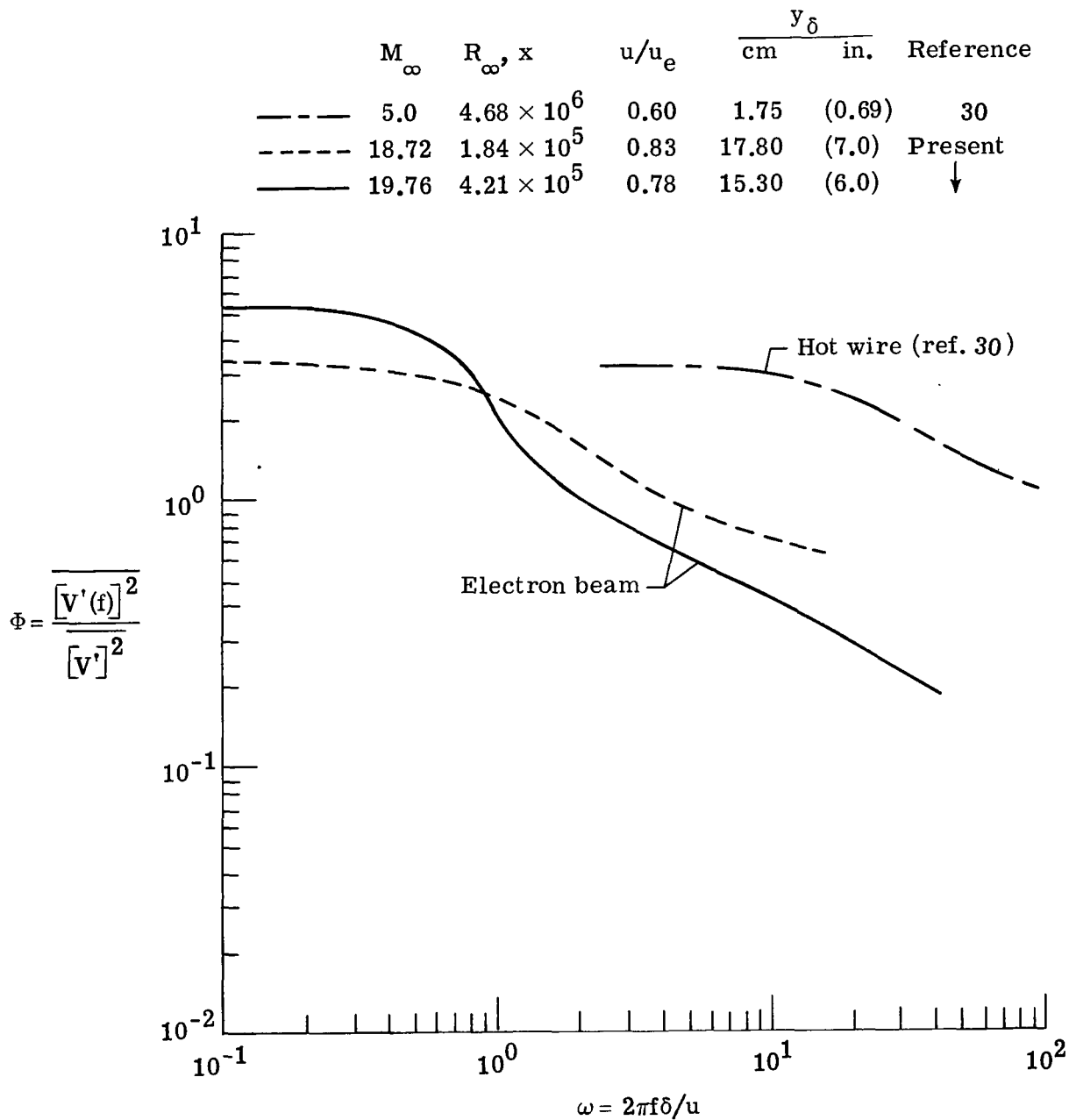


Figure 14.- Comparison of power spectra in free shear layers.

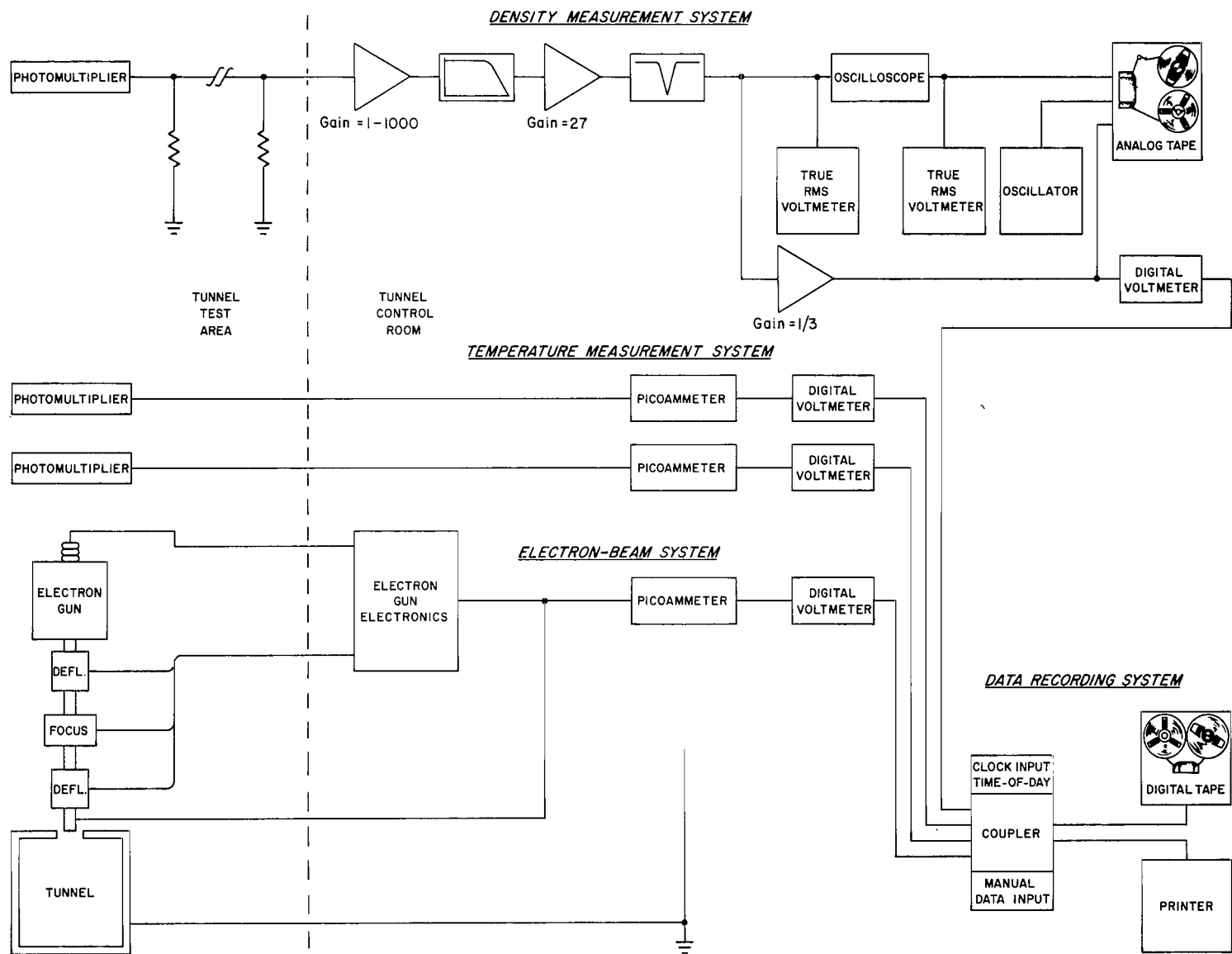


Figure 15.- Electron-beam density and temperature measurement system.

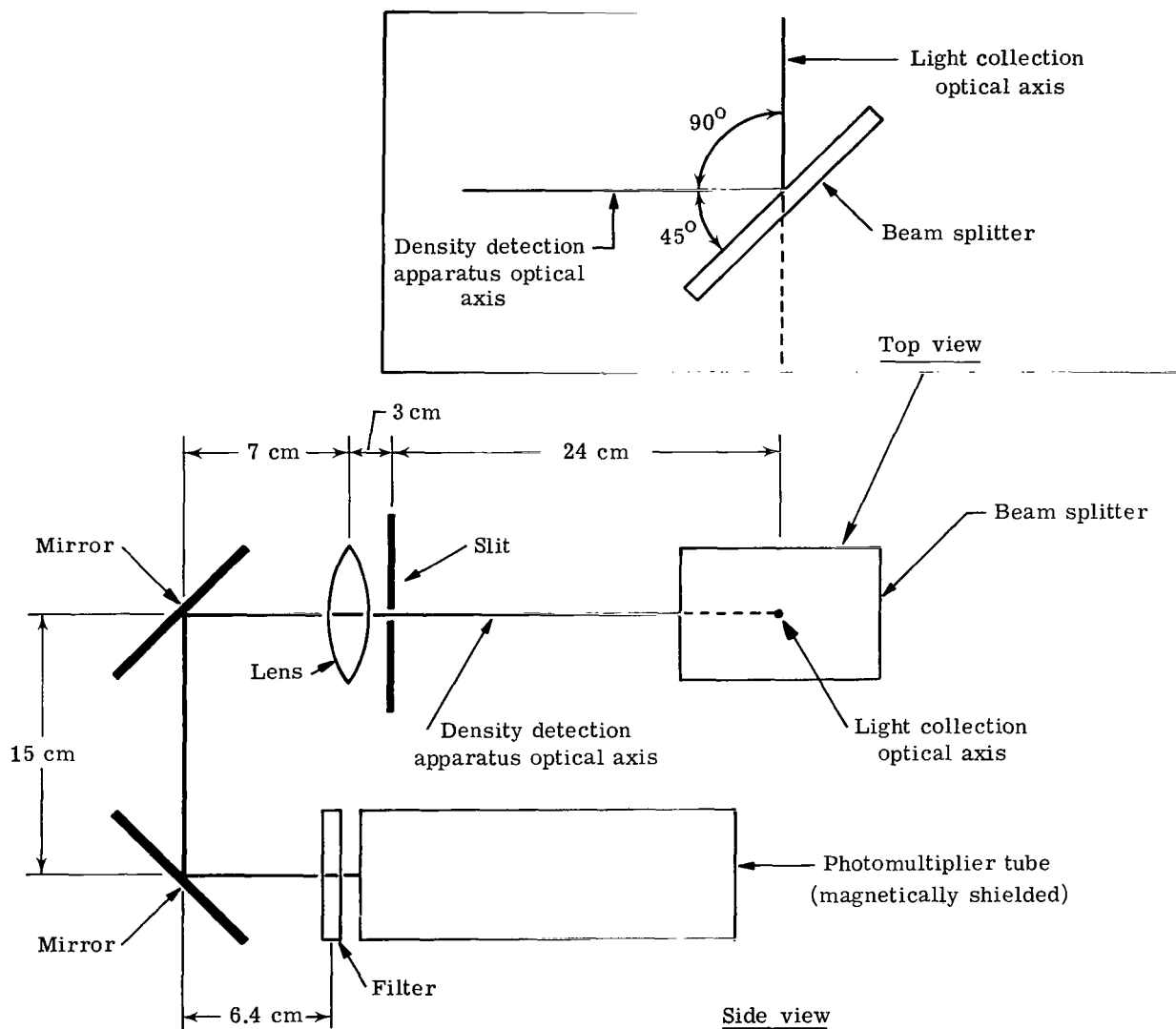


Figure 16.- Density measurement system.

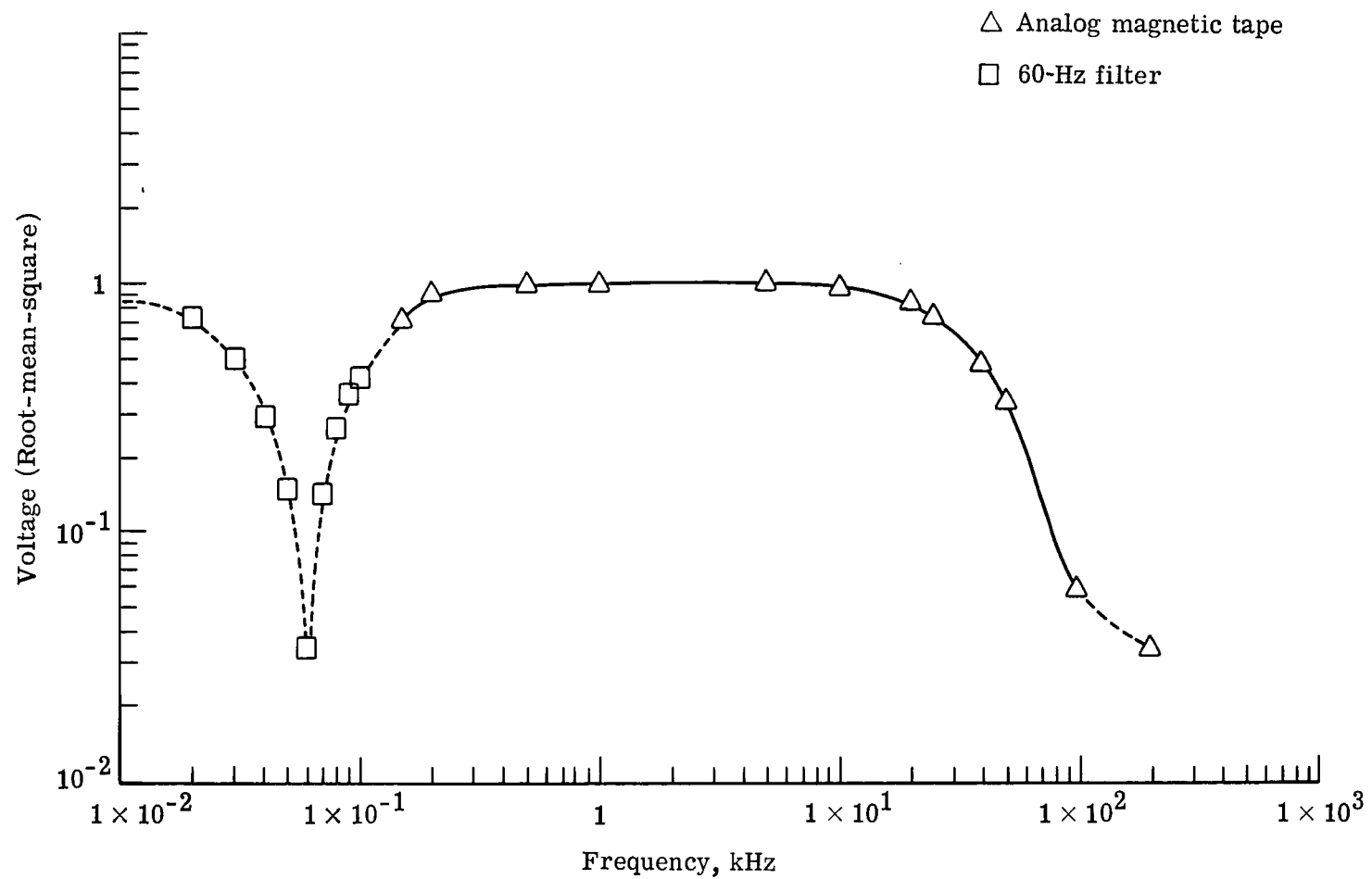


Figure 17.- Response of density measurement system.

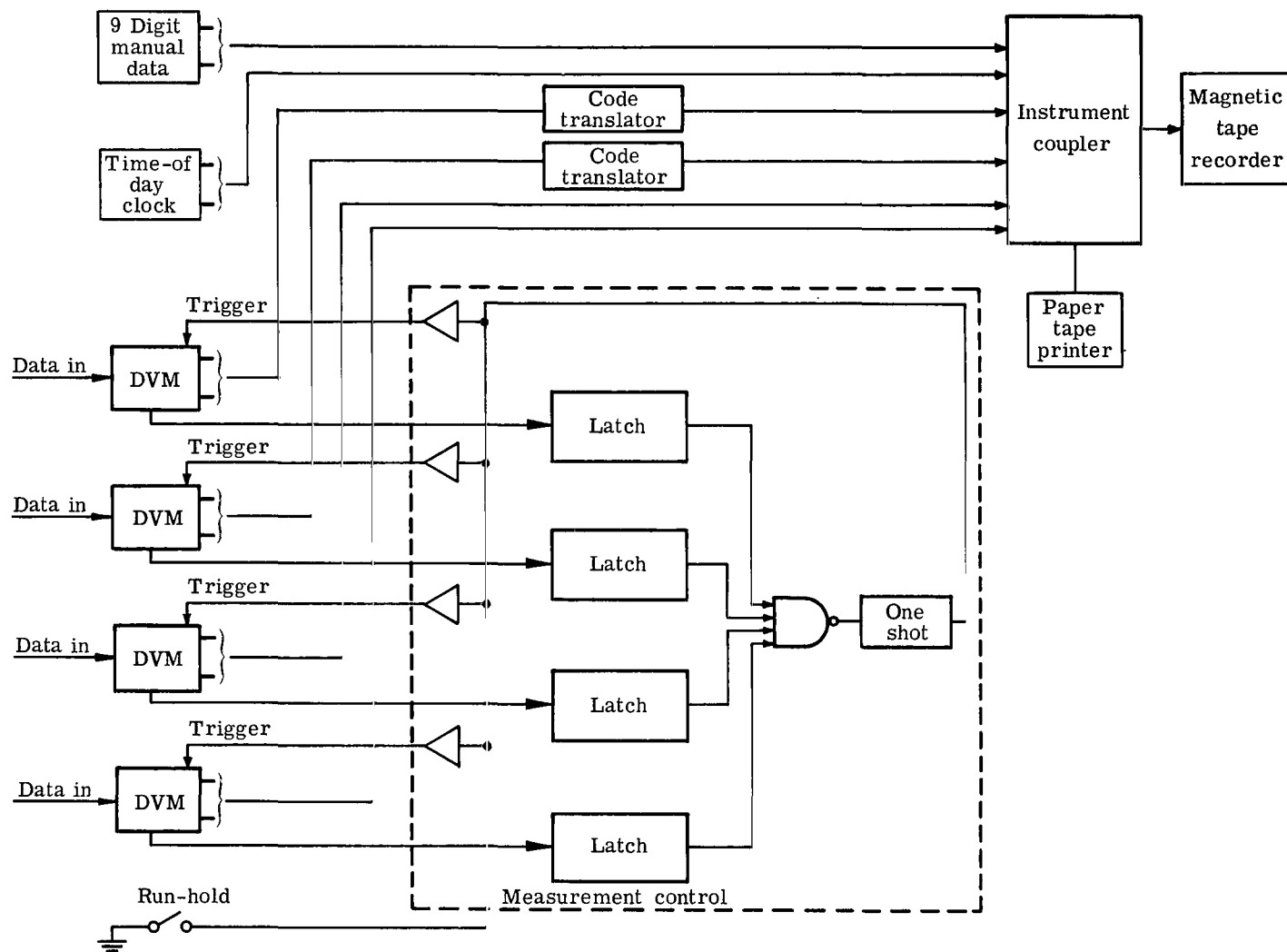


Figure 18.- Data system block diagram.

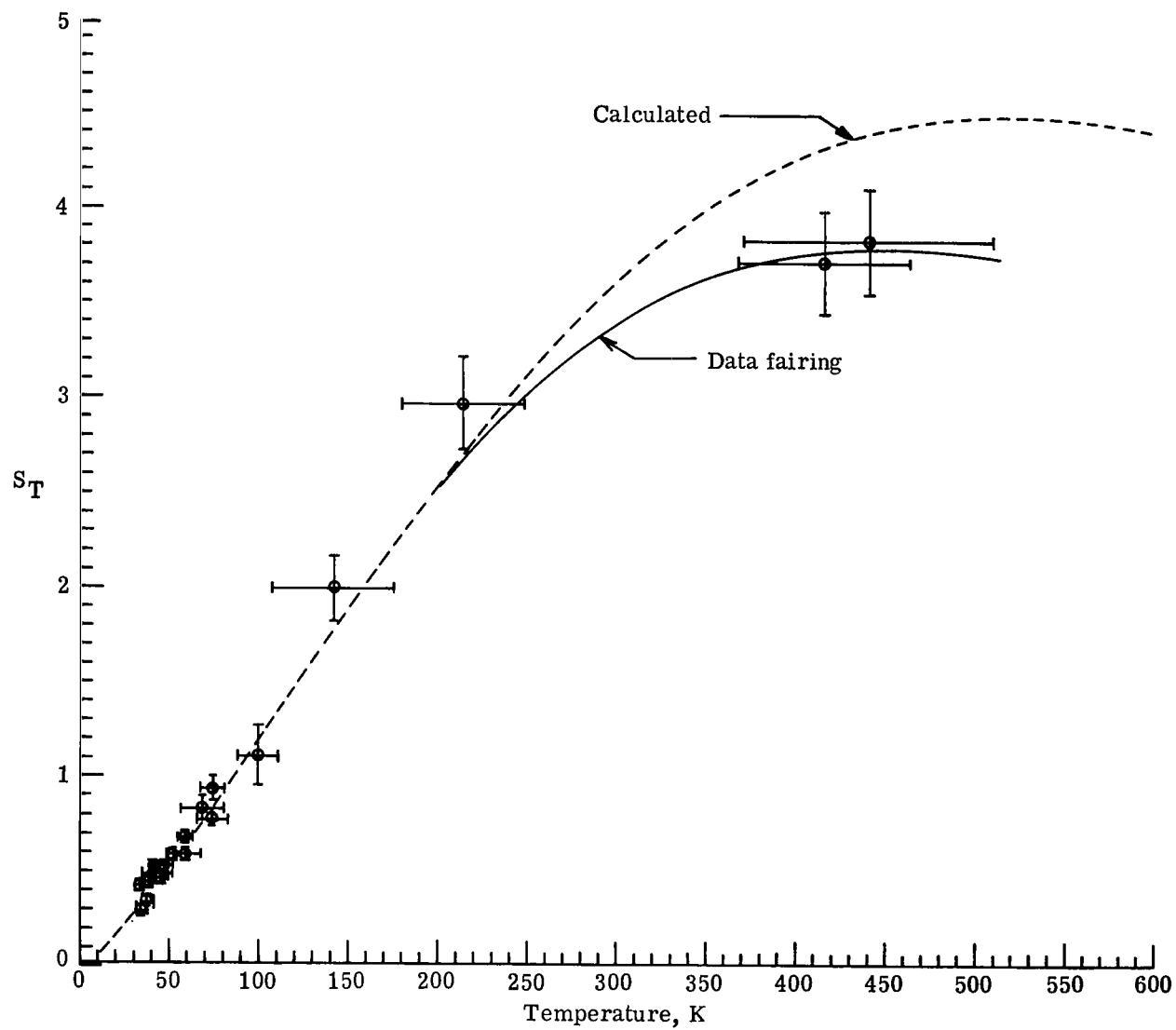


Figure 19.- Temperature calibration curve.

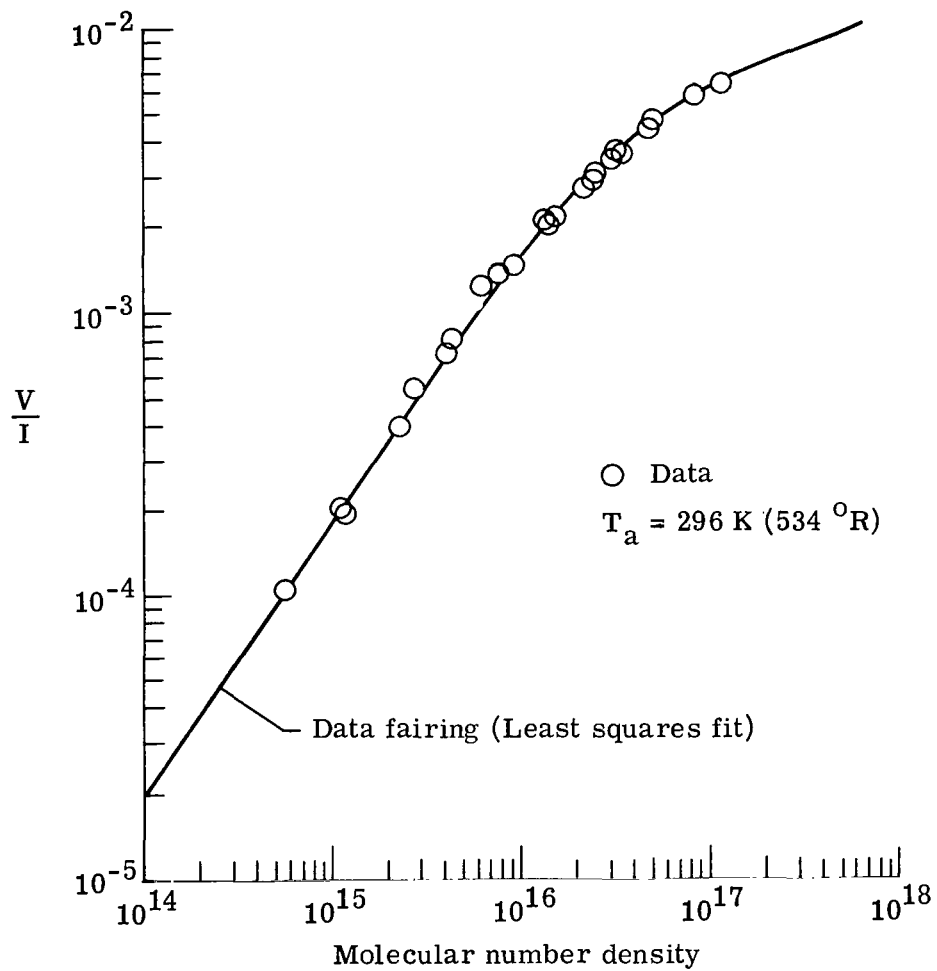


Figure 20.- Density calibration curve.



856 001 C1 U D 750822 S00903DS
DEPT OF THE AIR FORCE
AF WEAPENS LABORATORY
ATTN: TECHNICAL LIBRARY (SUL)
KIRTLAND AFB NM 87117

POSTMASTER: If Undeliverable (Section 158
Postal Manual) Do Not Return

"The aeronautical and space activities of the United States shall be conducted so as to contribute . . . to the expansion of human knowledge of phenomena in the atmosphere and space. The Administration shall provide for the widest practicable and appropriate dissemination of information concerning its activities and the results thereof."

—NATIONAL AERONAUTICS AND SPACE ACT OF 1958

NASA SCIENTIFIC AND TECHNICAL PUBLICATIONS

TECHNICAL REPORTS: Scientific and technical information considered important, complete, and a lasting contribution to existing knowledge.

TECHNICAL NOTES: Information less broad in scope but nevertheless of importance as a contribution to existing knowledge.

TECHNICAL MEMORANDUMS: Information receiving limited distribution because of preliminary data, security classification, or other reasons. Also includes conference proceedings with either limited or unlimited distribution.

CONTRACTOR REPORTS: Scientific and technical information generated under a NASA contract or grant and considered an important contribution to existing knowledge.

TECHNICAL TRANSLATIONS: Information published in a foreign language considered to merit NASA distribution in English.

SPECIAL PUBLICATIONS: Information derived from or of value to NASA activities. Publications include final reports of major projects, monographs, data compilations, handbooks, sourcebooks, and special bibliographies.

TECHNOLOGY UTILIZATION PUBLICATIONS: Information on technology used by NASA that may be of particular interest in commercial and other non-aerospace applications. Publications include Tech Briefs, Technology Utilization Reports and Technology Surveys.

Details on the availability of these publications may be obtained from:

SCIENTIFIC AND TECHNICAL INFORMATION OFFICE

NATIONAL AERONAUTICS AND SPACE ADMINISTRATION
Washington, D.C. 20546